Pre-Rift Evolution of Malawian High-Grade Basement Rocks

Leslie Huang

2017

Thesis presented for the degree of Master of Science in the

Department of Geological Sciences

University of Cape Town

Abstract

There is some controversy in terms of the basement geology of Malawi which ultimately stems from the overall lack of metamorphic studies conducted in the area. The geological complexity of Malawi comes from that fact that it sits at the intersection of three major orogenic belts: The Palaeoproterozoic Ubendian Belt, Mesoproterozoic Kibaran/Irumide Belt, and Pan African Mozambique Belt. Its complexity makes it difficult to unravel, especially in terms of identifying features of older orogenic events which have already experienced multiple metamorphic overprinting from subsequent events. This thesis provides a more detailed pre-rift evolution of the Malawian basement rocks by reporting ages and P-T conditions from four localities surrounding Lake Malawi, namely Chilumba, Mlowe, Maganga, and Mangochi. Results reveal that at 1985-1974 Ma, garnet-cordierite granulites were equilibrated under conditions of 760°C at 4.5-5 kbar possibly as a result of subduction-related magmatism. Subsequently, at 1100 Ma, charnockites were emplaced and metamorphosed under peak conditions of 770-780°C at 4.3-6 kbar due to Kibaran-age magmatic underplating. Remnants of the Irumide/Kibaran Orogeny is relatively scarce throughout Malawi and although the Mangochi charnockites were emplaced during Kibaran-age tectonism, it also experienced at least two different metamorphic events thereafter. The first occurred either during early stages of the East African orogen or Rodinia break-up at 900-800 Ma while the second occurred during the late stages of the East African orogen at 650-600 Ma. Possible remnants of the Kuunga Orogeny are recorded in Chilumba and Maganga as an amphibolite facies metamorphic event which took place around 570 Ma under peak conditions of roughly 660-670°C at 6-8 kbar. Findings of this study have not only provided a more detailed metamorphic history of Malawi but also paved way for future studies in the area to further explore why similar rocks found in such close proximity to each other preserve vastly different tectonic environments.

Plagiarism Declaration

I know that plagiarism is wrong. Plagiarism is to use anothers work and pretend that it is one's own. I have used the Harvard convention for citation and referencing. Each contribution to, and quotation in, this thesis from the work(s) of other people has been attributed, and has been cited and referenced. This thesis is my own work.

I have not allowed, and will not allow, anyone to copy my work with the intention of passing it off as his or her own work.

Leslie Huang

Acknowledgements

I would like to thank my supervisors, Dr Johann Diener and Dr Ake Fagereng, for their guidance and tremendous support throughout the past two years. Their patience and constructive feedback has been invaluable. I would also like to express my utmost gratutide to my family and friends who have supported and encouraged me throughout my Masters years. Further thanks is extended to the National Research Foundation (NRF) who provided the student funding that made this research project possible.

Leslie Huang

Contents

Chapter 1

Introduction

The underlying geology of Malawi is extremely complex simply due to the fact that it is located at the intersection of three major orogenic belts: The Ubendian Belt, Irumide Belt, and Mozambique Belt (Fig. 1.1), which were variably affected and reactivated by the Ubendian, Kibaran, Irumide, and Pan African orogenies (Ray, 1974; Ring *et al.*, 1997). Consequently, in order to further resolve various supercontinent reconstructions, one would need to unravel and understand the complex geology of Malawi. Not to mention, Malawi is a relatively ancient piece of continental crust that has been geologically active for a long time, having lived through multiple orogenies, and is again active as the southern propagation of the East African Rift system (Ring, 1994). The reason for this goes back to the Wilson Cycle theory, proposed by Wilson (1966), which suggests that oceans open and close along ancient suture zones formed during earlier supercontinent cycles. It was proposed that mobile belts, formed during supercontinent amalgamation, are essentially inherited zones of weakness, which are preferentially reactivated during later tectonic events and can still preserve overprinting P-T conditions and/or ages (Wilson, 1966; Lenardic *et al.*, 2000). Busch *et al.* (1997) applied this theory to the Grenville Orogen in Canada, and proposed that a local Robertson Lake shear zone (formed from the collision of two separate terranes during the Grenville Orogeny) was reactivated due its inherited weakness, resulting in possible rifting and continental break-up. The theory was also further explored and supported by Buiter & Torsvik (2014) who stated that continental break-up is preferentially initiated along ancient, pre-existing suture zones from earlier collisional events and that the opening of the South Atlantic Ocean (which started 134-126 Ma) likely occurred along Pan African sutures. Hence, the fact that Malawi sits at the intersection of multiple mobile belts (Fig. 1.1), each with inherited weakness, is key to why this piece of crust was not cratonised and, instead, preferentially reactivated during subsequent supercontinent cycles.

Given this, one would expect numerous studies in Malawi revolving around the metamorphic signatures and histories of different rock types, in efforts to further understand both the timing and overprinting relationships between the major orogenies themselves. Similar studies had been conducted in other parts of the Mozambique Belt in Tanzania (Muhongo & Lenoir, 1994; Appel *et al.*, 1998; Moller *et al.*, 2000; Sommer *et al.*, 2003) and Mozambique (Engvik *et al.*, 2007), where focus was placed on high grade Pan African granulites. However, relatively little research of this kind has been conducted in Malawi, with the exception of Andreoli (1984); Kroner *et al.* (1997, 2001). Most current interest in the area revolves around the mechanics of rift propagation and the occurrence of unusually deep earthquakes (Ring *et al.*, 1992; Ring, 1994; Fagereng, 2013).

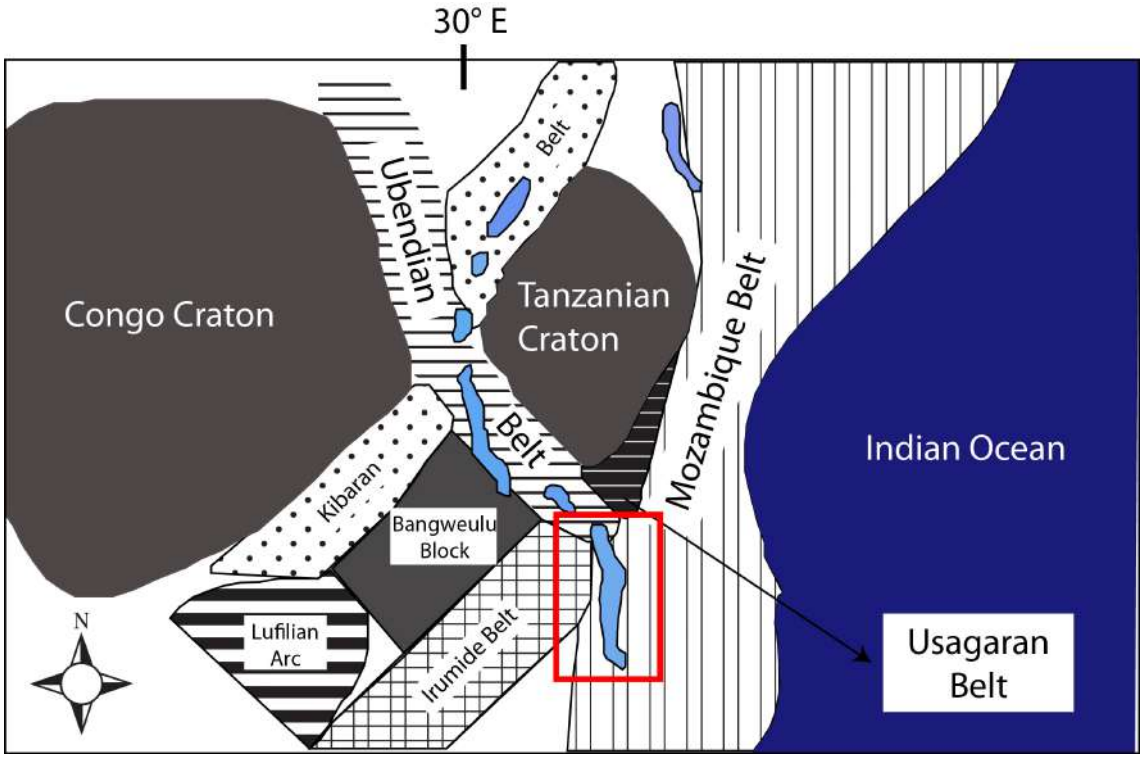

Figure 1.1: Map showing the locations of mobile belts in the East African region, where the location of Malawi is indicated in the red box. The area shaded in dark blue represents the Indian Ocean while areas shaded in light blue represent African lakes. (Modified after Ring *et al.* (1997)).

Considering the high P-T conditions and associated metamorphic facies of the mentioned orogenic events that affected the Malawian region, it is expected that the area would be made up predominantly of high pressure granulites and amphibolites. Although there are several studies

discussing ages and P-T conditions of granulites (Ring *et al.*, 1997; Andreoli, 1984; Kroner *et al.*, 2001), there is little research aimed at compiling ages and P-T conditions of all the rock types of Malawi in order to construct an overall geological history of the area.

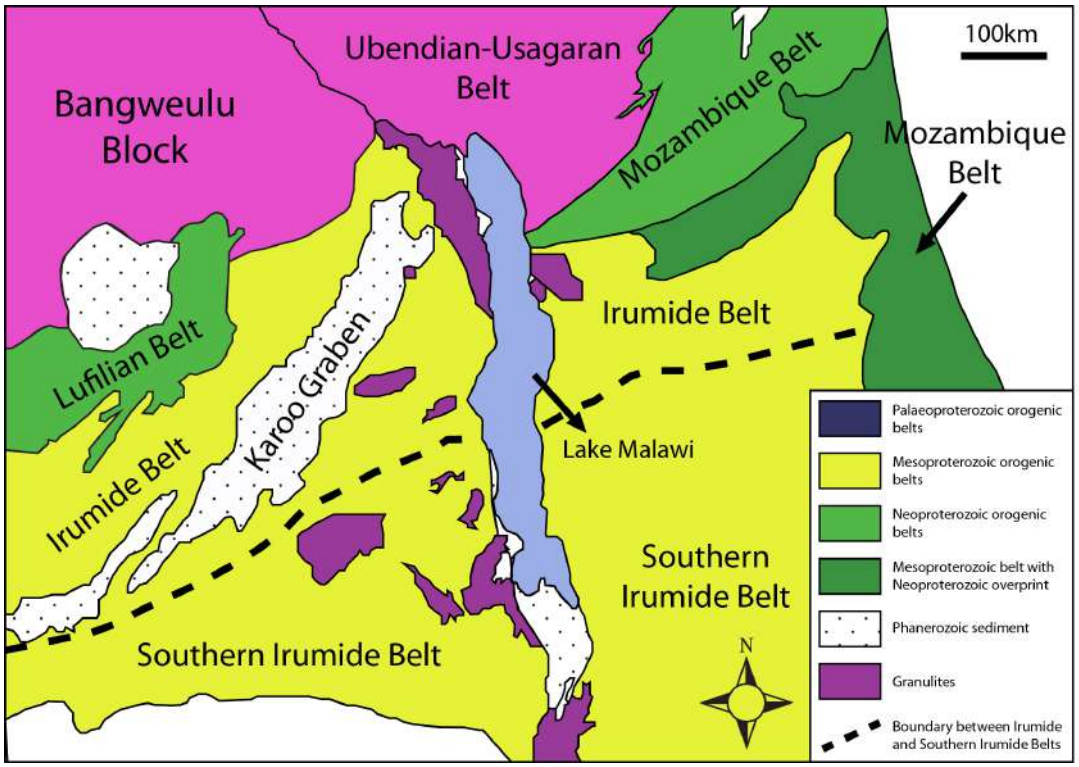

Figure 1.2: Map showing the regional geology of Malawi as suggested by Karmakar & Schenk (2016) which shows that Malawi consists mostly of Mesoproterozoic orogenic rocks (modified after Karmakar & Schenk (2016)).

Regions which have been affected by multiple overprinting orogenies, are often geologically complex and difficult to unravel, especially in terms of identifying features of older orogenic events which have already experienced some metamorphic overprinting from subsequent events. For example, extensive amounts of research has been conducted in areas such as East Antarctica (Corvino *et al.*, 2008; Phillips *et al.*, 2009) and the Grenville-aged belts in Canada (Corrigan *et al.*, 1994; Busch *et al.*, 1997) which focused on identifying and constraining multiple orogenic events recorded in the areas. The fact that Malawi has been affected by at least three orogenic events makes it an ideal example for further knowledge and understanding of the metamorphic history of each event. There are several regional geological maps of Malawi which are not entirely in agreement. For example, two recent maps of Malawi, provided by Karmakar & Schenk

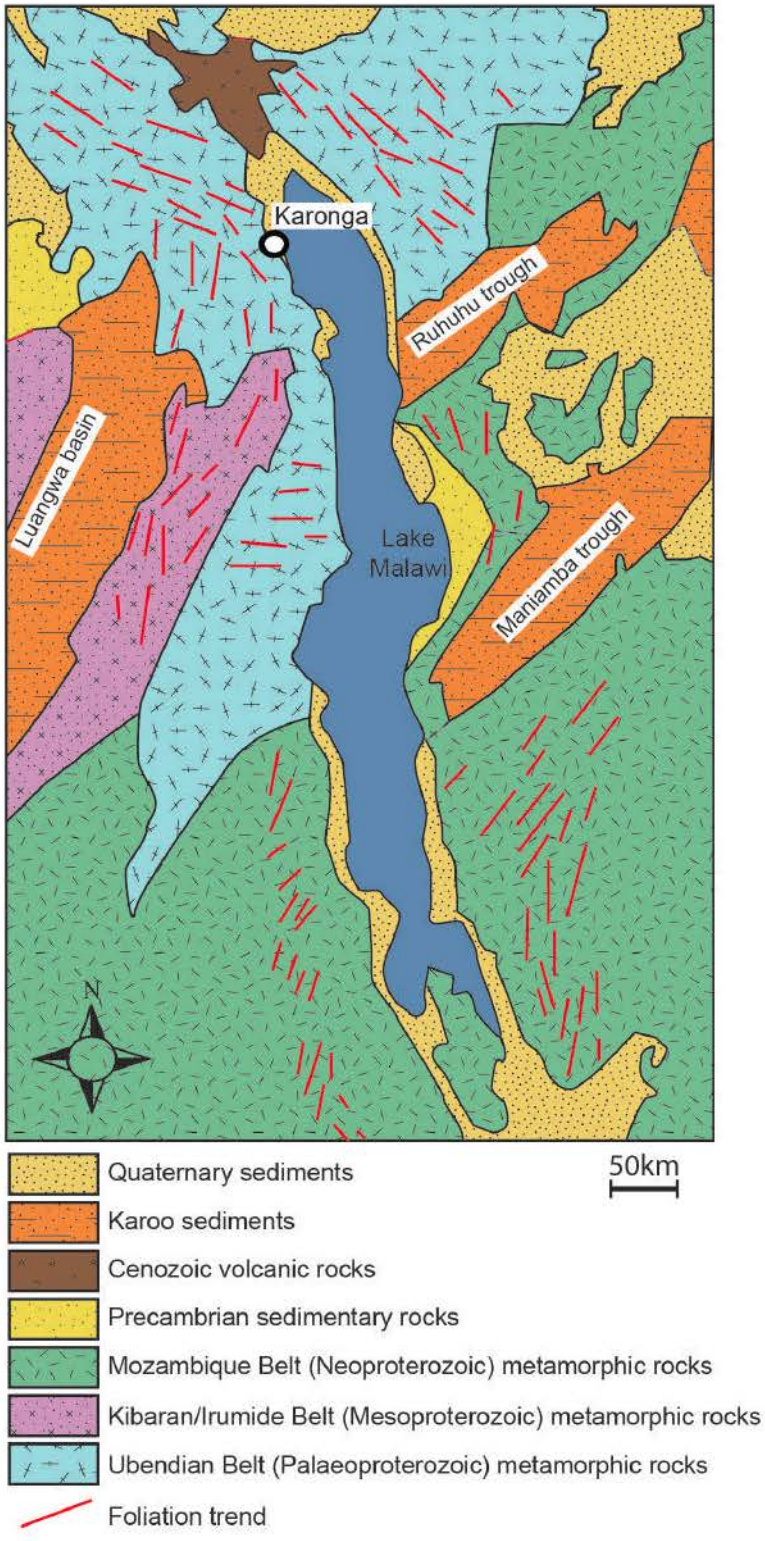

Figure 1.3: Distribution of the various orogenic belt terrains (ranging from Palaeoproterozoic to Neoproterozoic) and younger sediments around Lake Malawi as suggested by Fagereng (2013) which shows a concentration of Ubendian rocks to the north and Pan African rocks to the south (modified after Fagereng (2013)).

(2016) and Fagereng (2013) show significantly different geologies. The regional geology suggested by Karmakar & Schenk (2016) shows that most of Malawi consists of Mesoproterozoic orogenic rocks with some Neoproterozoic Mozambique Belt and Palaeoproterozoic Ubendian Belt rocks to the north of Lake Malawi (Fig. 1.2). Fagereng (2013), on the other hand, provides a map that suggests Malawi mainly consists of Palaeoproterozoic rocks to the north and Neoproterozoic rocks to the south, while Mesoproterozoic rocks appear to be quite scarce in this map (Fig. 1.3).

As a result, there appears to be some controversy in terms of the geology of Malawi as existing maps suggested by previous literature are not really at a consensus. This is essentially attributed to the scarcity of metamorphic studies conducted in Malawi and an overall incomplete geological history. Since little research has been conducted on the basement geology of Malawi, this thesis aims to construct a more detailed understanding of the Malawian geology and further constrain the specific timing and conditions of major orogenic events that shaped the Malawian geology observed today.

Overall, most studies in Malawi revolve around the age and P-T evolution of specific granulite terrains (Andreoli, 1984; Ring *et al.*, 1997; Kroner *et al.*, 2001; Ring *et al.*, 2002) rather than compiling a pre-rift metamorphic and tectonic history of the area using different P-T conditions recorded in rock types of different ages. Uncovering some of the metamorphic and tectonic history would contribute to further understanding the geological evolution of not just Malawi, but the orogenies themselves and how they influenced each other. As discussed before, the concentration of multiple mobile belts (and their inherited weakness) in Malawi allows for episodic reactivation during separate, major orogenic events, spanning from Eburnian to Pan African in age (Wilson, 1966; Lenardic *et al.*, 2000). Naturally, the Malawian basement would have preserved not only rocks of these ages, but parts of the P-T path which may identify the processes and tectonic environments responsible for supercontinent formation. As a result, this thesis aims to determine the P-T conditions under which these various rock types were formed and, subsequently, construct a more detailed metamorphic history of Malawi based on rock ages.

Aims and Objectives

The aims of this thesis are to investigate the metamorphic evolution of the high grade basement rocks from different localities around Lake Malawi through calculated P-T conditions and determine the timing of metamorphism in rocks from different localities. This will be done by analysing rocks collected from four locations around Lake Malawi. These aims will be achieved by:

1. Petrographic analyses of the rocks to identify characteristic minerals and describe any distinct metamorphic textures and fabric.

2. Electron Probe Microanalysis of minerals to determine typical mineral compositions and identify and characterise any variations in chemistry within and between rock types and localities.

3. Mineral equilibria modelling to calculate pseudosections that will constrain P-T conditions as well as any P-T paths based on mineral assemblage and retrograde textures.

4. Geochronology to determine the timing of metamorphism in order to assign P-T estimates to their relevant orogenic time periods.

5. Interpreting calculated ages and P-T conditions in attempts to determine where and how these rock types fit into their relevant orogenic events.

6. Discussing these interpretations to further contribute to existing interpretations of the area.

7. Ultimately constructing a more detailed chronological order of events in order to show the evolution of the basement geology spanning from the Eburnian to Pan African times.

Chapter 2

Orogenic Context of Malawian Geology

The 800-500 Ma Pan African Orogeny (De Waele *et al.*, 2003) was the last major orogenic event that shaped the overall geology of Malawi. However, there were three major orogenies that affected Malawi prior to this: the 2200-1800 Ma Ubendian-Usagaran, 1350-950 Ma Kibaran, and 1050-950 Ma Irumide orogenies (Ring, 1993; De Waele *et al.*, 2003). According to Fagereng (2013), the Palaeoproterozoic Ubendian, Mesoproterozoic Irumide, and Neoproterozoic Mozambique terrains are characterised by NW-SE, NE-SW, and roughly N-S trending structures, respectively. Regions along the Mozambique Belt in Malawi, Mozambique, and Tanzania are predominantly made up of high grade rocks associated with major orogenic events that will be discussed below, and later underwent Pan African metamorphic overprinting (Ring *et al.*, 2002; Sommer *et al.*, 2003). There are three main metamorphic styles recorded in different parts of the Mozambique Belt which have been described in previous literature: granulites, eclogites, and amphibolites. These rock types have been analysed mainly to constrain timing, P-T conditions, tectonic environments, and reconstructions of major orogenies (Muhongo & Lenoir, 1994; Appel *et al.*, 1998; Moller *et al.*, 2000; Sommer *et al.*, 2003; Boniface, 2009; Karmakar & Schenk, 2016).

2.1 Ubendian Orogeny

The east African section of the Ubendian Belt is between the Tanzanian Craton and Bangweulu Block (Boniface, 2009) and was formed during the Palaeoproterozoic Ubendian Orogeny between 2200-1800 Ma (De Waele *et al.*, 2003). The Ubendian Orogeny forms part of the Eburnian orogenic event and produced predominantly NW-SE structures, including the Mugesse Shear Zone

in northern Malawi (Ray, 1974). The Ubendian Belt is 600km in length and roughly 200km in width, extending from eastern Congo, through Tanzania, to northern Malawi (Muhongo *et al.*, 2002).

Moller *et al.* (1995) reported the oldest-known outcrop of eclogites of 2000 Ma formed by subduction of ancient oceanic lithosphere in the Usagaran Belt in Tanzania. The eclogites experienced conditions of 750-800°C at roughly 18 kbar and preserve a clockwise P-T path with near-isothermal decompression. Moller *et al.* (1995) proposed plate convergence (subduction) as the cause of deformation and associated metamorphism. Similarly-aged garnet-cordierite gneisses found in central Malawi were reported by Ring *et al.* (1997) as a result of low pressure granulite facies metamorphism, which peaked at 1985-1995 Ma, suggesting it was related to the Ubendian Orogeny. Although it experienced peak conditions of 750-850°C at 5-5.5 kbar, it was intercalated with lenses of enderbitic gneisses that are roughly 2000 Ma in age as well and record high pressure granulite facies conditions of up to 11 kbar in pressure (Ring *et al.*, 1997). Given the overlap in age as well as the significant difference in pressure conditions, it was concluded that the high and low pressure granulite facies metamorphism took place simultaneously and, consequently, likely formed part of a paired metamorphic belt. Ring *et al.* (1997) suggested that the garnet-cordierite granulites were part of the upper plate based on the lack of evidence that it was ever subjected to high pressures. Subsequently, the age of subduction proposed by Ring *et al.* (1997) is in agreement with that suggested by Moller *et al.* (1995). Boven *et al.* (1999) also constrained Ubendian subduction conditions based on kyanite-bearing eclogites, located in the Ubende Belt of western Tanzania, which yielded peak conditions of 720°C at 17 kbar. Pressure conditions suggested by Moller *et al.* (1995) and Boven *et al.* (1999) are therefore in close agreement. However, the difference in recorded pressures in Ubendian subduction-related eclogites in the Ubendian Belt may be attributed to retrogression. Boven *et al.* (1999) concluded that early stages of exhumation are recorded in retrograde eclogites with pressures ranging from 12-15 kbar, suggesting that Tanzania and Malawi may have experienced the same subduction conditions at roughly 2000 Ma.

In terms of the subsequent collisional event, a recent study by Kazimoto *et al.* (2015) analysed granulite facies rocks obtained from the Katuma Block in the north western Ubendian Belt of Tanzania that suggested peak conditions of roughly 770°C at 7 kbar. Kazimoto *et al.* (2015) attributed these conditions to what has been suggested by the authors as the final collisional event of the Ubendian Orogeny at 1840 Ma. This is in close agreement to ages reported by De Waele *et al.* (2003) who proposed that the Ubendian Orogeny started at 2200Ma and ended at roughly

1800Ma.

2.2 Kibaran and Irumide Orogenies

The 1350-950 Ma Kibaran Orogeny, which formed part of the Grenville orogenic event, has been previously recognised to be comprised of three main metamorphic terrains: the Kibaran Belt, the Irumide Belt and the Choma-Kalomo Block (De Waele *et al.*, 2003; Johnson *et al.*, 2005) and represented sutures of the Rodinia supercontinent (Boniface, 2009) as shown in Fig. 2.1. The Kibaran Belt itself was formed as a result of the Mesoproterozoic collision between the Tanzania Craton, Bangweulu block and the Congo Craton (Boniface, 2009). Peak P-T conditions of the Kibaran Orogeny in the Ubende region were acquired from Ubendian-aged rocks that were reworked during Kibaran metamorphism and yielded 700-750°C at 10 kbar (Boniface, 2009).

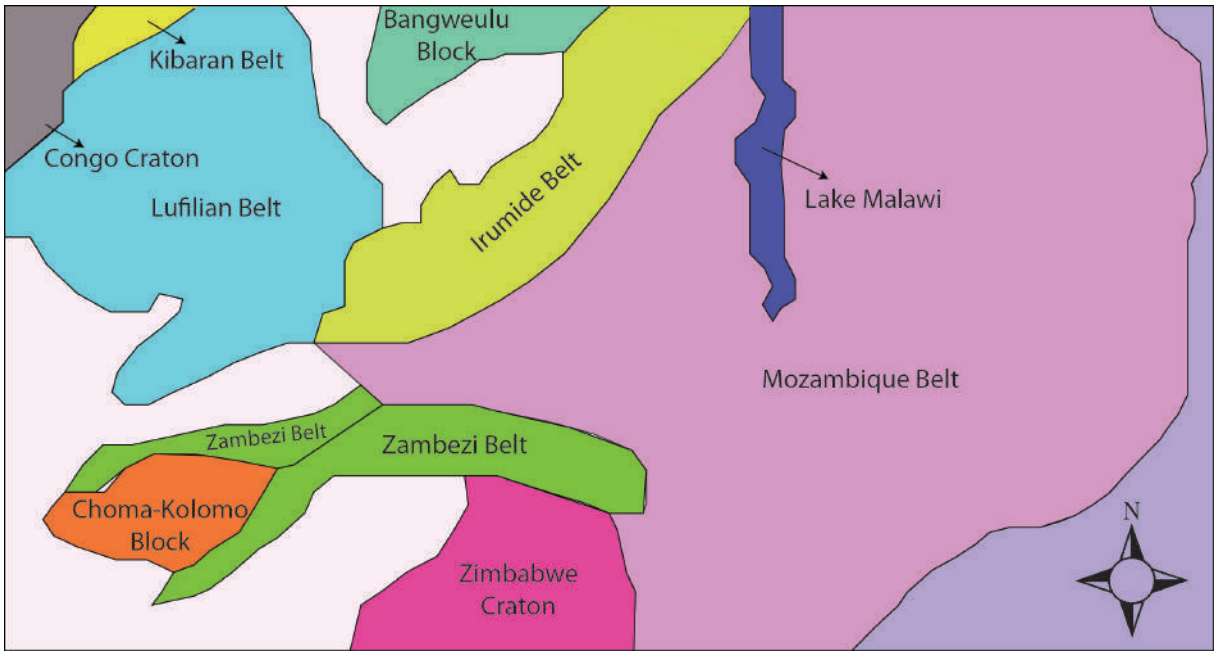

Figure 2.1: Simplified map showing the distribution of Kibaran-age metamorphic terrains: the Kibaran Belt, the Irumide Belt, and Choma-Kalomo Block, in relation to other mobile belts, cratons, and Lake Malawi. Areas shaded in white represent Phanerozoic sediments. (Modified after Johnson *et al.* (2005)).

The Irumide Belt is situated between the Bangweulu Block and Mozambique Belt and consists

of mainly NE-SW trending structures (De Waele & Mapani, 2002). It was also thought that the Irumide and Mozambique belts were linked in that both experienced Irumide magmatism and tectonism which was supported by Mesoproterozoic ages of 1150-1040 Ma (Kroner *et al.*, 1997) and 1150-1100 Ma (Manhica *et al.*, 2001) reported in the Mozambique Belt. These ages were in agreement with the proposed age of 1100 Ma by Daly (1986) for Irumide tectonism in Zambia. However, De Waele *et al.* (2003) reported age data obtained in central and northern Zambia that suggested Irumide magmatism and tectonism took place much later, at 1050-950 Ma. Consequently, the authors proposed that the Irumide and Mozambique Belts are not related but were developed separately and later juxtaposed during Neoproterozoic tectonic activities (De Waele *et al.*, 2003). Furthermore, De Waele *et al.* (2003) concluded that Kibaran magmatic and tectonic events are not recorded in the Irumide Belt and, therefore, unlikely correlated as well.

Similar to the Ubendian garnet-cordierite gneiss discussed by Ring *et al.* (1997), metapelitic rocks found in Chipata, Zambia, in the southern Irumide Belt was discussed extensively by Karmakar & Schenk (2016). Defined as a garnet-cordierite-spinel gneiss, Karmakar & Schenk (2016) suggested that these gneisses were the result of HT to UHT metamorphism based on the metamorphic texture of garnet grains replaced by symplectites of spinel and quartz. The P-T path of the gneiss, determined by Karmakar & Schenk (2016), shows a clockwise loop followed by isobaric cooling at 5-6 kb, suggesting cooling at mid-crustal levels. Additionally, the HT to UHT metamorphism was dated at 1030-1013 Ma, which chronologically places its occurrence just before arc magmatism at 1090-1000 Ma in the southern Irumide Belt and almost concurrent to intracrustal melting in the Irumide Belt at 1020-1000 Ma (Karmakar & Schenk, 2016). Given both its P-T path characteristics and determined ages, it was concluded that the HT to UHT metamorphism and the intracrustal melting was a result of subduction-related magmatism in the southern Irumide Belt, where it cooled at mid-crustal levels and later uplifted and exhumed during the Pan African event (Karmakar & Schenk, 2016).

An early study conducted by Andreoli (1984) analysed and discussed granulites in southern Malawi which yielded ages of 1085-850Ma. Based on the Mesoproterozoic ages obtained, it was then concluded that southern Malawi was not part of the Mozambique Belt (i.e. not Pan African) but part of the Kibaran Orogeny instead. It was subsequently suggested that the southern Malawi terrain is part of an island arc that was subducted during the Mesoproterozoic Kibaran orogeny. Later uplift and cooling resulted in the exposure of the granulites observed in southern Malawi presently (Andreoli, 1984).

However, Kroner *et al.* (2001) argued against this theory and suggested that southern Malawi is indeed part of the Mozambique Belt and is one of several terrains, part of East Gondwana, which all amalgamated during the collision of East and West Gondwana. Kroner *et al.* (2001) supported this claim by dating high grade gneisses and metapelites in southern Malawi which determined three distinct events: 1. Late Kibaran granitoid intrusions (1040-929 Ma), 2. Pan African granitoid intrusions (710-550 Ma), and 3. Thermal peak of Pan African granulite metamorphism (571-549 Ma). The authors proposed that Pan African metamorphism would have caused extensive metamorphic overprinting and multiple age signatures, making it difficult to identify characteristics of older orogenic events (Kroner *et al.*, 2001). Kroner *et al.* (1997) reported ages from the granulite terrain in southern Malawi and concluded that although Kibaran-aged magmatism occurred at 1000-1100 Ma, high grade metamorphism only occurred about 550-575 Ma during the Pan African Orogeny.

Charnockites have been reported in southern Malawi by both Andreoli (1984) and Kroner *et al.* (2001) and described as orthopyroxene-bearing granulites that are dark-green in colour and granoblastic in texture (Andreoli, 1984). Although Andreoli (1984) interpreted these charnockites to have possibly formed as a result of granite intrusions associated with the magmatic arc setting mentioned above, their P-T conditions were not constrained. Kroner *et al.* (2001) determined P-T conditions of these charnockites to range between 848-940°C but no pressure conditions were determined. However, Kroner *et al.* (2001) used the recorded anticlockwise, isobaric cooling P-T paths of other granulites in the surrounding region to suggest that granulites in southern Malawi were formed by magmatic underplating.

2.3 Pan African Orogeny

The Pan African Orogeny occurred roughly at 800-500 Ma (De Waele *et al.*, 2003), forming the Mozambique Belt which stretches from southern Mozambique to southern Ethiopia and is defined as a suture that marks the amalgamation of East and West Gondwana (Ring *et al.*, 1997; Muhongo & Lenoir, 1994). Peak conditions for the orogenic event recorded in Tanzania were suggested to be 750-800°C at roughly 12-13 kbar and subsequent amphibolite facies retrogression occurred at 550-700°C at 5-8 kbar (Sommer *et al.*, 2003). Ring *et al.* (2002), however, suggested slightly higher retrograde conditions of 750-800°C at roughly 6 kbar, as a result of near-isothermal

decompression, recorded in northern Malawi. Ultimately, Pan African tectonism and high grade metamorphism resulted in significant overprinting of older orogenic features from the Ubendian, Irumide and Kibaran orogenies (Ring *et al.*, 1997). The Pan African Orogeny not only created N-S trending structures but also reactivated older pre-existing structures such as the Ubendian-aged Mugesse Shear Zone (Ray, 1974; Appel *et al.*, 1998). Additionally, the Palaeoproterozoic basement rocks of Malawi were metamorphosed under amphibolite and granulite facies conditions during the Pan African Orogeny (Boniface, 2009).

There are two prevalent interpretations of the associated high pressure granulites found along the Mozambique Belt (Moller *et al.*, 2000). The first interpretation revolves around the idea that there was one, continuous collision of East and West Gondwana, resulting in high grade metamorphic granulites prior to 600 Ma (Moller *et al.*, 2000). It was then assumed that the age of metamorphism of the granulites indicated the age of the collision which marked the final amalgamation of East and West Gondwana. The second interpretation suggests that the formation of Gondwana involved two distinct orogenic events: (1) the collision of the India, Madagascar, Sri Lanka, East Antarctic Craton and Kalahari Craton (IMSLEK) terranes with the Congo Craton and Arabian Nubian Shield (ANS) between 800-650 Ma. This was termed the East African Orogen; (2) a later, subsequent collision between Australia and Antarctica with the rest of Gondwana (i.e. IMSLEK-Congo-ANS) at 570-530 Ma, and was termed the Kuunga Orogen (Meert *et al.*, 1995; Meert & van der Voo, 1997; Moller *et al.*, 2000; Meert, 2003). In other words, the amalgamation of Gondwana essentially involved a multi-phase assembly instead of describing the assembly as a single suture event (Meert, 2003). However, this model was later amended by Collins & Pisarevsky (2005) who proposed that India did not collide with the Congo Craton and Arabian Nubian Shield (ANS) until late Neoproterozoic. As a result, the Kuunga orogen actually encompasses the collision of India with Australia/Antarctica as well and redefined to have occurred at 570-500 Ma, 30 Ma later than that proposed by Meert (2003).

Extensive work has been conducted on Pan African granulites along the Mozambique Belt, mainly in Tanzania (Muhongo & Lenoir, 1994; Appel *et al.*, 1998; Moller *et al.*, 2000; Sommer *et al.*, 2003) and Mozambique (Engvik *et al.*, 2007). In previous literature, differences in interpretations of tectonic environments in the Mozambique Belt often stems from extensive retrogression of Pan African rocks. For example, while Muhongo & Lenoir (1994) concluded that the 695±4 Ma granulites in the Mozambique Belt were formed during the subduction-collision event during the final amalgamation of Gondwana, Appel *et al.* (1998) suggested that according to Meert *et al.* (1995),

the final assemblage of Gondwana had not occurred until 150 Ma years later, at 550 Ma. Appel *et al.* (1998) showed that the high grade granulites lack a distinctive clockwise P-T path with near isothermal decompression that is compatible with continental collision. It was then proposed that formation of the high grade granulites could be explained by magmatic underplating, instead of continental collision (Appel *et al.*, 1998).

Suprisingly, little to no research has been conducted on Pan African granulites in Malawi to date and hence, not much is known about them. However, Ring *et al.* (2002) reported on the first occurrence of Pan African 530 Ma eclogites in Malawi. Although described as heavily retrogressed garnet-amphibolites, Ring *et al.* (2002) reported rare clinopyroxene and, subsequently, used its elevated jadeite content to determine that the rock was, initially, exposed to high pressure conditions of 17-18 kbar. The inferred P-T path, determined by thermobarometry, of the eclogites shows distinct isothermal decompression after reaching peak pressure conditions, characteristic of subduction zone settings. In addition to P-T conditions, trace element patterns indicate that the eclogite precursor not only predates the Mozambique Ocean, but is likely thinned continental crust that was subducted after the closure of the ocean itself. As a result, Ring *et al.* (2002) concluded that the eclogites mark the final amalgamation of East and West Gondwana, in a subduction-collision transition tectonic setting. Some literature describing high-grade granulites along the Mozambique Belt have acknowledged that they have been heavily retrogressed to amphibolites, also involving some decompression as indicated by distinct decompression plagioclase rims around garnets (Ring *et al.*, 2002; Sommer *et al.*, 2003). Besides the eclogite facies event, there was another amphibolite facies metamorphic event in Malawi reported by Ring *et al.* (2002) which occurred at 580-550 Ma, south of the Mugesse Shear zone. It was concluded that since these amphibolites did not record high pressures, it is unlikely that they are the products of overthickened crust during the Pan African Orogeny (Ring *et al.*, 2002).

Chapter 3

Outcrop Geology

Samples were collected from four localities surrounding the Lake Malawi, namely the Chilumba garnet-amphibolites (M07, M08, and M09), Mlowe granulites (M13 and M14), Maganga amphibolites and schists (M16, M17, and M18), and Mangochi Charnockites (M21 and M22). Rock types were named according to their localities as shown in Fig. 3.1.

Chilumba Garnet Amphibolite (M07, M08, and M09)

Approximately 50 km south of Karonga, along the western boundary of Lake Malawi, lies the Chilumba basement block (Fig. 3.1). Ring *et al.* (2002) reported the first occurrence of Pan African eclogites in Malawi, found in the Chilumba region. These eclogites recorded pressures of up to 17 kbar and were proposed to have formed during the subduction-collision transition which marked the final amalgamation of east and west Gondwana at 530 Ma (Ring *et al.*, 2002). However, Ring *et al.* (2002) also reported adjacent amphibolites that formed during a shearing event south of the Mugesse Shear zone. These amphibolites were suggested to have formed at least 30 Ma before the eclogite facies event (Ring *et al.*, 2002). Samples collected in Chilumba for this study were characterised as garnet amphibolites and observed to possess two distinct textures:

- Coarse-grained, massive biotite-garnet-hornblende amphibolites which appear to be retrogressed (sample M07) and occur as lenses within garnet-feldspar migmatitic gneiss (Fig. 3.2 (a)). The garnet-feldspar gneiss is defined by strong deformed fabric (Fig. 3.2 (b)) with steep N-S foliation and shallow N-dipping lineation.
- Finer-grained garnet amphibolites (samples M08 and M09).

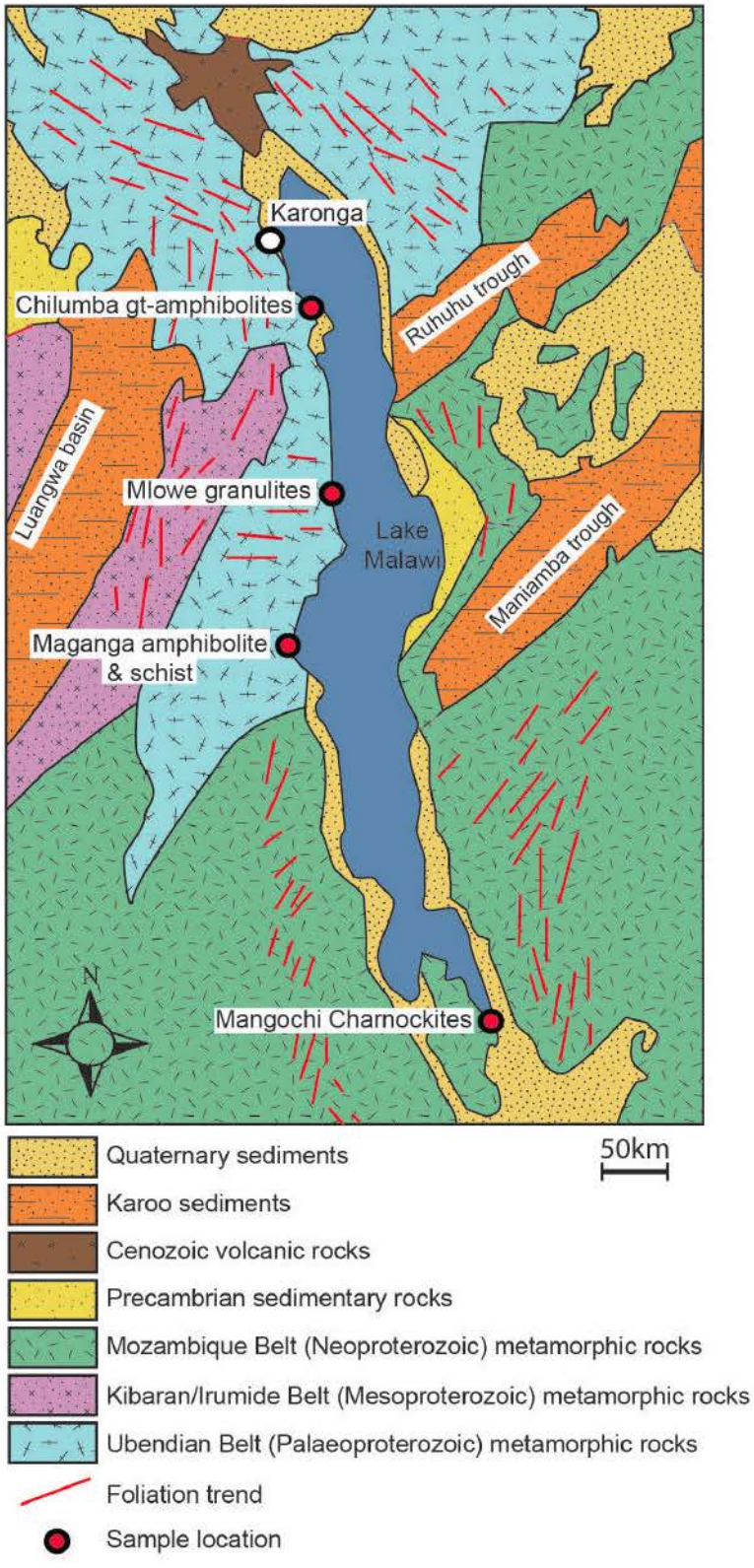

Figure 3.1: Regional map of Malawi, surrounding Lake Malawi, showing rock type, orogenic belts, structural trends, and sample locality (modified after Fagereng (2013)).

Figure 3.2: Field photographs from the Chilumba locality. (a) Garnet-feldspar migmatitic gneiss containing lens of sample M07 garnet-amphibolites. (b) Deformation within the gneiss suggests shearing. (c) Showing M08 and M09 which occur as fine-grained garnet-amphibolites.

Mlowe Granulites (M13 and M14)

A further 100 km south of Chilumba, large boulders of garnet-cordierite granulites were found at Mlowe, at the shore of Lake Malawi (Fig. 3.3 (a)). Similar garnet-cordierite granulites in this area were reported by Ring *et al.* (1997) which yielded an age of 1985-1995 Ma and interpreted to have been the upper plate of a paired metamorphic belt that underwent Ubendian-aged subduction. The granulite ages yielded by Ring *et al.* (1997) are consistent with Ubendian subduction ages recorded in Tanzania (Moller *et al.*, 1995; Boven *et al.*, 1999). They are also consistent with the map in Fig. 3.1 which shows the Mlowe region within the Ubendian Belt. The granulites collected for this study possess two different textures:

- Sample M13 (shown in Fig. 3.3 (b)) contains large garnet nodules, of up to 2-3 cm in diameter, and distinct leucosomes that wrap around the aforementioned garnets (Fig. 3.3 (c)).
- Although also possessing distinct leucosome patches, M14 does not contain large garnet

nodules as observed in M13 (Fig. 3.3 (d)).

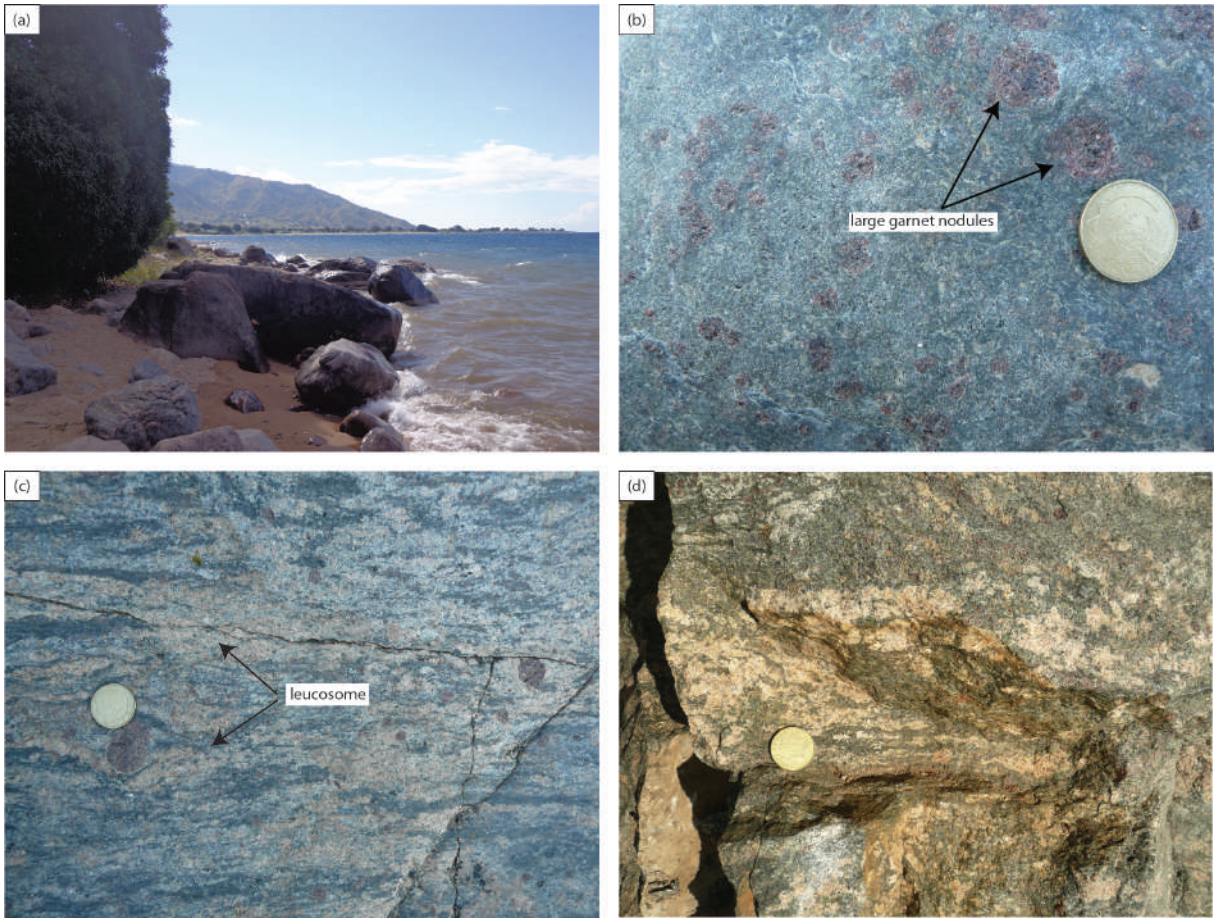

Figure 3.3: Field photographs from the Mlowe locality. (a) Granulites were found as boulders along the boundaries of Lake Malawi at Mlowe. (b) M13 contains large garnet nodules of up to 2-3 cm in diameter. (c) Shows leucosomes in sample M13 that wrap around garnet nodules. (d) Shows presence of leucosomes in M14 and the absence of large garnets seen in M13. Scale: coin = 25 mm.

Maganga Amphibolites and Schists (M16, M17, and M18)

The Maganga region has not been discussed in any existing literature but Fig. 3.1, modelled after that of Fagereng (2013), suggests the Maganga region falls within the Ubendian Belt. Two significantly different rock types were collected at Maganga for this study (located another 100 km south of Mlowe, along the lake):

- Foliated Amphibolites (M16 and M17): the fine-grained hornblende amphibolite (Fig. 3.4) was found amongst retro-sheared schists in a shallowly dipping basement with N-S trending foliation. Sample M17 appeared to be a fresher sample of M16, as it is coarser-grained and

appears to be less retrogressed.

- Schists (M18): micaceous muscovite-schists were observed on the beach which appeared to have a flat fabric, parallel to the shoreline that has a roughly N-S trend. Distinct porphyroblasts of biotite were also seen.

Figure 3.4: Outcrop photo of the Maganga amphibolite which is defined as fine-grained with N-S trending foliation.

Mangochi Charnockites (M21 and M22)

At the southern-most tip of Lake Malawi (200 km south of Maganga), green charnockitic two-pyroxene garnet granulites were found along a scarp at Mangochi Pass. The scarp was observed to be N-S trending and dipping west at roughly 50°. Although the map in Fig. 3.1 shows the region to be part of the Mozambique Belt, similar orthopyroxene-bearing granulites were discussed by Andreoli (1984) in the Blantyre-Zomba region of southern Malawi. These granulites were described as green to dark-green in colour with a granoblastic texture and resembles typical charnockites (Andreoli, 1984). Andreoli (1984) proposed that the granulites were formed as a

result of granite intrusions associated with a magmatic arc setting during Irumide tectonism. Ages spanning from 1100 Ma to roughly 570 Ma of granulites located in southern Malawi have been reported as well (Kroner *et al.*, 1997, 2001).

Chapter 4

Petrography and Mineral Chemistry

4.1 Petrography

Chilumba Garnet-amphibolites (M07, M08, and M09)

The garnet-amphibolites are characterised as fairly equigranular rocks, consisting of garnet, hornblende, plagioclase, quartz and accessory minerals rutile, ilmenite, and titanite. The anhedral hornblende grains range roughly between 0.25 mm to 1.5 mm while the an- to subhedral garnet grains range between 0.25 mm to 0.5 mm. Plagioclase is not only found in the finer grained matrix, but also as distinct rims around garnet grains (see Fig. 4.1 (a)). These plagioclase rims are relatively thin and occur particularly around garnet grains (Fig. 4.1 (a)). The amphibolites show little to no mineral alignment and have a distinct granoblastic texture. There are also distinct magnetite-plagioclase sympletites that occur throughout the rock (Fig. 4.1 (c)). Proportionally, there is approximately 75% hornblende, 10% garnet, 10% plagioclase, and 5% magnetite. These features are consistent throughout samples M08 and M09. However, sample M07 shows some very fine-grained biotite mats that occur as a replacement texture on the edges of garnet grains (Fig. 4.1 (b)). The fine-grained bioite also seem to have formed along cracks within the garnet. Subsequently, the modal abundance for sample M07 is approximately 50% hornblende, 25% garnet, 10% plagioclase, 10% biotite, and 5% magnetite.

Mlowe Garnet-cordierite-granulites (M13 and M14)

Samples M13 and M14 have very similar textures and therefore microphraphs of one of the samples have been chosen to represent and illustrate the described textures in Fig. 4.2 to avoid repetition. The M13 garnet-cordierite granulite is made up of large poikiloblasts of garnet (ranging roughly from 2 cm to 5 cm) set in a finer-grained matrix of fine-grained garnet (0.5 mm to 1.5 mm), sillimanite (up to 0.5 mm), fine-grained fibrolite sillimanite, biotite (roughly 0.25 mm), cordierite

(roughly 1 mm), spinel (up to 1 mm), plagioclase, alkali feldspar (2 mm to 3 mm), corundum (0.5 mm to 1 mm)), quartz (up to 0.5 mm), and magnetite (up to 2 mm) (Fig. 4.2 (a)). Accessory minerals include magnetite and monazite. The distinct gneissic texture is defined by light and dark bands (each roughly 1 cm thick) throughout the rock. The light bands consist of cordierite, feldspar and quartz, while the dark bands consist of garnet, biotite, sillimanite, magnetite, and spinel (Fig. 4.2 (b)). The strong fabric, limited to the dark bands, is defined by the alignment of biotite and sillimanite.

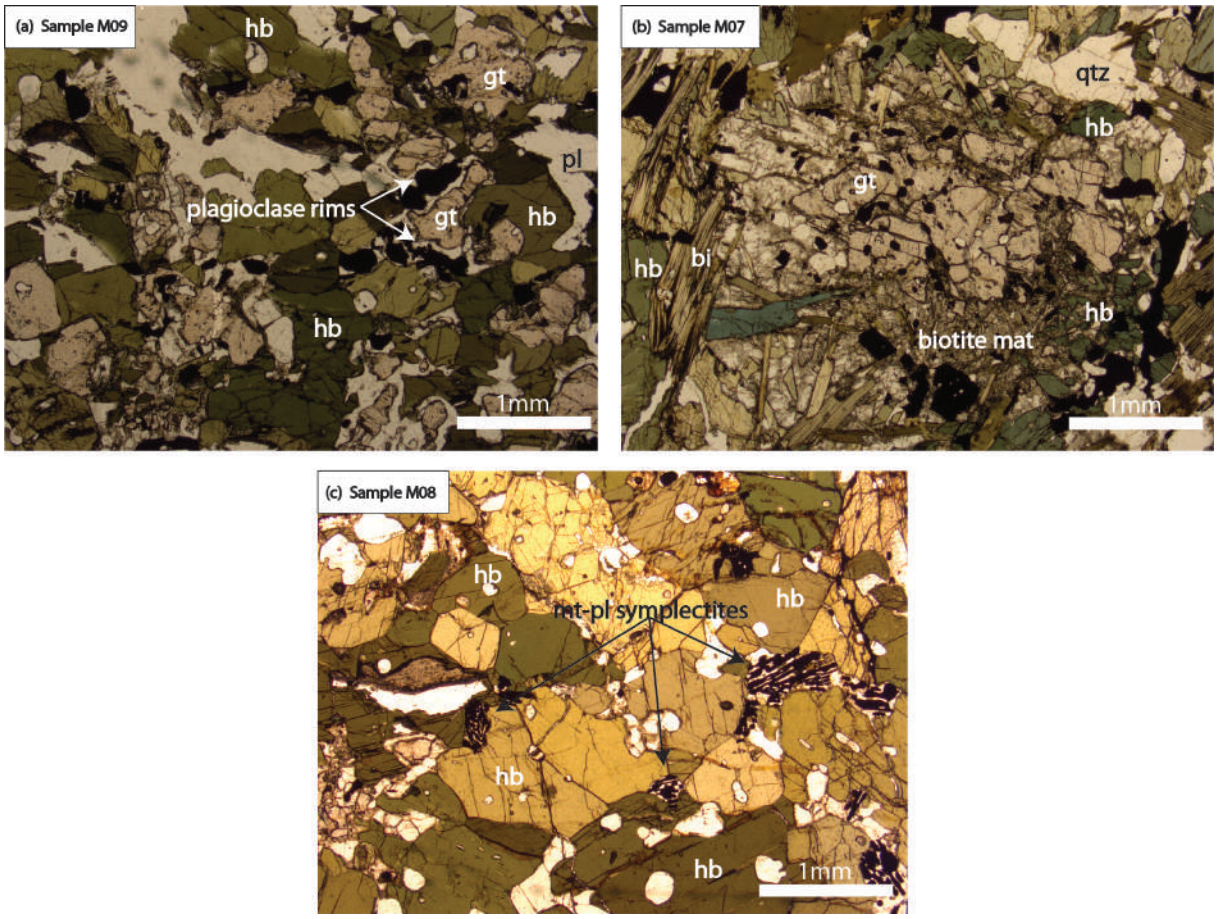

Figure 4.1: (a) Typical texture of samples M08 and M09, showing distinct decompression plagioclase rims, as indicated by the label, as well as matrix plagioclase. (b) Shows some alteration of garnet grains in M07. (c) Shows magnetite-plagioclase symplectites. All images were taken in plane polarised light.

Poikiloblastic garnets in M13 are characterised by its large grain size and multiple inclusions of spinel, magnetite, and corundum. Fig. 4.2 (c) and (d) shows instances of a symplectite-like texture where finer-grained garnets have almost completely replaced spinel and magnetite. This

is mainly supported by the fact that the garnet grains appear to more stable than the symplectites themselves. This feature is not observed in sample M13 garnet nodules and occurs only in the finer-grained garnets. Additionally, the finer-grained garnets are generally found in the dark bands that wrap around poikiloblastic garnets. It is, therefore, likely that the poikiloblastic garnets and the finer-grained garnets formed during two distinct growth events. Similarly, sillimanites also appear to have two different textures. Larger-grained sillimanites occur as well-equilibrated grains (Fig. 4.2 (e)), while the finer-grained, fibrolite sillimanites occur on the edges of cordierite grains (Fig. 4.2 (f)). Biotite occurs as a replacement texture around the coarser-grained sillimanite grains (Fig. 4.2 (e)).

Modal abundance for M13 is roughly 55% garnet, 15% cordierite, 10% sillimanite, 10% feldspar (and quartz), 5% biotite, and 5% spinel and magnetite. Sample M14, however, does not have large garnet nodules and, therefore, consists of approximately 40% cordierite, 20% sillimanite, 15% feldspar (and quartz), 10% garnet, 10% biotite, and 5% spinel and magnetite. Rare amounts of corundum are observed in both M13 and M14 granulites and occur exclusively as inclusions within the garnets, being isolated from the matrix (Fig. 4.2 (g)). Although samples M13 and M14 garnet-cordierite granulites share the same petrography, M13 has garnet nodules as well was finer-grained garnets while M14 does not have these nodules and contain only the finer-grained garnets up to 1-1.5 mm in size.

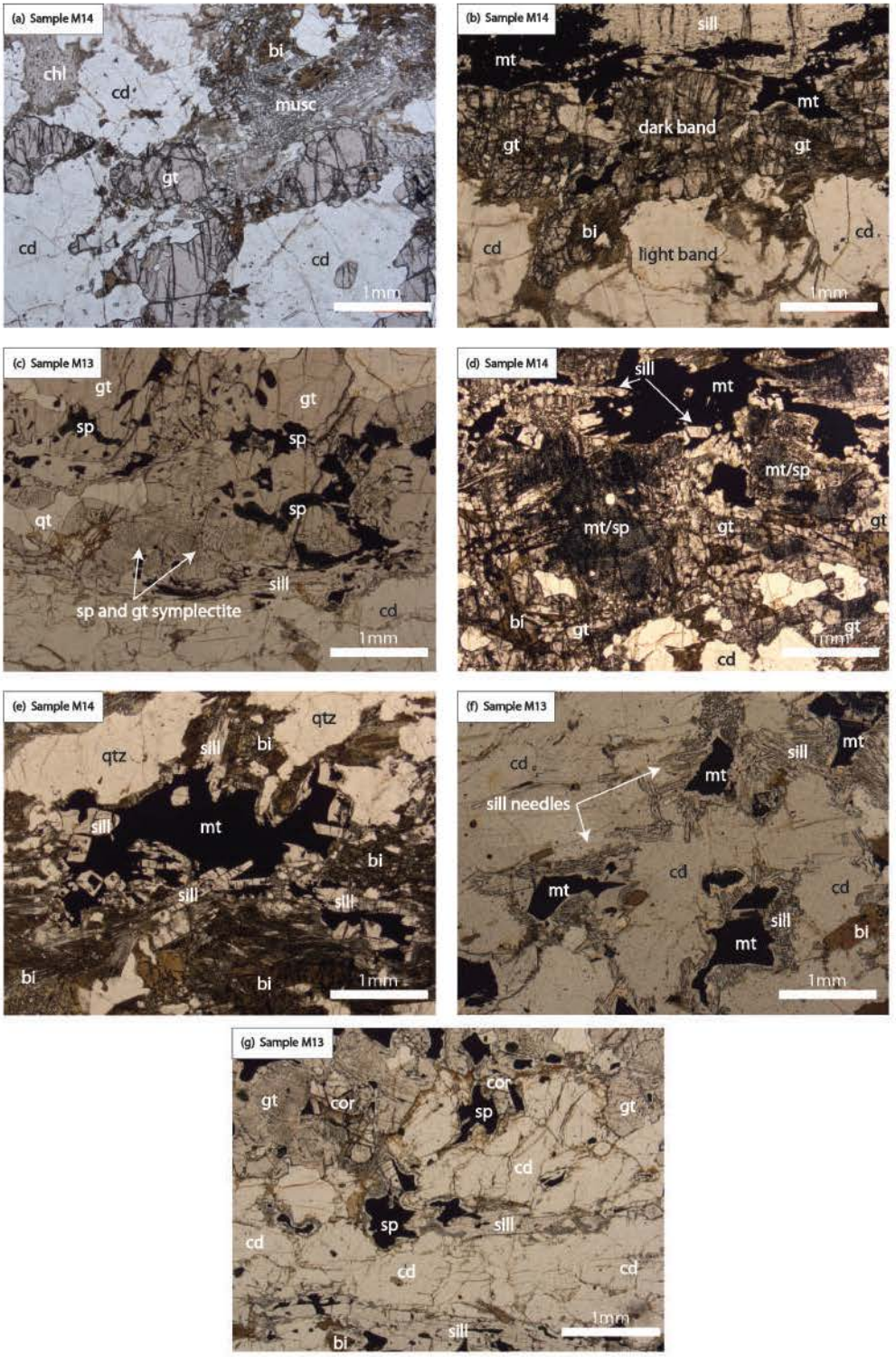

Figure 4.2: (a) Shows fabric, defined by alignment of sillimanite and biotite, which wraps around the garnet grains. (b) Gneissic texture defined by distinct light and dark bands. (c) garnet grains with symplectites of spinel. (d) Texture showing garnet almost completely replacing magnetite grains. (e) Biotite needles that appear to be replacing first generation sillimanite grains. (f) Fibrolite sillimanite forming along the edges of cordierite grains. (g) Sample M13 corundum grains occurring as inclusions of garnets and spinel.

Maganga Amphibolites (M16 and M17) and Schists (M18)

The sample M17 hornblende-amphibolite consists of approximately 80% hornblende, 10% plagioclase, 5% quartz, 5% magnetite and <1% titanite and rutile. In contrast to the granoblastic Chilumba amphibolites, these amphibolites shows a distinct fabric defined by the alignment of hornblende grains and the orientation of elongated quartz-plagioclase aggregates. The hornblende grains are generally <0.25 mm, while the oxides are <1mm (Fig. 4.3 (a)). Sample M16 mainly differs from M17 in that it is significantly finer-grained and contains a higher proportion of biotite (Fig. 4.3 (b)). As a result, its modal abundance for M16 is 85% hornblende, 10% plagioclase-quartz matrix, and 5% biotite. Overall, this hornblende-amphibolite differs to the previously described garnet-amphibolite in such that these amphibolites lack garnet, has a more well-defined fabric, and is finer-grained.

Found at the same location is the sample M18 metapelitic schist that consists of staurolite, kyanite, garnet, and biotite porphyroblasts set in a fine-grained matrix of muscovite, chlorite, plagioclase, and quartz (Fig. 4.3 (c)). Kyanite grains are approximately 8mm, staurolite grains range from 0.5-5 mm, garnet 0.5-2 mm, and biotite grains between 0.25-3 mm. The strong schistose fabric is defined by the alignment of the micas, muscovite and chlorite, and appear to wrap around the biotite porphyroblasts. However, the garnet, kyanite and staurolite clearly overprints the fabric (Fig. 4.3 (c), (d) and (f)). Additionally, the quartz matrix has a characteristic annealed texture (Fig. 4.3 (e)). The overall modal abundance is 50% muscovite, 20% quartz, 10% staurolite, 5% kyanite, 5% garnet, 5% chlorite, and 5% biotite.

Mangochi Charnockites (M21 and M22)

The charnockites consists of clinopyroxene (<1 cm), orthopyroxene (<0.5 mm), garnet (<1 cm), plagioclase (range from <0.5 mm to 3 cm), oxides (apatite, ilmenite and magnetite), quartz and small amounts of biotite, titanite and zircon. The overall texture is shown in Fig. 4.4 (a)). There is no obvious fabric present in the charnockites and they have a distinct granoblastic, coarse-grained, and equigranular texture. There is, however, a distinct perthitic exsolution feature observed in the feldspar grains where patches of alkali feldspar are found in the plagioclase and vice versa (Fig. 4.4 (b)). Modal abundances are roughly 35% plagioclase, 35% alkali feldspar, 15% pyroxene, 10% oxides (apatite, ilmenite, and magnetite), 5% garnet, and <1% of biotite. Samples M21 and M22 are extremely similar in texture and modal abundance.

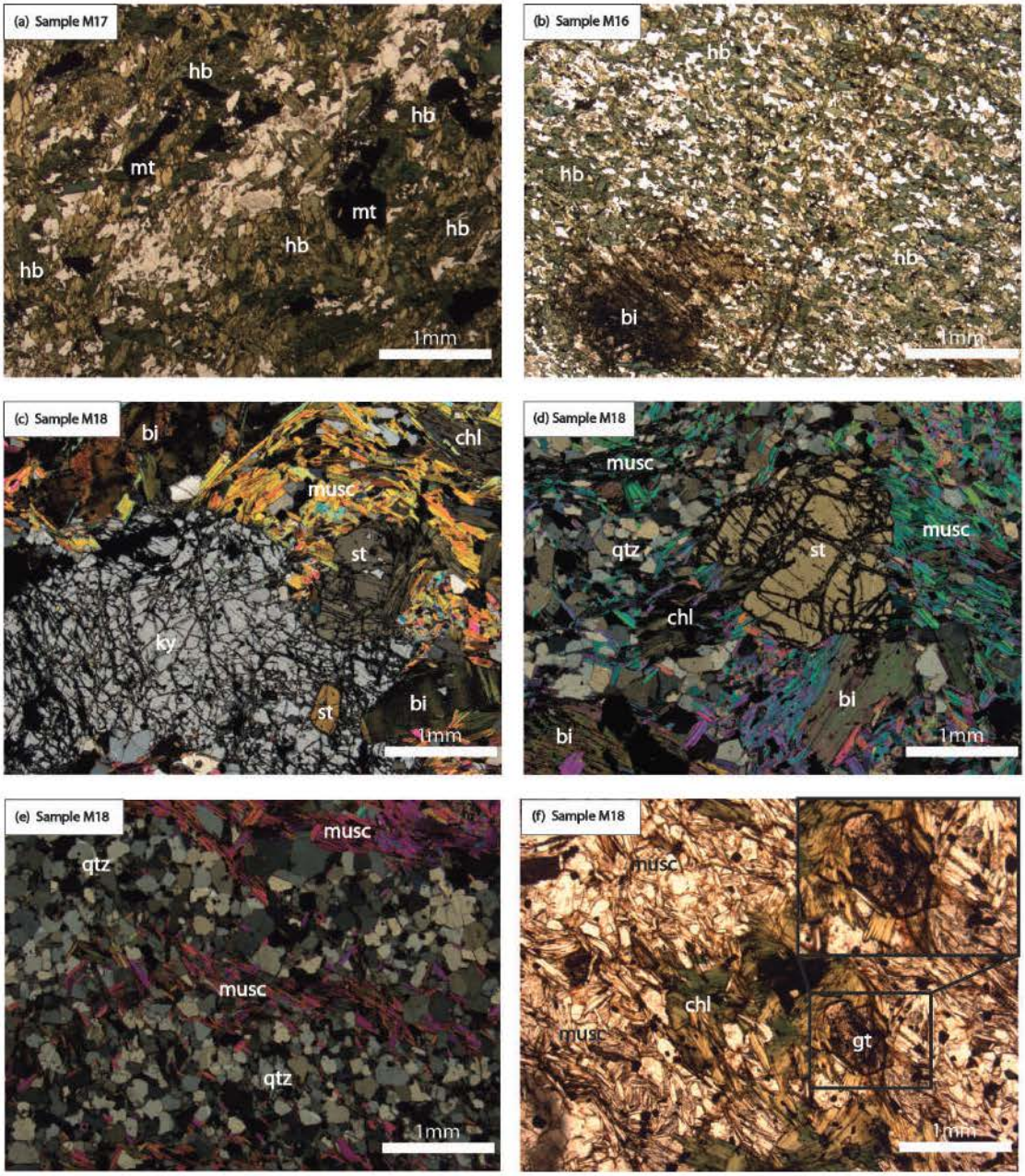

Figure 4.3: (a) Shows texture of sample M17 (taken in PPL). (b) Sample M16, which is characterised as being finer-grained and has likely experienced some alteration (taken in PPL). (c) M18 shows the presence of major minerals such as kyanite, staurolite and biotite as well as the fabric, defined by the alignment of muscovite and chlorite (taken in PPL). (d) Staurolite grain in M18 overprinting the fabric (taken in XPL). (e) Annealed quartz is predominant throughout sample M18 (taken in XPL). (f) Shows the fabric being overprinted by garnet (taken in PPL).

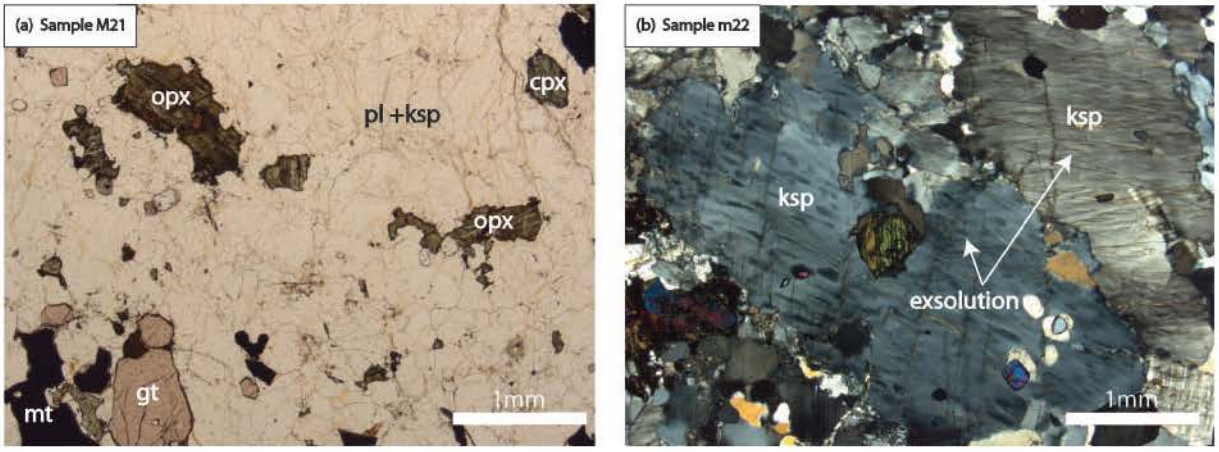

Figure 4.4: (a) Sample M21 showing the typical granoblastic texture of the Mangochi charnockites. (b) Sample M22 showing the distinct perthitic exsolution feature of feldspars.

4.2 Mineral Chemistry

Mineral compositions were acquired using the JEOL JXA-8100 Electron Probe Micro-Analyser at the University of Cape Town. Carbon-coated polished thin sections were analysed with an acceleration voltage of 15kV, a current of 20μA and a beam diameter of 3μm. Counting times for all elements were 5 seconds for backgrounds and 10 seconds per peak. Data were processed using the ZAF matrix corrections and reduced using the procedure of Pouchou and Pichoir. Analyses were quantified using natural standards, followed by stoichiometric re-calculations done on Excel. Summaries of the processed mineral chemistry for the samples are presented in Tables 4.1 to 4.4 below and in the appendix.

Chilumba Garnet Amphibolites (samples M07, M08, and M09)

Garnet: the garnets in sample M07 have almandine content (where Xalm = Fe/(Fe+Mn+Mg+Ca)) between 0.58 and 0.61, grossular content (where Xgrs = Ca/(Fe+Mn+Mg+Ca)) from 0.21 to 0.23, pyrope content (where Xgrs = Mg/(Fe+Mn+Mg+Ca)) between 0.11 and 0.15, and spessartine content (where Xsps = Mn/(Fe+Mn+Mg+Ca)) from 0.06 to 0.08 (Table 4.1). Garnets found in M08, however, show slightly lower Xalm of 0.53 to 0.56, marginally higher Xgrs of between 0.22 and 0.29, also slightly higher Xpyr of 0.16 to 0.18, and lower Xsps of 0.02 to 0.05 (Table 4.1). In M09, Xalm lies between 0.55 and 0.60, Xgrs from 0.23 to 0.26, Xpyr between 0.16 and 0.18, and Xsps consistently at 0.03 (Table 4.1). It seems that the garnet compositions from M08 and M09 are more similar than that of M07 and no zoning was observed.

Feldspar: as mentioned previously, feldspar in the Chilumba garnet-amphibolites occur in the matrix and as rims around garnets. The matrix feldspars occur as plagioclase with negligible orthoclase solid solution (Table 4.1). The matrix plagioclase in sample M07 has anorthite content, Xan (where Xan = Ca/(Ca+Na+K)), from 0.77 to 0.78 (Table 4.1). In sample M08, Xan is considerably lower, lying between 0.43 and 0.50 (Table 4.1). Compositions for M09 overlap with those of M08 Xan and ranges from 0.36 to 0.48 (Table 4.1). Although the plagioclase rims are textually unusual, they were not further examined in terms of the mineral chemistry.

Amphibole: amphiboles in the garnet-amphibolites occur as hornblendes. In sample M07, the XFe = 0.58-0.60 (where XFe = Fe/(Mg+Fe)). In samples M08 and M09, XFe is higher and ranges from 0.65 to 0.67 and 0.66 to 0.68, respectively (Table 4.1). Al content in sample M07 lies between 2.43 and 2.67 cations per formula unit (Table 4.1). The Al content for samples M08 and M09 are similar to that of M07 and are 2.51-2.59 and 2.44-2.60 cations per formula unit, respectively (Table 4.1). Na content for sample M07 ranges from 0.34 to 0.40 cations per formula unit while that of samples M08 and M09 are slightly higher with values 0.41-0.47 and 0.42-0.50 cations per formula unit, respectively (Table 4.1).

Mlowe Granulites (samples M13 and M14)

Garnet: as previously discussed in the Petrography, the Mlowe granulites contain two types of garnets: coarser grained garnet nodules and finer-grained garnets. Mineral composition analyses showed that there is no compositional variance between the two types of garnets. Additionally, the garnet compositions of M13 and M14 are fairly consistent, with little variation between and within the grains as well as between the two samples. In sample M13, the almandine composition (Xalm) lies between 0.71 and 0.72, grossular composition (Xgrs) from 0.02 to 0.03, pyrope composition (Xpyr) between 0.21 and 0.22, and spessartine composition (Xsps) from 0.04 to 0.05 (Table 4.2). Compositions in M14 are similar with Xalm between 0.70 and 0.71, Xgrs between 0.01 and 0.03, Xpyr between 0.22 and 0.23, and Xsps consistently at 0.05 (Table 4.2). Overall, garnet compositions appear to be consistent throughout the samples and no zoning was observed even in cm-sized porphyroblasts.

Feldspar: the granulites have both plagioclase and alkali feldspar present. Plagioclase in sample M13 occur as albite and have albite composition (Xab where Xab = Na/(Ca+Na+K))) between 0.98 and 0.99. Plagioclase in sample M14, however, has lower albite and higher anorthite com-

positions, with Xab between 0.73 and 0.78 and Xan from 0.21 to 0.27 (Table 4.2). The alkali feldspar in sample M13 occurs as orthoclase (K-feldspar) with Xab between 0.07 and 0.20. The alkali feldspar in sample M14 is fairly similar to that of M13, where Xab lies between 0.07 to 0.30 (Table 4.2). Overall, the plagioclase compositions between M13 and M14 are significantly different, while the alkali feldspar compositions are consistent between them.

Cordierite: cordierite in sample M13 has XFe between 0.37 and 0.41 while the cordierite in sample M14 has XFe ranging from 0.39 to 0.41 (Table 4.2). As a result, the cordierite compositions for the two samples are rather similar.

Sillimanite: Similarly to the Mlowe garnets discussed above, coarser-grained sillimanites as well as the fibrolite sillimanites in the rocks are compositionally the same. Sillimanite compositions are consistent between and within the two samples. Samples M13 and M14 sillimanites have similar Al contents ranging from 1.97 to 1.99 and 1.93 to 1.99 cations per formula unit, respectively (Table 4.2).

Biotite: biotite in sample M13 has XFe values between 0.59 and 0.62 while sample M14 has slightly lower XFe values from 0.50 to 0.55 (Table 4.2). K content for sample M13 lies between 0.91 and 0.96 cations per formula unit while that of M14 is slightly higher, ranging from 0.90 to 1.01 cations per formula unit (Table 4.2). Ti content for samples M13 and M14 are 0.13-0.17 and 0.08-0.15 cations per formula unit, respectively (Table 4.2). Al content for samples M13 and M14 are 1.52-1.58 and 1.49-1.65 cations per formula unit, respectively (Table 4.2).

Corundum: for both samples M13 and M14, the corundum has Al values of 1.99 cations per formula unit and Fe values of 0.01 cations per formula unit throughout the measured grains (Table 4.2). Given the extremely small amounts of Fe, the mineral occurs as pure corundum for both samples.

Spinel: in sample M13, the Al content ranges between 1.88 and 1.94 cations per formula unit (assuming four oxygens), Fe content lies between 0.76 and 0.80 cations per formula unit, Mg content from 0.29 to 0.31 cations per formula unit, and Zn content is consistently 0 throughout the grains (refer to appendix). In sample M14, the Al content is slightly higher and lies between 2.08 and 2.10 cations per formula unit (refer to appendix). Fe and Mg contents are lower and ranges from 0.63 to 0.67 and 0.17 to 0.18 cations per formula unit, respectively. Although sample

M13 has no Zn, sample M14 spinel has Zn ranging between 0.30 and 0.34 cations per formula unit (refer to appendix).

Table 4.1: Representative mineral compositions for Chilumba garnet amphibolites

	M07				M08			M09		
	gt	pl	hb	bi	gt	pl	hb	gt	pl	hb
SiO_2	37.35	52.77	43.82	37.60	38.19	56.53	41.47	38.61	58.75	41.33
TiO_2	0.06	0.02	0.82	1.57	0.13	0.02	1.71	0.10	0.01	1.68
Al_2O_3	21.96	30.43	14.22	17.07	21.92	28.37	14.44	21.80	26.32	14.81
Cr_2O_3	0	0	0.07	0.04	0.03	0.04	0	0.01	0	0.01
FeO	26.39	0.11	15.74	15.91	25.11	0.16	18.27	25.04	0.16	18.33
MnO	3.43	0.03	0.58	0.07	1.82	0.02	0.19	1.26	0.03	0.15
MgO	3.44	0	11.46	14.67	4.22	0	9.62	4.21	0.01	9.12
CaO	7.32	12.45	11.11	0.19	8.98	8.75	11.85	8.96	8.14	12.04
Na_2O	0	4.43	1.35	0.19	0	5.84	1.57	0.05	6.78	1.48
K_2O	0	0.03	0.50	8.04	0	0.21	1.42	0	0.23	1.24
Total	99.95	100.27	99.67	95.35	100.41	99.93	100.54	100.03	100.42	100.20
Oxygens	12	8	23	11	12	8	23	12	8	23
Si	2.96	2.38	6.36	2.78	2.98	2.53	6.12	3.01	2.62	6.11
Ti	0	0	0.09	0.09	0.01	0	0.19	0.01	0	0.19
Al	2.05	1.62	2.43	1.49	2.02	1.50	2.51	2	1.38	2.58
Cr	0	0	0.01	0	0	0	0	0	0	0
Fe	1.75	0	1.91	0.99	1.64	0.01	2.25	1.63	0.01	2.27
Mn	0.23	0	0.07	0	0.12	0	0.02	0.08	0	0.02
Mg	0.41	0	2.48	1.62	0.49	0	2.11	0.49	0	2.01
Ca	0.62	0.60	1.73	0.01	0.75	0.42	1.87	0.75	0.39	1.91
Na	0	0.39	0.38	0.03	0	0.51	0.45	0.01	0.59	0.42
K	0	0	0.09	0.76	0	0.01	0.27	0	0.01	0.23
Total	8.01	5	15.56	7.77	8	4.98	15.80	7.98	4.99	15.74

Table 4.2: Representative mineral compositions for Mlowe granulites

	M13								M14							
	gt	pl	ksp	cd	sill	bi	cor	sp	gt	pl	ksp	cd	sill	bi	cor	sp
SiO_2	37.47	68.91	65.34	49.88	37.71	36.78	0.01	0	37.79	61.91	64.91	49.58	37.12	37.53	0.03	0
TiO_2	0.02	0.02	0	0	0	2.70	0.06	0	0.06	0.05	0.02	0	0.05	2.13	0.01	0.02
Al_2O_3	22.07	19.69	18.78	33.58	61.96	17.97	101.87	57.27	22.05	24.61	18.67	33.58	61.67	17.64	101.76	58.50
Cr_2O_3	0	0	0	0.01	0.01	0.09	0.07	2.32	0	0.01	0.02	0	0.02	0.01	0.09	0.65
FeO	32.35	0.02	0.03	6.62	0.70	17.95	0.60	33.45	31.45	0.08	0.03	6.25	0.74	16.14	0.64	26.04
MnO	1.78	0.02	0.01	0.10	0.03	0	0.01	0.14	2.25	0.02	0	0.10	0.03	0.04	0.02	0.13
MgO	5.70	0	0	9.56	0.01	13.04	0	7.01	5.79	0	0	9.59	0.01	0	0.01	3.84
CaO	0.75	0.28	0	0	0.02	0	0	0	0.85	5.43	0	0.03	0.01	0	0	0
Na_2O	0.01	11	0.80	0.10	0.02	0.26	0	0	0.04	8.19	0.75	0.16	0	0.10	0.01	0
K_2O	0	0.05	15.58	0	0	10.19	0	0	0	0.09	15.90	0.02	0.01	10.92	0	0
NiO	0	0	0	0	0	0	0	0.34	0	0	0	0	0	0	0	0.13
ZnO	0	0	0	0	0	0	0	0	0	0	0	0	0	0	0	14.67
Total	100.14	99.99	100.53	99.86	100.46	98.97	102.63	100.53	100.28	100.39	100.30	99.31	99.65	98.76	102.58	103.98
oxygens	12	8	8	18	5	11	3	4	12	8	8	18	5	11	3	4
Si	2.96	3	2.99	5.01	1.02	2.68	0	0	2.97	2.73	2.99	5.00	1.01	2.73	0	0
Ti	0	0	0	0	0	0.15	0	0	0	0	0	0	0	0.12	0	0
Al	2.06	1.01	1.01	3.98	1.97	1.55	1.99	1.89	2.05	1.28	1.01	4.00	1.98	1.51	1.99	1.93
Cr	0	0	0	0	0	0	0	0.05	0	0	0	0	0	0	0	0.01
Fe	2.14	0	0	0.56	0.02	1.10	0.01	0.78	2.07	0	0	0.53	0.02	0.98	0.01	0.61
Mn	0.12	0	0	0.01	0	0	0	0	0.15	0	0	0.01	0	0	0	0
Mg	0.67	0	0	1.43	0	1.42	0	0.29	0.68	0	0	1.44	0	1.54	0	0.16
Ca	0.06	0.01	0	0	0	0	0	0	0.07	0.26	0	0	0	0	0	0
Na	0	0.93	0.07	0.02	0	0.04	0	0	0.01	0.70	0.07	0.03	0	0.01	0	0
K	0	0	0.91	0	0	0.95	0	0	0	0.01	0.93	0	0	1.01	0	0
Ni	0	0	0	0	0	0	0	0.01	0	0	0	0	0	0	0	0
Zn	0	0	0	0	0	0	0	0	0	0	0	0	0	0	0	0.30
Total	8.01	4.96	4.99	11.01	3.00	7.88	2	3.03	8	4.98	5	11.01	3.00	7.91	2	3.03

Maganga Amphibolites and Schists (samples M16, M17, and M18)

Feldspar: feldspar in samples M16 and M17 occurs as plagioclase with negligible orthoclase solid solution. In sample M16, the albite content (Xab) lies between 0.66 and 0.69 (Table 4.3). Similar compositions are found in sample M17 with Xab from 0.59 to 0.66 (Table 4.3). Feldspar in the schist (M18), however, occurs as more albite-rich plagioclase (or oligoclase) with higher Xab of 0.80 to 0.81 (Table 4.3).

Amphibole: the amphiboles in samples M16 and M17 occur as hornblende with XFe = 0.68-0.70 (Table 4.3). Overall, the XFe values are fairly consistent throughout the Maganga amphibolites. Na content for sample M16 ranges from 0.32 to 0.39 cations per formula unit while that of sample M17 is extremely similar and ranges from 0.32 to 0.36 cations per formula unit (Table 4.3). Al content for sample M16 lies between 2.33 and 2.52 cations per formula unit and that of sample M17 is slightly lower at 2.16-2.46 cations per formula unit (Table 4.3). There are no amphiboles in the schist M18.

Garnet: the garnet composition in sample M18 is fairly consistent and has little variation between grains. The almandine content (Xalm) lies between 0.62 and 0.63, grossular content (Xgrs) from 0.06 to 0.08, pyrope content (Xpyr) consistently at 0.11, and spessartine (Xsps) from 0.19 to 0.20 (Table 4.3). Zoning within the garnet grains was not observed. In other words, the composition is consistent within and between the garnet grains.

Phyllosilicates: the micas are exclusively found in the sample M18 schist and not in the M16 and M17 amphibolites. Chlorite in sample M18 has XFe ranging between 0.59 and 0.60 as well as Al(IV) from 1.97 to 2 cations per formula unit (Table 4.3). Chlorite compositions have little variation between grains. Biotite found in sample M18 has XFe ranging from 0.61 to 0.64 and K content between 0.69 and 0.91 cations per formula unit (Table 4.3). Ti content of the biotites lie between 0.07 and 0.09 cations per formula unit (Table 4.3). Muscovite in sample M18 has XFe values ranging from 0.75 to 0.84, while its K content lies between 0.79 and 0.84 cations per formula unit (Table 4.3). Na content of the muscovite is fairly consistent between the grains and ranges from 0.18 and 0.21 cations per formula unit (Table 4.3).

Staurolite: the staurolites are exclusively found in the M18 schist. The XFe values of staurolites range from 0.94 to 0.97 (Table 4.3).

Mangochi Charnockites (samples M21 and M22)

Garnet: the garnets in sample M21 have almandine composition (Xalm) consistently at 0.68, grossular composition (Xgrs) between 0.21 and 0.22, pyrope composition (Xpyr) at 0.02, and spessartine composition from 0.08 to 0.09. Similarly, sample M22 has Xalm consistently at 0.70, Xgrs consistently at 0.02, Xpyr consistently at 0, and Xsps consistently at 0.1. Zoning was not observed as the compositions throughout each individual grains and across the sample are consistent.

Feldspar: the charnockites contain both alkali feldspar and plagioclase that show exsolution features throughout. In sample M21, the plagioclase grains have an albite composition (Xab) from 0.73 to 0.75, anorthite composition (Xan) between 0.24 and 0.25, and orthoclase composition (Xor) from 0.01 to 0.02 (Table 4.4). The alkali feldspar exsolution in these plagioclase grains occur as orthoclase with Xab between 0.08 and 0.10 (Table 4.4). Alkali feldspars in M21 have Xab between 0.09 and 0.16 (Table 4.4). As a result, it appears the large alkali feldspar grains have slightly higher Xab than alkali feldspar exsolution found in plagioclase (Table 4.4). Subsequently, the plagioclase exsolution found in alkali feldspar grains have Xab from 0.74 and 0.76, Xan between 0.23 and 0.26, and Xor from 0 to 0.01 (Table 4.4). It appears the plagioclase exsolution has the same composition as the large plagioclase grains.

For sample M22, the plagioclase grains have Xab of 0.75, Xan consistently between 0.24 and 0.25, and Xor consistently at 0 to 0.01 (similar to that of plagioclase grains in M21) (Table 4.4). The alkali feldspar exsolution in the plagioclase grains occur as orthoclase, having Xab consistently at 0.1 (which is, again, similar to that of M21) (Table 4.4). Alkali feldspar grains occur as orthoclase as well, with Xab consistently at 0.1 (Table 4.4). These alkali feldspar grains have exsolutions of plagioclase that has Xab from 0.7 to 0.8, Xan consistently at 0.2, and Xor consistently at 0 (Table 4.4). Overall, compositions across the two samples are rather similar and exsolution compositions are consistent with that of the large grains.

Pyroxene: for sample M21, XFe values for ortho- and clinopyroxene range from 0.95 to 0.96 and 0.93 to 0.94, respectively (Table 4.4). The Al content for the orthopyroxene is low and lies between 0.01 and 0.02 cations per formula unit (Table 4.4). For the clinoproxene in sample M21, the jadeite content (Na/(Na+Ca)) ranges from 0.03 to 0.04 and its Al content lies between 0.04 and 0.05 cations per formula unit (Table 4.4). Consequently, the jadeite composition of the clinopyroxene is extremely low.

In sample M22, the XFe values for ortho- and clinopyroxene are slightly higher than that of M22 and are 0.96 and 0.93-0.96, respectively (Table 4.4). The Al content of orthopyroxene is similar to

that of sample M21 as it is 0.01-0.02 cations per formula unit (Table 4.4). Jadeite compositions for clinopyroxene in M22 is extremely similar to that of M21, where Na/Na+Ca sits between 0.00 and 0.03 (Table 4.4).

Table 4.3: Representative mineral compositions for Maganga amphibolites and schists

	M16			M17		M18						
	hb	pl	bi	hb	pl	gt	pl	st	ky	musc	chl	bi
SiO_2	41.98	60.19	36.20	43.05	58.80	37.37	64.65	27.94	37.03	45.83	25.44	36.87
TiO_2	0.64	0	1.62	0.59	0.01	0.04	0	0.51	0.01	0.72	0.02	1.53
Al_2O_3	14.11	24.47	17.09	13.18	26.75	37.37	64.65	27.94	37.03	45.83	25.44	36.87
Cr_2O_3	0.01	0	0.04	0.06	0	0.04	0	0.51	0.01	0.72	0.02	1.53
FeO	19.63	0.26	22.85	20.15	0.09	27.86	0.06	14.61	1.45	2.59	24.62	19.80
MnO	0.40	0.02	0.20	0.19	0.08	8.58	0.03	0.59	0.09	0.04	0.32	0.16
MgO	8.56	0	13.44	8.93	0.02	2.75	0.02	1.83	0.07	0.49	16.72	11.49
CaO	11.57	6.85	0.07	11.88	7.96	2.01	3.61	0	0.02	0.01	0	0
Na_2O	1.31	7.43	0.09	0.57	0.07	0.01	8.81	0.04	0	1.49	0.05	0.36
K_2O	0.55	0.06	7.49	0.57	0.07	0	0.04	0	0.01	9.63	0	9.67
Total	98.76	99.28	99.09	99.81	100.21	100.05	99.42	100.68	100.98	95.33	90.77	98.44
Oxygens	23	8	11	23	8	12	8	26	5	11	14	11
Si	6.29	2.70	2.67	6.39	2.61	3	2.86	4.28	1.00	3.07	2.57	2.72
Ti	0.07	0	0.09	0.07	0	0	0	0.06	0	0.04	0	0.08
Al	2.49	1.29	1.48	2.31	1.40	2.03	1.16	9.96	1.98	2.72	2.81	1.61
Cr	0	0	0	0.01	0	0	0	0	0	0	0	0
Fe	2.46	0.01	1.41	2.50	0	1.87	0	1.87	0.03	0.15	2.08	1.22
Mn	0.05	0	0.01	0.02	0	0.58	0	0.08	0	0	0.03	0.01
Mg	1.91	0	1.48	1.98	0	0.33	0	0.42	0	0.05	2.52	1.26
Ca	1.86	0.33	0.01	1.89	0.38	0.17	0.17	0	0	0	0	0
Na	0.38	0.65	0.01	0.35	0.56	0	0.75	0.01	0	0.19	0.01	0.05
K	0.11	0	0.70	0.11	0	0	0	0	0	0.82	0	0.91
Total	15.63	4.98	7.86	15.62	4.96	7.99	4.94	16.68	3.01	7.04	10.03	7.87

Table 4.4: Representative mineral compositions for Mangochi charnockites

	M21							M22						
	gt	pl	pl inclusions	ksp	ksp inclusions	opx	cpx	gt	pl	pl inclusions	ksp	ksp inclusions	opx	cpx
SiO_2	36.65	62.99	62.71	64.98	64.93	47.41	48.59	36.78	63.11	61.80	66.34	64.35	47.26	49.13
TiO_2	0.02	0.03	0.03	0.02	0.07	0.05	0.09	0.08	0	0	0.05	0.03	0.11	0.03
Al_2O_3	20.50	24.03	23.74	18.81	18.51	0.24	0.93	20.82	23.14	23.88	18.67	19.10	0.28	0.76
Cr_2O_3	0	0	0.01	0.02	0	0.02	0	0.03	0.03	0	0	0	0.02	0
FeO	30.88	0.09	0.08	0.05	0.06	46.56	29.92	31.21	0.10	0.05	0.03	0.04	47.67	27.97
MnO	3.93	0.05	0.02	0.01	0.03	2.26	1.98	3.45	0.04	0.06	0.04	0	1.94	1.15
MgO	0.49	0	0	0.01	0	0.93	17.16	0.29	0	0	0	0	1.85	1.88
CaO	7.61	4.88	5.14	0.01	0	0.93	17.16	7.68	4.76	4.79	0	0	0.90	19.33
Na_2O	0	8.15	8.21	0.99	0.94	0	0.33	0.01	8.34	8.33	1.18	1.00	0.05	0.28
K_2O	0	0.21	0.16	15.24	15.48	0	0.01	0	0.14	0.12	13.68	13.79	0	0
Total	100.09	100.43	100.09	100.13	100.07	99.76	100.25	100.35	99.67	99.03	99.99	98.32	100.07	100.53
oxygens	12	8	8	8	8	6	6	12	8	8	8	8	6	6
Si	2.98	2.77	2.77	2.99	2.99	2.02	1.99	2.97	2.80	2.76	3.02	2.99	2.02	1.99
Ti	0	0	0	0	0	0	0	0	0	0	0	0	0	0
Al	1.96	1.25	1.24	1.02	1.01	1.01	0.04	2.00	1.21	1.26	1.00	1.05	0.01	0.04
Cr	0	0	0	0	0	0	0	0	0	0	0	0	0	0
Fe	2.10	0	0	0	0	1.66	1.02	2.08	0	0	0	0	1.70	0.95
Mn	0.27	0	0	0	0	0.08	0.04	0.26	0	0	0	0	0.07	0.04
Mg	0.06	0	0	0	0	0.14	0.12	0.04	0	0	0	0	0.12	0.11
Ca	0.66	0.23	0.24	0	0	0.04	0.75	0.66	0.23	0.23	0	0	0.04	0.84
Na	0	0.70	0.70	0.09	0.08	0	0.03	0	0.72	0.72	0.10	0.09	0	0.02
K	0	0.01	0.01	0.89	0.91	0	0	0	0.01	0.01	0.79	0.82	0	0
Total	8.04	4.96	4.97	4.99	5	3.97	4	8.02	4.96	4.98	4.93	4.94	3.97	4.00

Chapter 5

Inferred Equilibrium Mineral Assemblages

This chapter aims to interpret the relationship between minerals (in particular, distinct metamorphic textures) for each rock type in order to infer the most likely equilibrium mineral assemblages. Determining the equilibrium mineral assemblage is required for determining metamorphic conditions and P-T paths from calculated pseudosections.

Chilumba garnet-amphibolites

The Chilumba garnet amphibolites have an unusual granoblastic texture that is quite different from what would be expected of a typical amphibolite such as that observed in the Maganga amphibolites. In all samples M07, M08, and M09, the plagioclase not only forms part of the fine-grained matrix, but also sometimes occurs as distinct rims, particularly (but not exclusively) surrounding garnet grains (Fig. 4.1 (a)). It is possible that the rock was always plagioclase bearing but formed new plagioclase from garnet breakdown which may or may not have formed as a response to decompression. Since the mineral chemistry of plagioclase rims were not examined further, its mineral composition cannot be compared with that of matrix plagioclase to confirm this hypothesis. Although the Xan of the matrix plagioclase is similar for samples M08 and M09, the elevated Xan of 0.77-0.78 in M07 is interpreted to not be an accurate representation since sample M07 has been heavily retrogressed. This is shown by the biotite mats throughout the rock which predominantly surround garnet grains and give a patchy texture in the rock which may be the result of post-peak metamorphic hydrothermal alteration since it replaces peak garnet and therefore was not part of the story at the peak P-T that this study is interested in. Taking into account the textures discussed above, it can be inferred that the peak mineral assemblage likely

consisted of garnet (with Xalm from 0.53 to 0.60), hornblende (with XFe from 0.60-0.68), quartz and matrix plagioclase (with Xan 0.40 to 0.50). A retrograde assemblage of garnet, hornblende, biotite, quartz and possibly decompression plagioclase formed after that.

Mlowe granulites

In general, cordierite, garnet and feldspar, and their grain boundaries, appear to be fairly well equilibrated (Fig. 4.2 (a)) as they do not form part of any distinct retrograde textures. Fig. 4.2 (f) shows coarser-grained, first generation sillimanite being overgrown by biotite and fine-grained, fibrolite second generation sillimanite. Compositionally, both first and second generation sillimanites are very similar, with Al content from 1.93-1.99 cations per formula unit. Texturally, however, they are distinctly different and most likely represent two distinct sillimanite growth events. Fine-grained, second generation sillimanite also forms replacement textures around cordierite, suggesting that the second sillimanite growth occurred subsequent to peak metamorphism (Fig. 4.2 (b)). These secondary sillimanites may have formed due to melt crystallisation during retrogression and hence does not form part of the peak assemblage. Similarly, the two generations of garnets share the same mineral composition but are texturally very different. The first generation garnet nodules are coarser-grained while second generation finer-grained garnets are characterised by distinct spinel and magnetite symplectites (Fig. 4.2 (c) and (d)) which are not seen in the garnet nodules. The second generation garnets appear to be consuming the spinel and magnetite from the rims of the grains, suggesting that they also formed after peak metamorphism (Fig. 4.2 (d)). A small but noticeable amount of corundum observed throughout the granulites is mostly isolated from the matrix and therefore likely not part of the equilibrium mineral assemblage. The origin of the corundum is undetermined but may occur as a pseudomorph of an earlier trapped inclusion or the result of some sort of exsolution. However, the latter in unlikely since they are large, well-formed grains. The biotite mats occur as a replacement texture of first generation sillimanite and most likely formed subsequent to peak metamorphism as well. Additionally, the distinct light and dark bands are likely leucosomes and melanosomes, respectively, which is a strong indication that melt formed part of the equilibrium mineral assemblage as well. It can then be inferred that the most likely equilibrium mineral assemblage for the Mlowe granulites then consists of first-generation garnet, first-generation sillimanite, cordierite, feldspar (alkali feldspar and plagioclase), spinel, quartz and magnetite and that this assemblage equilibrated in the presence of melt. A retrograde assemblage of second generation sillimanite, second generation garnet, cordierite, feldspar, spinel, biotite, quartz and magnetite formed subsequent to that.

Maganga amphibolites and schists

The observed mineral assemblage for sample M16 mainly includes hornblende, plagioclase, biotite, and quartz. These minerals appear to be mostly in equilibrium with each other with the exception of some biotite alteration textures which possibly formed due to hydrothermal alteration (Fig. 4.3 (b)). Sample M17, on the other hand, is coarser-grained than M16 and has the mineral assemblage hornblende, plagioclase, quartz, magnetite and accessory titanite and rutile. Mineral compositions for the two samples are quite similar, where feldspar Xab ranges from roughly 0.60-0.69 and hornblende XFe from 0.68-0.70 (as discussed in Mineral Chemistry). Although minerals in both M16 and M17 share similar compositions and are mostly in equilibrium, M17 does not contain alteration biotite and therefore more accurately represents the peak mineral assemblage. As a result, the equilibrium mineral assemblage includes hornblende, plagioclase and quartz (Fig. 4.3 (a)). Biotite was then introduced after peak metamorphism and formed part of the retrograde assemblage.

The schist (sample M18) is significantly different to the amphibolites in terms of both mineral assemblage and textures. The annealed texture of the quartz matrix shown in Fig. 4.3 (e) strongly suggests that the rock remained at reasonably high temperatures (likely at igneous conditions) where the quartz matrix was re-cyrstallised. However, it is unknown to what extent the rock actually recrystallised and re-equilibrated in terms of its mineral assemblage as well as textures. Despite this, the minerals do appear to be in equilibrium in the presence of each other, particularly kyanite, staurolite and garnet. The alignment of muscovite and chlorite define a strong schistose fabric that appears to wrap around the biotite grains (figure 3.3 (c)) while garnet, kyanite and staurolite truncate and overprint the fabric (Fig. 4.3 (c), (d) and (f)). Given the relationship between the abovementioned minerals and the fabric, it appears as though the biotite is pre- to syn-kinematic while garnet, kyanite and staurolite are post kinematic. Overall, equilibrium mineral assemblage likely consists of kyanite, staurolite, garnet, muscovite, chlorite, plagioclase, quartz and biotite.

Mangochi charnockites

The charnockites have a characteristic granoblastic, coarse-grained and equigranular texture which is likely due to exposure to relatively high temperatures. An interesting texture found in both samples M21 and M22, is represented by the exsolution features in feldspars, where alkali feldspars have plagioclase exsolution and vice versa. Alkali feldspar grains have higher Xab than alkali feldspar exsolution found in plagioclase (Xab of 0.09-0.16 for large alkali feldspar

grains compared to 0.08-0.10 for alkali feldspar exsolution) while plagioclase grains share the same composition as plagioclase exsolution in alkali feldspar (with Xab from 0.73 to 0.76). Feldspar compositions for the two samples are also fairly similar. The exsolution texture is strongly suggestive of the initial assemblage containing ternary feldspar at high temperatures (likely at igneous conditions). After cooling and/or decompression, the ternary feldspar likely then separated into respective plagioclase and alkali feldspar components. Given that the rock possesses an igneous-like granoblastic texture and that it was likely formed under igneous conditions, these granulites probably melted at some point. As a result, the likely equilibrium mineral assemblage includes clinopyroxene, orthopyroxene, garnet, alkali feldspar, plagioclase, melt, magnetite, quartz and biotite.

Chapter 6

Mineral Equilibria Modelling

P-T conditions for the relevant samples were determined through pseudosection calculations using THERMOCALC (version 3.37; Powell & Holland (1988)). Pseudosections were produced using the model system MnO-Na_2O-CaO-FeO-MgO-Al_2O_3-SiO_2-H_2O-TiO_2-Fe_2O_3 (MnNCKFMASHTO) for metapelites and Na_2O-CaO-FeO-MgO-Al_2O_3-SiO_2-H_2O-TiO_2-Fe_2O_3 (NCFMASHTO) for mafic rocks. Mineral phases included in the metapelites modelling were garnet, plagioclase-K-feldspar, biotite, orthopyroxene, cordierite, sillimanite, muscovite-paragonite, spinel-magnetite, ilmenite-hematite, and liquid. The activity-composition relations are taken from White *et al.* (2014), quartz and aqueous fluid (H_2O) are pure end-member phases, and the presence of quartz and ilmenite was assumed in these samples. The pressure and temperature ranges for which pseudosections were calculated are 2-18kbar and 500-880°C. Mineral phases included in the mafic modelling were garnet, plagioclase-K-feldspar, chlorite, rutile, titanite, spinel-magnetite, orthopyroxene, liquid, quartz, H_2O (all taken from White *et al.* (2014)), clinopyroxene and amphibole (taken from Green *et al.* (2016)). Quartz and aqueous fluid (H_2O) are pure end-member phases and their presence was assumed in all the mafic samples. The pressure and temperature ranges for which the mafic pseudosections were calculated are 2-13kb and 540-900°C.

Bulk rock compositions of the samples were acquired using X-ray Fluorescence analysis with a Philips X'Unique II wavelength-dispersive spectrometer housed at the University of Cape Town. A summary of the XRF data for the samples are presented in Tables 6.1 and 6.2. This data was then recalculated for input into THERMOCALC by disregarding negligible amounts of P_2O_5, SO_3, Cr_2O_3, and converting 10% and 15% of total Fe to Fe^{3+} for metapelites and mafics, respectively. Subsequent to removing the negligible amounts of P_2O_5, a correction for CaO was made by subtracting the P from Ca and multiplying it by the Ca:P ratio of 3.3. H_2O content was assumed for all granulite samples (i.e. the Mlowe granulite and Mangochi charnockites) based on the fact

that these are residual rocks that have lost melt and are therefore not fluid-saturated. The H_2O content was then chosen such that the inferred peak assemblages were

	M-08	M-09	M-13	M-14	M-16	M-17	M-18	M-21	M-22
SiO_2	43.61	47.04	45.31	64.03	49.46	48.94	59.91	59.42	59.44
TiO_2	3.01	2.89	1.79	0.96	2.97	2.72	0.63	0.59	0.53
Al_2O_3	13.87	13.64	30.33	17.56	12.60	12.20	19.88	17.32	17.28
Fe_2O_3	19.24	18.36	15.55	8.88	15.72	16.61	7.43	7.72	7.31
MnO	0.28	0.28	0.22	0.21	0.25	0.22	0.13	0.20	0.17
MgO	6.66	5.85	5.30	2.35	5.59	5.27	2.11	0.19	0.17
CaO	9.34	9.00	0.05	0.47	9.18	9.57	0.44	3.38	3.20
Na_2O	1.21	1.32	0.24	0.76	1.93	1.92	1.46	4.24	4.13
K_2O	1.19	0.97	0.88	3.57	0.84	0.43	4.36	5.53	5.94
P_2O_5	0.28	0.27	0.02	0.05	0.30	0.31	0.11	0.15	0.14
SO_3	0.01	0.01	0.00	0.00	0.00	0.01	0.00	0.00	0.00
Cr_2O_3	0.01	0.01	0.06	0.03	0.01	0.01	0.02	0.00	0.00
NiO	0.01	0.01	0.03	0.01	0.01	0.01	0.01	0.01	0.01
H_2O-	0.23	0.15	0.13	0.10	0.21	0.14	0.28	0.15	0.18
LOl	0.92	0.40	0.34	0.49	0.66	0.30	2.82	0.07	0.16
Sum	99.89	100.21	100.24	99.47	99.74	99.66	99.59	98.98	98.67

Table 6.1: Whole-rock XRF results of the relevant samples used for pseudosection calculations (in wt%).

stable immediately above the residuum solidus (White & Powell, 2002). Consequently, the H_2O content for Mlowe granulites were assumed to be 3.5%, while that of the Mangochi charnockites were assumed to be 0.2%.

For the Mlowe granulites, it was previously discussed that although a small but noticeable amount of corundum is present in sample M13, it is isolated from the matrix and, therefore, does not constitute as part of the bulk rock composition. As a result, some Al was removed from the bulk composition of samples M13 and M14 for modelling purposes, as a means of disregarding the corundum as part of the peak assemblage and bulk rock composition. More specifically, the Al content for sample M13 was reduced from 21% to 18%. Since the amount of corundum in sample

	M-08	M-09	M-13	M-14	M-16	M-17	M-18	M-21	M-22
SiO_2	48.32	51.59	53.22	72.02	54.16	53.53	70.10	68.00	68.36
TiO_2	2.51	2.38	1.58	0.81	2.45	3.06	0.56	0.51	0.46
Al_2O_3	9.06	8.82	21.00	11.64	8.13	7.87	13.71	11.68	11.71
Fe_2O_3	16.04	15.15	13.74	7.51	12.96	13.68	6.54	6.65	6.33
MnO	0.27	0.26	0.22	0.20	0.23	0.21	0.13	0.19	0.17
MgO	11.00	9.57	9.28	3.93	9.12	8.59	3.68	0.33	0.29
CaO	10.66	10.15	0.04	0.49	10.31	10.74	0.37	3.90	3.72
Na_2O	1.30	1.40	0.27	0.83	2.05	2.03	1.66	4.70	4.61
K_2O	0.84	0.68	0.66	2.56	0.59	0.30	3.25	4.04	4.36
O	1.20	0.00	0.00	0.00	0.00	1.00	0.30	0.40	0.40

Table 6.2: Bulk rock composition for the relevant samples used in the pseudosection modelling (in mol%).

M14 is close to none, and therefore negligible, no adjustments were made to its Al content. Spinel in the Mlowe granulites are characterised by Ni and Zn content (where Zn content is only found in sample M14 spinels). However, since THERMOCALC modelling does not accommodate for Ni and Zn content in spinel calculations, the stability of the spinel modelled by THERMOCALC and shown on the pseudosections below was not taken at face value. For the Chilumba and Maganga amphibolites, it is worth noting that although small amounts of magnetite are observed in thin section, it is not calculated to be part of the equilibrium assemblage. Calculated pseudosections are presented in Fig. 6.1 to Fig. 6.4.

Chilumba Garnet-Amphibolites (M08 and M09)

The overall topologies of the M08 and M09 pseudosections are quite similar (Fig. 6.1). At temperatures below 570-580°C, phase boundaries are steep, suggesting that reactions are generally sensitive to temperature in this range. From 450°C, as temperature increases, glaucophane is consumed, hornblende becomes stable, and actinolite and albite are consumed. Between approximately 500°C and 580°C, epidote, titanite and chlorite are consumed, while garnet and rutile become stable. From this point, the phase boundaries are less steep as they become slightly more pressure-sensitive. From 590°C, plagioclase becomes stable and allows for the stabilisation of hornblende, rutile, garnet, and plagioclase which is the observed mineral assemblage in M08 and M09. Thereafter, diopside becomes stable at high temperatures (from 680°C) and pressures (above 8 kbar).

The observed mineral assemblage in samples M08 and M09 is hornblende, rutile, garnet, and plagioclase. According to the calculated psuedosections, the stability field for this assemblage is anywhere above 635°C and 4.8 kbar, for sample M08, or anywhere above 650°C and 5 kbar, for sample M09. Given the large P-T range, the stability fields for both M08 and M09 were contoured based on grossular content (Xgrs) of garnets in percentages, where the calculated isopleths would be able to further narrow the P-T fields. The measured Xgrs of garnets in sample M08 and M09 was averaged to be roughly 25% (based on Xgrs discussed in the Mineral Chemistry and shown in Table 4.1) and therefore suggests P-T conditions of ≥635°C at 4.8-5.5 kbar and ≥650°C at 5-5.5 kbar, for samples M08 and M09, respectively (red shaded area in Fig. 6.1). Both calculated pseudosections appear to be in close agreement as they show extremely similar pressure and temperature conditions. Essentially, the observed mineral assemblage places the stability field at low-medium pressure and medium-high temperature amphibolite facies conditions.

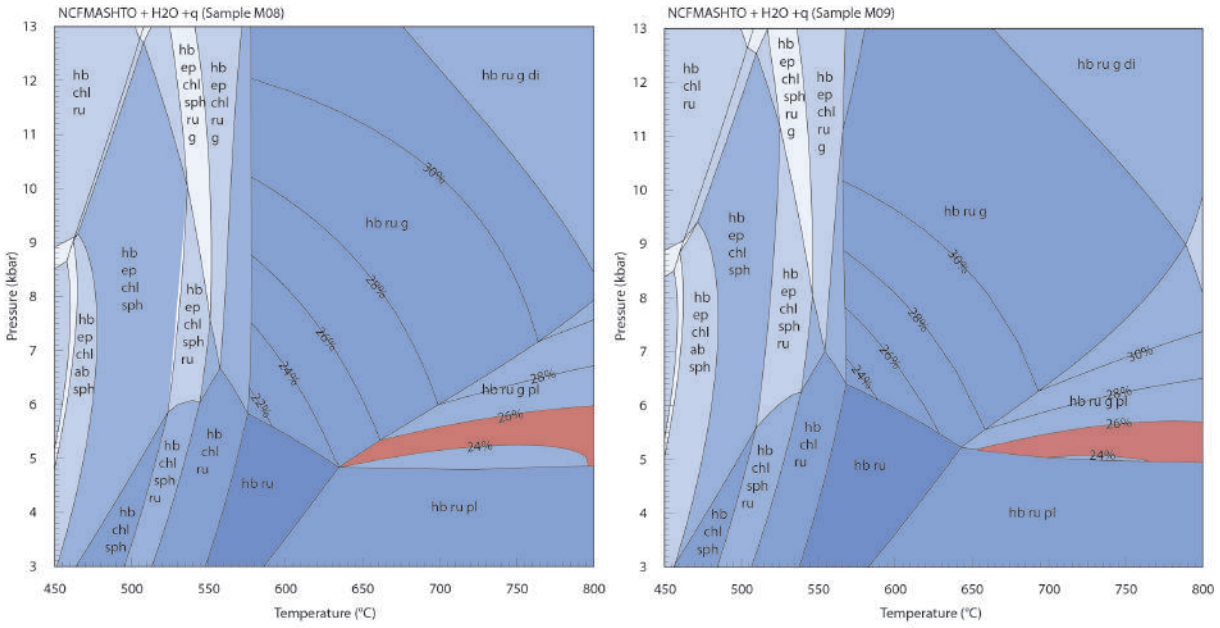

Figure 6.1: Pseudosection of samples M08 and M09, with assemblage fields contoured according to Xgrs in percentages. Narrowed stability fields are shaded in red.

Mlowe Granulites (M13 and M14)

Although the topologies of samples M13 and M14 are quite different, they are both characterised as fairly complex pseudosections that involve a large number of minerals and low-variance assemblage fields. For sample M13, at low pressures (≤4 kbar) and high temperatures (≥800°C),

orthopyroxene becomes stable, quickly followed by the consumption of garnet, quartz, spinel, and K-feldspar. Between 2.4 kbar and 5 kbar, sillimanite and magnetite become stable (in order of increasing pressure). At pressures above 5 kbar, the rock melts anywhere below roughly 750°C while at pressures below 5 kbar, the rock melts between 750°C and 820°C. As pressures increase from approximately 4 kbar to 6.5 kbar, plagioclase becomes stable below 770°C and K-feldspar is consumed above 770°C. Both the plagioclase and K-feldspar phase boundaries intersect at roughly 770°C, which allows for extremely narrow fields where these two feldspars co-exist. As a result, the stability field for the observed mineral assemblage lies in the ranges 760-780°C at 5-5.8 kbar. However, given the presence of melt in the granulites, the peak P-T conditions would then lie along the solidus, resulting in an even more precise P-T condition of 760°C at 5kb as indicated in the red circle in Fig. 6.2.

For M14, the pseudosection shares similar topologies with that of M13 at temperatures above ±700°C and pressures below ±6 kbar (figure 6.2). However, at lower temperatures, this pseudosection is defined by larger stability fields and more pressure-sensitive phase boundaries. With increasing pressure (between 650°C and 700°C), sillimanite becomes stable, followed by the consumption of magnetite and cordierite. With increasing temperature, the rock reaches the solidus and melts between 760°C and 810°C, and thereafter follows a similar trend to that of sample M13. There is an extremely small field which allows for the co-existence of magnetite, liquid (melt), and biotite. Additionally, the presence of melt suggests that peak P-T conditions also lies along the solidus, providing a precise P-T condition of 760°C at 4.5 kbar (as indicated in the red circle in Fig. 6.2). Given the observed mineral assemblage in M13 and M14 is garnet, plagioclase, alkali-feldspar, biotite, cordierite, sillimanite, magnetite, and melt (shown in Figure 6.2 in the circled areas), it appears the two samples suggest the same temperature and similar pressure conditions. Overall, this associated P-T condition indicates low-pressure granulite facies conditions.

Maganga Amphibolites (M17) and Schists (M18)

At low temperatures, the topology of the M17 pseudosection resembles that of the Chilumba garnet-amphibolites. At temperatures below approximately 550°C, the phase boundaries are fairly steep and, hence, are generally more temperature sensitive. From 450°C to 550°C, garnet and hornblende become stable, while glaucophane, actinolite, and epidote are consumed. At conditions below 9.5 kbar and 570°C, albite is consumed as well. At temperatures higher than 550°C, reaction lines are less steep and stability fields are larger in general. Between 520°C and 720°C,

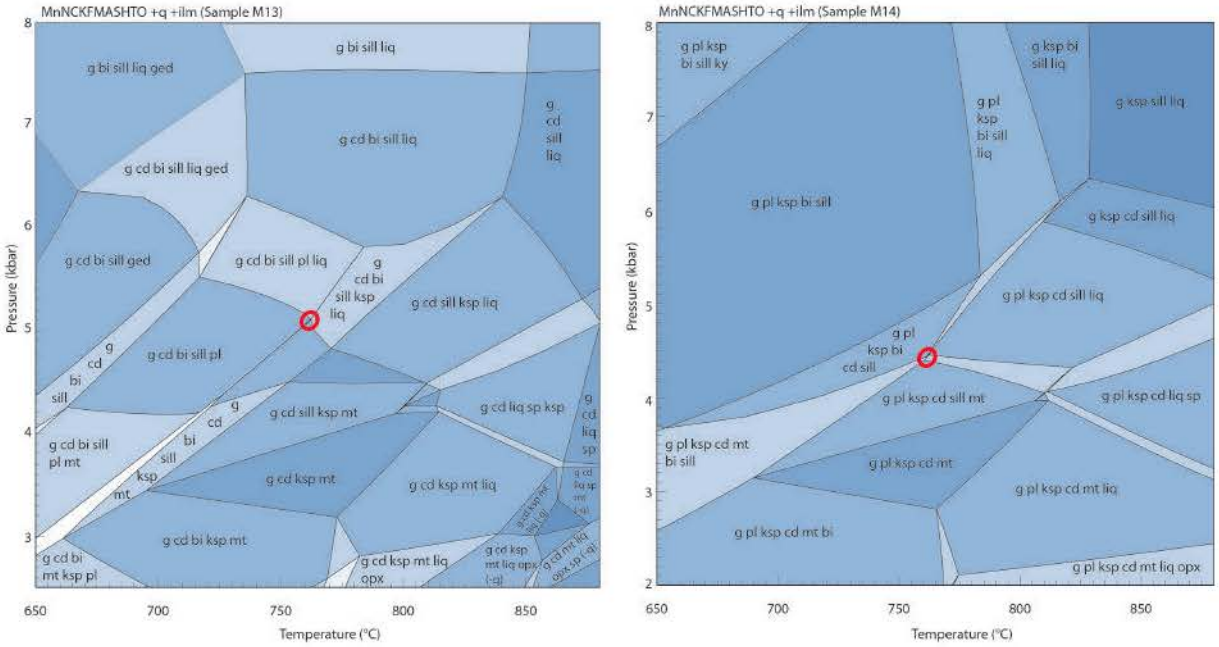

Figure 6.2: Pseudosection of sample M13 and M14 with their respective stability fields indicated by red circles.

plagioclase becomes stable (at low temperatures, plagioclase stabilises at low pressures and at high temperatures, plagioclase stabilises at high pressures). At higher pressures (approximately $\geq$8 kbar), diopside becomes stable and, with a slight increase in pressure, titanite is consumed. The observed mineral assemblage lies in the large hornblende-titanite-rutile-plagioclase stability field, which allows for the presence of plagioclase and absence of garnet and albite. According to the calculated pseudosection, this field is anywhere above 530°C and up to 8.5 kbar.

Given the large stability field (and wide P-T range) in which the assemblage lies, the field was contoured for Xan of plagioclase, which was determined to be roughly between 30% and 45% based on M17 plagioclase mineral chemistry (Table 4.3). Subsequently, the stability field was narrowed slightly to conditions of 525-750°C and anywhere below 8.5 kbar, as indicated in the shaded area shown in Fig. 6.3. The overall medium-high temperature at low-medium pressures suggest amphibolite facies conditions.

The topology of sample M18 pseudosection differs significantly to that of M17, as it is defined and dominated by relatively steep phase boundaries. At temperatures below 550°C (depending on pressure), garnet becomes stable and is followed by the consumption of epidote. Between 550°C and 660°C, and in order of increasing temperature, biotite, staurolite, and kyanite become stable while chlorite is consumed soon after. However, staurolite becomes consumed fairly quickly

after its stabilisation, resulting in narrow fields which allow for the co-existence of kyanite and staurolite. The rock then starts to melt (stabilise liquid) between 660°C and 700°C. Thereafter, in order of increasing temperatures, H_2O is consumed, followed by the consumption of plagioclase, paragonite, and muscovite. Above 650°C, biotite is consumed anywhere higher than 16 kbar. Kyanite is generally stable throughout the pseudosection, except under temperatures below 660°C and less than 14 kbar. The observed mineral assemblage for sample M18 is kyanite, staurolite, garnet, plagioclse, muscovite, chlorite, biotite and ilmenite. However, the calculated pseudosection does not show any field where all the abovementioned minerals co-exist. It has been established in the Inferred Equilibrium Mineral Assemblage chapter that kyanite, staurolite, and garnet appear to be the most stable and well-equilbrated minerals in the schist. Given that the extremely narrow fields which allow for the co-existence of kyanite, staurolite, and garnet, there are ultimately two most likely stability fields for the schist which do not require the rock to melt. The first possible stability field is shown as Assemblage A in Fig. 6.3 and does not include plagioclase as part of the equilibrium mineral assemblage. This extremely small field suggests a relatively precise P-T condition of 650°C at 15 kbar (Fig. 6.3). The second possible stability field is shown as Assemblage B in Fig. 6.3 and does not include chlorite as part of the equilibrium mineral assemblage. This field is also relatively small and suggests a narrow P-T range of 660-670°C at 6-8 kbar. P-T conditions associated with Assemblage B (Fig. 6.3) are more consistent with conditions recorded in the M17 amphibolites. Although both possible stability fields share similar temperature conditions ranging from 650-670°C, the suggested pressure conditions differ by roughly 7-9 kbar, which is quite a significant amount. Overall, the suggested P-T conditions of M18 observed mineral assemblage are either very high pressure amphibolite facies conditions or low-medium pressure amphibolite facies conditions.

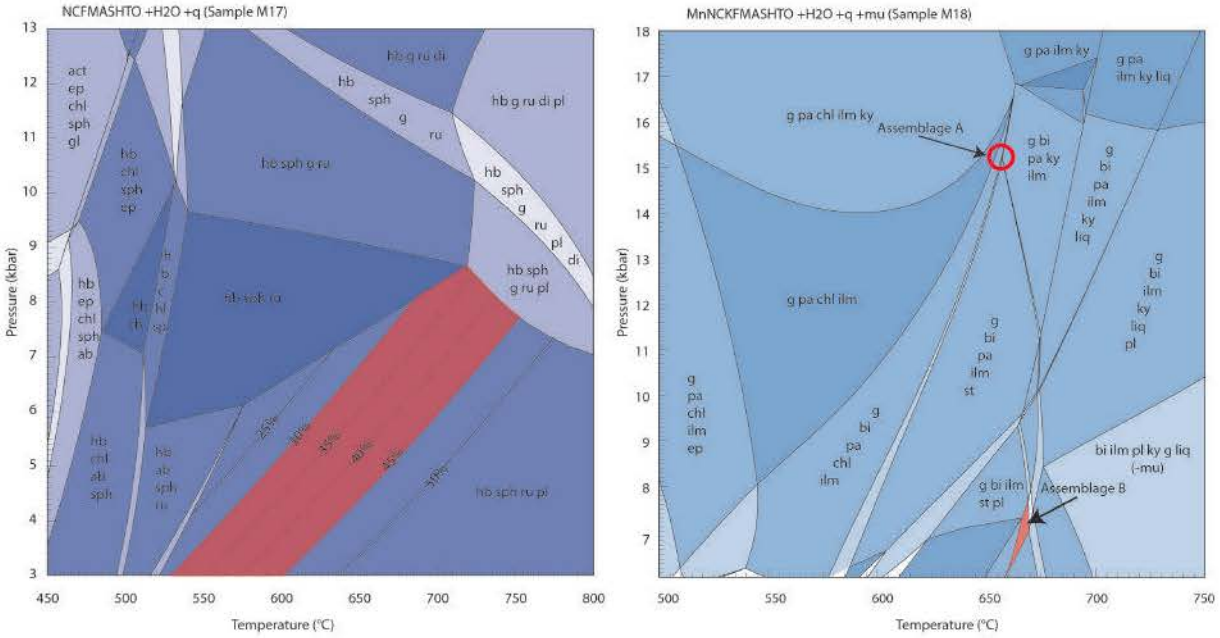

Figure 6.3: Pseudosections of samples M17 and M18. For sample M17, the assemblage field was contoured according to Xan (expressed in percentages). The narrowed stability field is shaded in red. For sample M18, two possible stability fields are shown as Assemblages A and B.

Mangochi Charnockites (M21 and M22)

The topologies of samples M21 and M22 are near identical and, hence, show the same temperature conditions for the observed mineral assemblage. Overall, the pseudosections appear to be dominated by relatively flat, pressure-sensitive phase boundaries. With increasing pressure, garnet becomes stable from 3-5 kbar, magnetite is consumed at 5-6 kbar, and orthopyroxene is consumed at 5.6-7.5 kbar. With increasing temperature, the rock melts and liquid/melt is introduced between 740-800°C at 2-10 kbar. Immediately after the stability of melt, biotite is consumed. The inferred equilibrium mineral assemblages for M21 and M22 is garnet, orthopyroxene, diopside, plagioclase, alkali-feldspar, biotite, magnetite, and melt (liquid) which falls in a small field that allows for the co-existence of magnetite, garnet, melt, and biotite shown in Fig. 6.4. The presumed presence of melt as part of the assemblage was discussed in the previous chapter. This places the assemblage in a small range of 770-780°C at 4.2-6 kbar for both samples M21 and M22. This field lies at low pressure and high temperature conditions, characteristic of granulite facies conditions.

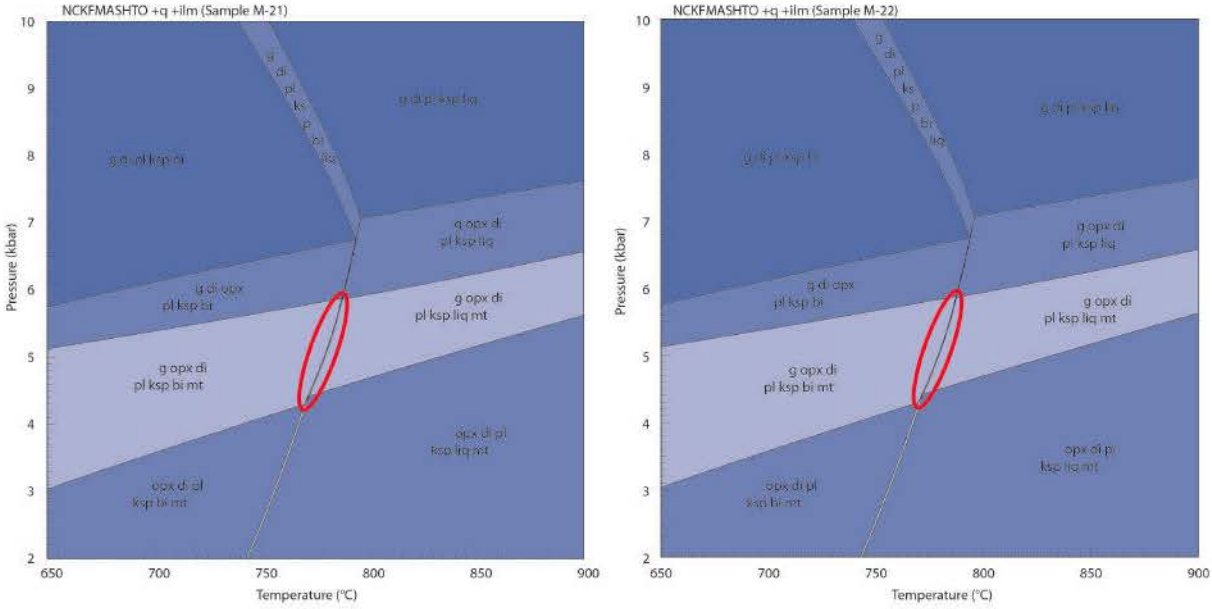

Figure 6.4: Pseudosections of samples M21 and M22 with stability fields (according to the observed mineral assemblage) indicated within the red circle.

Chapter 7

U-Pb Geochronology

Monazite is consumed during the production of melt and, consequently, formed by melt crystallisation in suprasolidus aluminous metapelites (Kelsey *et al.*, 2008; Spear & Pyle, 2010). As a result, monazite ages yielded by U-Pb analyses reflects that of T peak metamorphism and rarely preserves ages of older events (Kelsey *et al.*, 2008; Spear & Pyle, 2010). Although inheritance is less common in the case of monazites, it is not the case with regards to zircons, as they are commonly preserved as older, inherited zircons in the residuum or melt (Kelsey *et al.*, 2008). Titanite, on the other hand, is generally found in mafic rocks and is stable to its highest temperatures (up to granulite facies conditions). Due to the fact that titanite reacts readily during metamorphism, ages yielded by U-Pb analyses are more likely to represent that of metamorphic crystallisation and unlikely to be reset by diffusion (Frost *et al.*, 2000).

A total of five samples (M08, M09, M14, M17, and M22) were selected for in situ U-Pb analysis of titanite, monazite, and/or zircon using the laser ablation mass spectrometer (LA-SF-ICP-MS) housed at the University of Stellenbosch, South Africa. The Chilumba garnet-amphibolites (samples M08 and M09) and Maganga amphibolite (sample M17) were dated using in-situ titanite grains. The Mlowe granulite (sample M14) was analysed using monazite grains and the Mangochi charnockite (sample M22) was dated using zircon grains.

Methodology

All five samples were prepared as polished thick sections (80-100 μm) and were analysed under the petrographic microscope to locate titanite, monazite, and zircon grains. Thereafter, these grains were characterised using the electron microprobe (EMP) for both mineral composition and BSE imaging (see Fig. 7.1). All U-Pb isotope analyses used to determine sample ages were

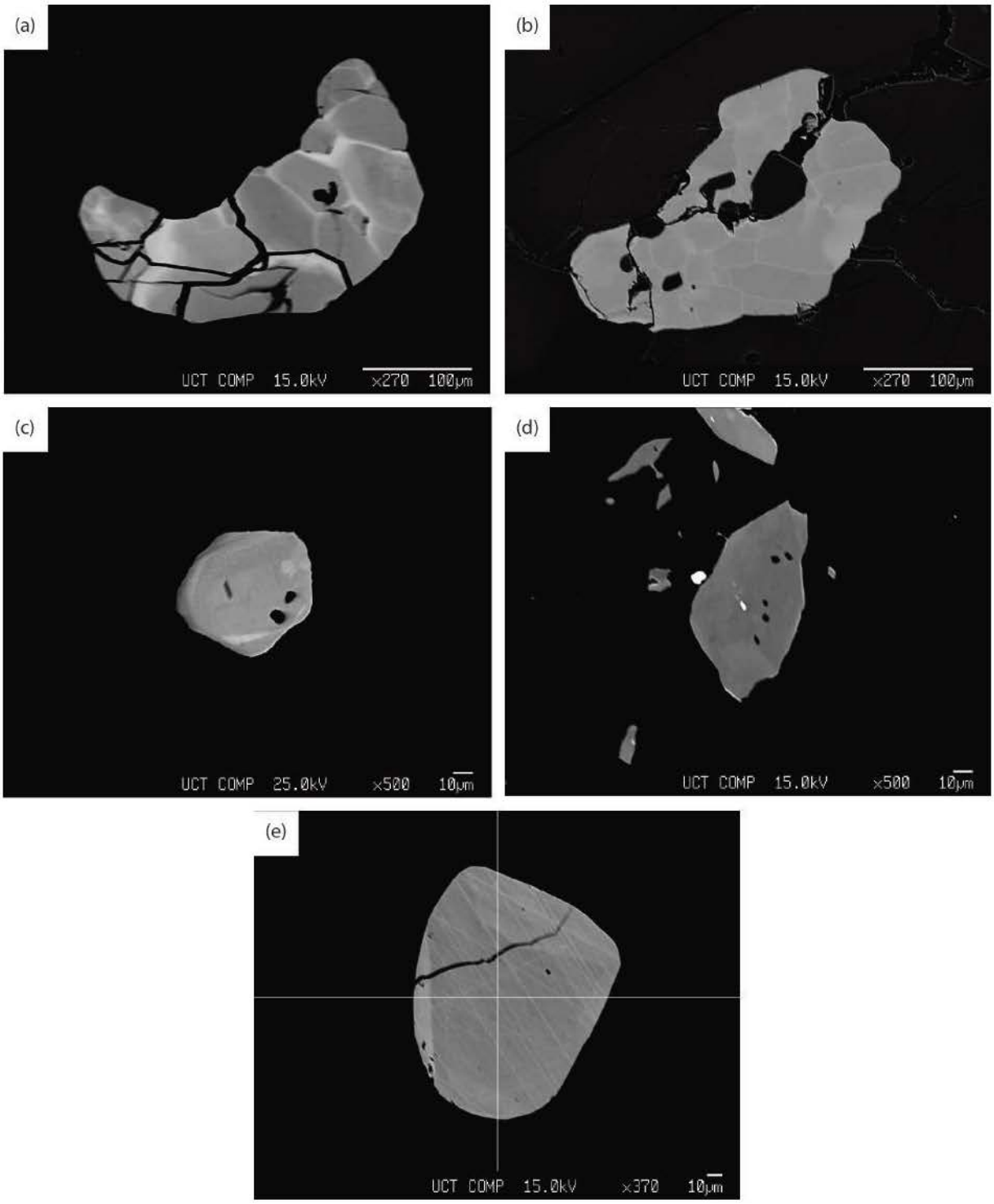

Figure 7.1: Back-scattered electron (BSE) images of titanite, monazite, and zircon grains used for U-Pb isotopic analyses. (a) and (b) show typical titanite grains analysed in samples M08 and M09 of the mafic Chilumba garnet amphibolites; (c) shows a representative monazite grain analysed from sample M14 of the pelitic Mlowe granulites with distinct concentric zoning; (d) shows one of the titanite grains analysed from sample M17 of the Maganga amphibolites; (e) subrounded zircon grain in sample M22 of the Mangochi charnockites.

obtained at the Central Analytical Facility, Stellenbosch University and acquired by the laser ablation - single collector - magnetic sectorfield - inductively coupled plasma - mass spectometry (LA-SF-ICP-MS), employing a Thermo Finnigan Element2 mass spectometer coupled to an ASI Resolution SE50 excimer laser ablation system.

In total, 107 spots were analysed from the selected 5 samples, where 57 of those spots were in titanite grains (M08, M09, and M17), 26 were in monazite grains (M14), and 24 were in zircon grains (M22). The titanite grains analysed were irregular in shape and zoning (no definite or clear trend) and ranged from 55 to 350 μm (figure Fig. 7.1 (a), (b), and (d)). Monazite grains, however, ranged from being round to elongated in shape and vary in size from 30 to 300 μm. Zoning (in terms of BSE brightness) is common amongst the monazite grains, where it occurs as concentric or patchy (Fig. 7.1 (c)). The analysed zircon grains ranged from sub-rounded to rectangular in shape and range between 35 and 300 μm (Fig. 7.1 (e)).

Ages for all samples were acquired from titanites, monazites and zircons by single spot analyses with spot diameters of 30 μm, 9 μm and 20 μm, respectively and all with a crater depth of roughly 10-15 μm. For titanite analyses, the GJ1 zircon was used as primary calibration material (Jackson *et al.*, 2004). The Khan titanite (Heaman, 2009), used for quality control, was repeatedly analysed and provided results that were in excellent agreement with the published ages. For monazite analyses, the USGS 44069 monazite was used as primary calibration material (Aleinikoff *et al.*, 2006). The Thompson Mine (Williams *et al.*, 1996) and Itambe (Goncalves *et al.*, 2016) monazite reference materials were used for quality control and results were in good agreement with the published ages. For zircon analyses, the Plesovice (Slama *et al.*, 2008) and M127 (Nasdala *et al.*, 2008; Mattinson, 2010) zircon reference materials were used for quality control and results were also in excellent agreement with the published ID-TIMS ages. The methods used for all data analysis and processing are as described by Frei & Gerdes (2009) and calculation of concordia ages and plotting of concordia diagrams were conducted using Isoplot/Ex 3.0 (Ludwig, 2003).

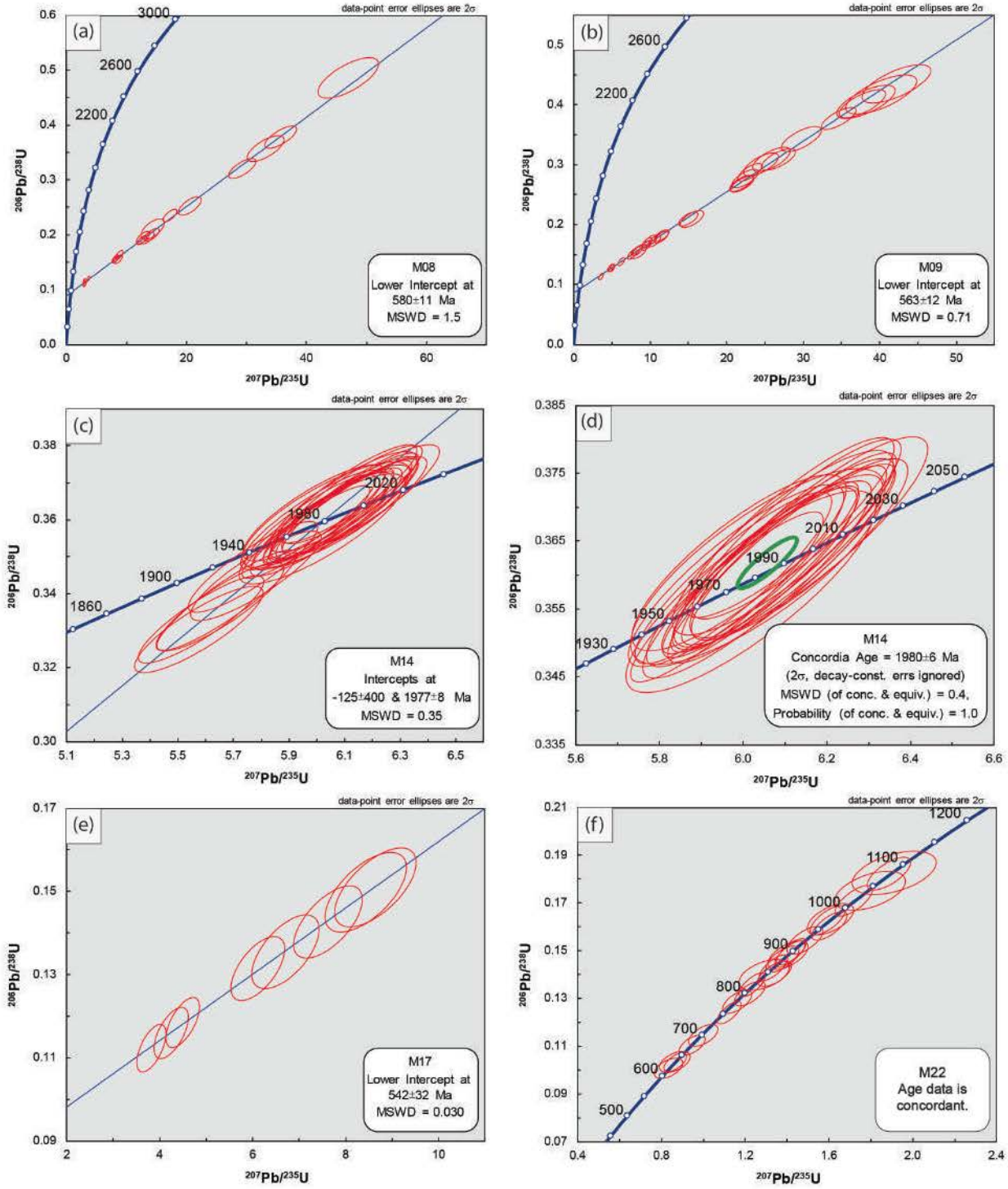

Figure 7.2: U-Pb Concordia diagrams for all 5 samples (from 4 different localities) and their respective ages. (a) Sample M08 Chilumba discordant age data; (b) sample M09 Chilumba discordant age data; (c) sample M14 discordant age data; (d) sample M14 Mlowe granulite concordant age data; (e) sample M17 Maganga amphibolite discordant age data; (f) sample M22 Mangochi charnockite concordant age data with ages ranging from roughly 600-1100Ma.

Results

Chilumba garnet-amphibolites

For samples M08 and M09, titanite grains were used for U-Pb isotopic analyses, where a total of 48 spots (19 spots for sample M08 and 29 spots for sample M09) were analysed. The grains ranged in size from 55-350μm and 65-300 μm for samples M08 and M09, respectively. Most spots give discordant ages but all lie on a concordia that yields an age of 580 $\pm$11Ma, defined by the lower intercept (Fig. 7.2 (a)). Analyses in sample M09 also yield a discordant age of 563 $\pm$12Ma, defined by the lower intercept (Fig. 7.2(b)). Overall, the two ages are within uncertainty of each other, indicating that metamorphism occurred somewhere around 575-569 Ma.

Mlowe granulites

Sample M14 was selected for U-Pb isotopic analyses to determine ages for the Mlowe granulites. In this sample, monazite grains were used for U-Pb analyses, where 26 spots were analysed and grains ranged between 30 μm and 300 μm. These grains yielded both discordant and concordia ages. The discordant ages fall on a discordia line with a lower intercept of 1977$\pm$8 Ma (Fig. 7.2 (c)), while the concordia age is 1980$\pm$6 Ma (Fig. 7.2 (d)). Both discordant and concordia ages are within uncertainty of each other, indicating that metamorphism occurred somewhere around 1985-1974 Ma.

Maganga amphibolites

In sample M17, titanite grains were used for U-Pb isotopic analyses, where 9 spots were analysed. Ttitanite grains ranged in size from 20-60 μm and yielded discordant ages that fall on a discordia line with a lower intercept of 542$\pm$32 Ma (Fig. 7.2 (e)). Hence, metamorphism likely occurred somewhere around 574-510 Ma.

Mangochi charnockites

Sample M22 was selected for U-Pb analyses on in-situ zircon grains present in the charnockites. A total of 24 spots were analysed and the zircon grains ranged between 30 μm and 300 μm. Ages from individual spots are mostly concordant but have multiple age signals ranging from roughly 600 Ma to 1100 Ma (Fig. 7.2 (f)). The frequencies of different age signals are presented in Fig. 7.3. The youngest ages between 600-650 Ma are observed in 3 analyses, followed by a total of 9 analyses that show ages between 800-900Ma. The oldest ages between 950-1100 Ma is observed in a total of 7 analyses. Essentially, age signals recorded seem to cluster around 600-650 Ma, 800-900 Ma, and 950-1100 Ma.

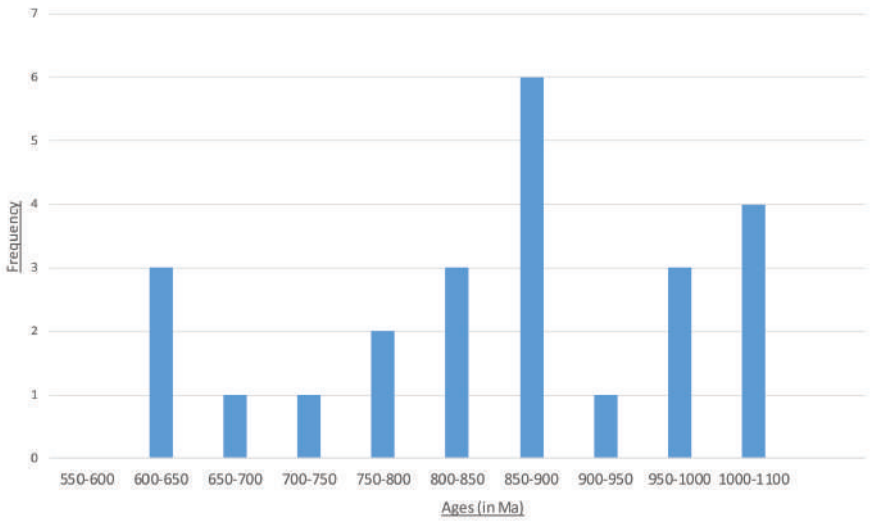

Figure 7.3: Graph showing the frequency of different age signals recorded in the Mangochi charnockites spanning from 1100 Ma to 600 Ma. Age signals recorded in Mangochi are clustered around 600-650 Ma, 800-900 Ma and 950-1100 Ma.

The aformentioned U-Pb age results for all five samples (taken from four different localities) have been summarised in Table 7.1.

	Age Type	No. of analyses	Upper	2_σ	Lower	2_σ	MSWD	Prob of Conc.
Sample M08	Discordia	19	-	-	580	11	1.5	-
Sample M09	Discordia	29	-	-	563	12	0.71	-
Sample M14	Discordia	26	1977	8	-	-	0.35	-
Sample M14	Concordia	26	1980	6	-	-	0.4	1.0
Sample M17	Discordia	9	-	-	542	32	0.030	-
Sample M22	Concordia	24	-	-	-	-	-	-

Table 7.1: Summary of U-Pb ages (in Ma) for all 5 samples. MSWD represents the mean square weighted deviation. Prob of Conc. represents the probability of concordance. Sample M22 shows multiple age signals along the concordia, hence some of its data are not specified.

Chapter 8

Discussion

8.1 Metamorphic History

The P-T conditions determined for various rock types surrounding Lake Malawi confirm that they were formed at a range of metamorphic conditions and at different times, which are mainly amphibolite and granulite facies conditions with varying pressure and temperature ranges (see Table 8.1 and Fig. 8.5 for summarised P-T conditions).

The Chilumba garnet-amphibolites yielded P-T conditions of $\geq$635°C at 4.8-5.5 kbar (for sample M08) and $\geq$650°C at 5-5.5 kbar (for sample M09). This was based on measured Xgrs and the observed mineral assemblage of hornblende, garnet, rutile, and plagioclase, shown as the shaded area in red on Fig. 8.1. Texturally, it has been observed that plagioclase occurs both in the matrix and as what appears to be decompression rims around garnet grains. Since the mineral composition of these plagioclase rims were not analysed, it cannot be said for certain whether or not the two plagioclase textures represent two growth events. Additionally, if there was indeed a second growth event during decompression, it cannot be constrained nor discussed without comparisons between compositional differences.

Ring *et al.* (2002) analysed similar garnet-amphibolites in northern Malawi and used rare occurrences of clinopyroxene with elevated jadeite composition to constrain pressure conditions to 17-18 kbar. Ring *et al.* (2002) then concluded that these amphibolites are 530 Ma in age and were heavily retrogressed eclogites, formed during the subduction-collision event that marked the final amalgamation of East and West Gondwana. However, Ring *et al.* (2002) also discussed other amphibolites which yielded ages of 580-550 Ma and found adjacent to the aforementioned eclogites, south of the Mugesse Shear zone. These amphibolites were suggested to have formed under

conditions of 600-750°C at 5-9 kbar during a shearing event 30 Ma prior to the eclogite facies metamorphism (Ring *et al.*, 2002). Although the P-T conditions yielded in this study are similar to that of those proposed for shearing-induced amphibolites, the overall granoblastic texture is quite inconsistent with metamorphism associated with shearing.

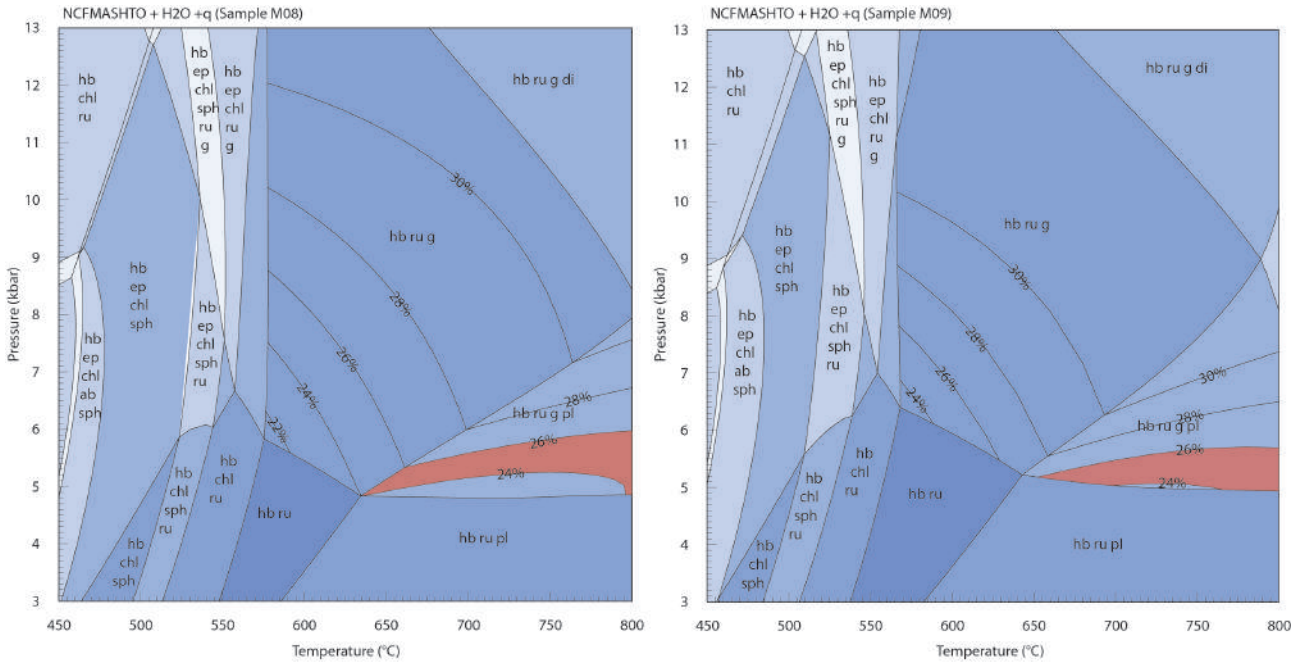

Figure 8.1: Pseudosections of samples M08 and M09, with general stability fields contoured according to grossular content (in percentages) and narrowed P-T ranges are shaded in red.

Further south from Chilumba, lies the Mlowe Granulites (samples M13 and M14), where both samples yielded similar P-T conditions of 760°C at 4.5-5 kbar. These conditions were based on the observed mineral assemblage of garnet, plagioclase, alkali-feldspar, biotite, cordierite, sillimanite, magnetite, and melt (circled in Fig. 8.2). Based on retrograde textures of garnet, sillimanite and biotite observed in the granulites (discussed previously in the Inferred Equilibrium Mineral Assemblages chapter), it has been inferred that biotite and second generation garnet and sillimanite were formed after peak metamorphic conditions. A possible scenario for which these second generation sillimanite and garnets formed is that when the rock crossed the solidus during its retrograde path and melt was produced, the melt likely then reacted with peak assemblage cordierite. Subsequent melt crystallisation formed fine-grained sillimanite along cordierite grain edges. This melt crystallisation could have also formed the second generation garnets as well. Similar interpretations have been made by Diener *et al.* (2008) for central Australian granulites.

If such was the case, the most likely path from melt-production to the crystallisation of second generation sillimanite and garnet is represented by the black arrows in Fig. 8.2. These arrows essentially show a general direction from the melt-bearing peak assemblage to the actual solidus where the melt would have crystallised. Futher interpretations of the P-T path prior to this cannot be made as these psuedosections are not applicable for the prograde or pre melt-loss history of the granulites.

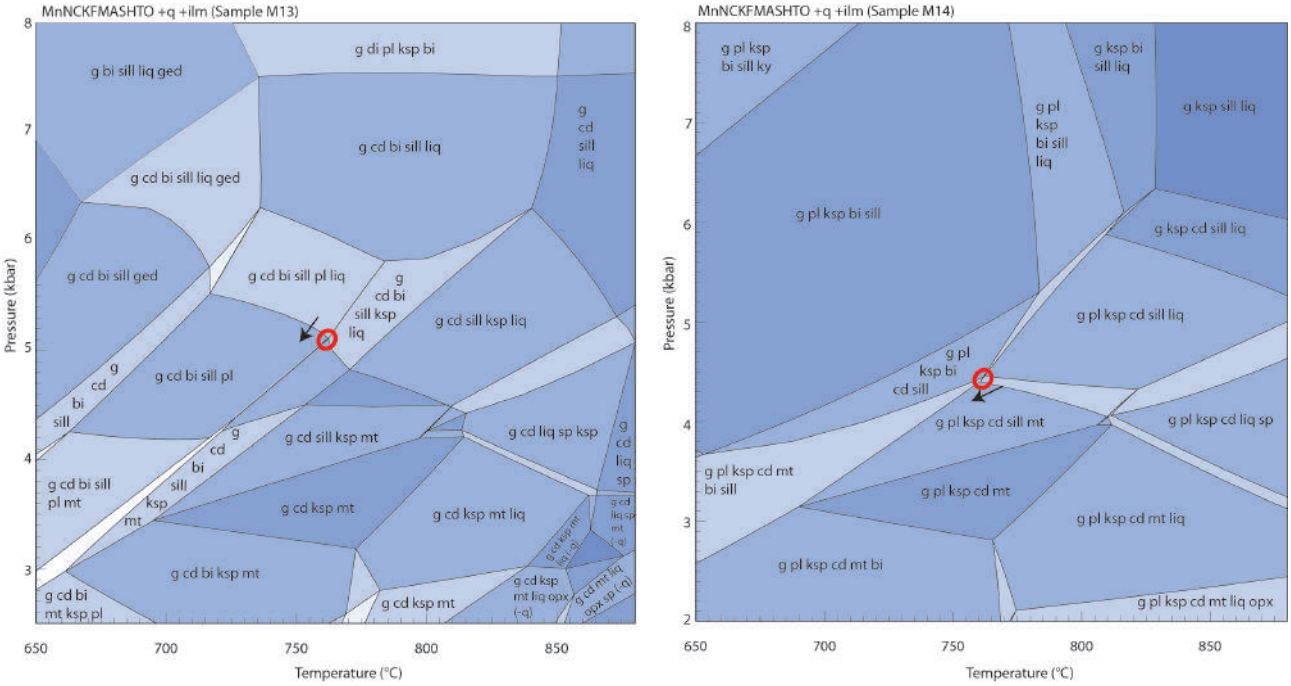

Figure 8.2: Pseudosections of samples M13 and M14, where the peak condition stability fields are circled in red. The black arrows represent the general direction of the retrograde path from the melt-bearing field to the actual solidus where melt crystallisation occurred.

Similar granulites from Malawi were discussed by Ring *et al.* (1997) and referred to as cordierite-garnet amphibolites which recorded rather similar P-T conditions of 750-850°C at 5-5.5 kbar. These granulites were interpreted as part of a Ubendian paired metamorphic belt which was part of the upper plate during a subduction event and, hence, never subjected to high pressure conditions (Ring *et al.*, 1997). This theory was based on the fact that the low pressure granulites were intercalated with high pressure enderbitic gneiss which recorded subduction-like pressure conditions (Ring *et al.*, 1997).

Samples collected in Maganga differ significantly in terms of mineral assemblage and P-T conditions, despite the fact that they were found in close proximity to each other. The amphibolites (sample M17) contain the mineral assemblage hornblende, plagioclase, quartz titanite, and rutile. With the combination of the observed mineral assemblage and Xan, a relatively wide P-T range of 525-750°C at <8.5 kbar is predicted (Fig. 8.3). The amphibolites are generally well-equilibrated and do not show any obvious retrograde textures to suggest approximate P-T paths. The overall P-T ranges suggest medium-high temperature and low-medium pressure amphibolite facies conditions.

The observed mineral assemblage for sample M18 is kyanite, staurolite, garnet, plagioclase, muscovite, chlorite, biotite, and ilmenite. As previously discussed, the pseudosection does not show a stability field which allows for the co-existence for all the observed minerals and hence, two possible stability fields were proposed (shown as assemblage A and B on Fig. 8.3). Assemblage A excludes plagioclase from the equilibrium mineral assemblage and suggests a P-T condition of 650°C at 15 kbar. Assemblage B, on the other hand, excludes chlorite from the assemblage and suggests a P-T range of 660-670°C at 6-8 kbar. Although both temperatures are quite similar, the pressures differ by a significant amount of 7-9 kbar.

Given that samples M17 and M18 were collected at the same location, in theory, they should yield similar P-T conditions. Although Assemblage B suggests similar P-T conditions to that of sample M17, conditions associated with Assemblage A is at significantly high pressures that are not recorded in M17. If sample M17 was indeed subjected to pressure conditions recorded by Assemblage A of 15 kbar, the amphibolite should include garnet and diopside as part of the mineral assemblage. Similarly, if Assemblage B was exposed to the P-T conditions recorded by sample M17, the schist likely would be melting and not have kyanite as part of the mineral assemblage (Fig. 8.3). Additionally, if sample M17 really was subjected to such high pressure conditions, it seems unlikely that the amphibolite did not record it. As a result, the most likely P-T conditions for the sample M18 schist is that recorded by Assemblage B of 660-670°C at 6-8kbar. Consequently, the overlap in P-T conditions of M17 and Assemblage B of sample M18 allows further constraint of the P-T range to 660-670°C and 6-8 kbar which overall suggests medium-pressure amphibolite facies conditions.

The Mangochi Charnockites are defined by the inferred equilibrium mineral assemblage of garnet, orthopyroxene, clinopyroxene, plagioclase, alkali-feldspar, biotite, magnetite, and melt (liquid).

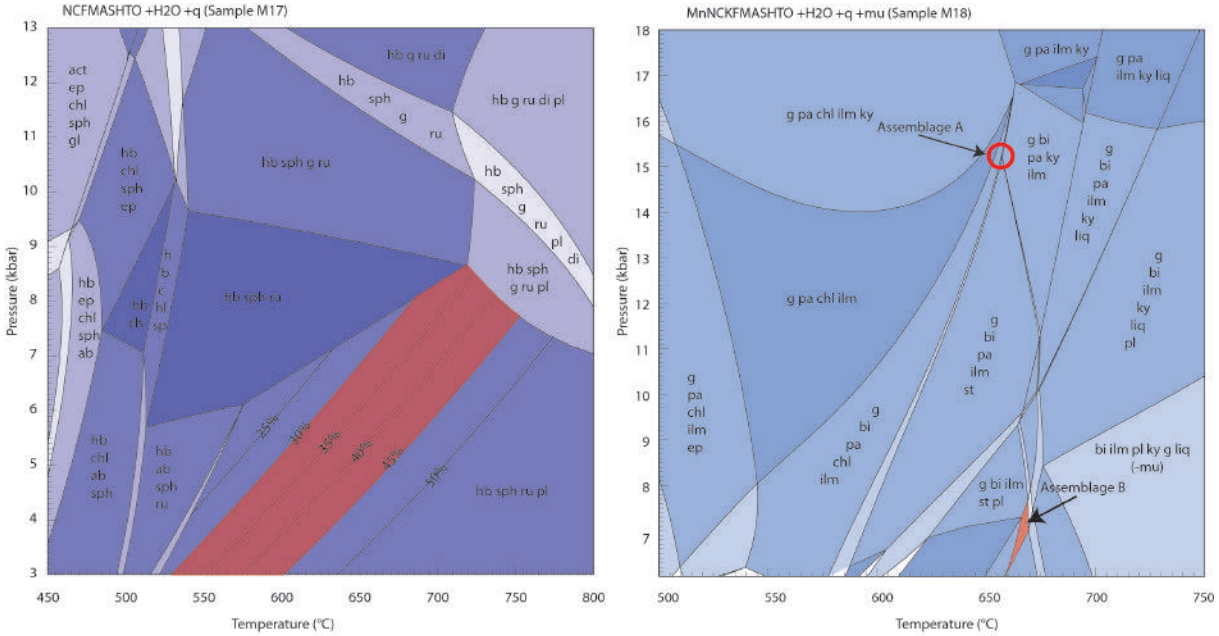

Figure 8.3: Pseudosections of samples M17 and M18, where stability fields are shaded in red or indicated by a red circle. Sample M17 is contoured according to Xan (in percentages). For sample M18, Assemblages A and B represent the two possible P-T ranges discussed.

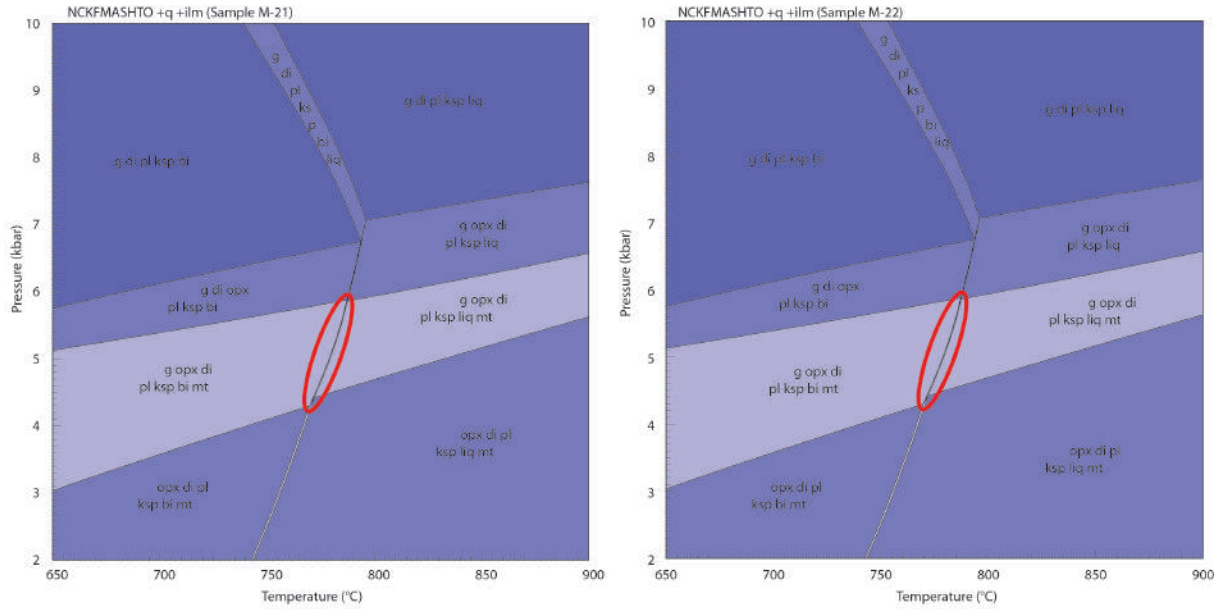

Figure 8.4: Pseudosections of samples M21 and M22 with stability fields indicated with red circles.

This suggests a P-T range of 770-780°C at 4.3-6 kbar for both samples M21 and M22 (Fig. 8.4). However, the charnockites' distinct perthitic exsolution texture of the feldspars suggest the rock initially contained ternary feldspar at high temperatures and likely under igneous conditions. Overall, the P-T conditions suggest low pressure, high temperature granulite facies conditions.

Similar granulites were mentioned by Andreoli (1984) in the Zomba-Blantyre region of southern Malawi and suggested to have been formed in magmatic arc environment associated with the Kibaran-age continental collision event. Kroner *et al.* (2001) later proposed that granulites in southern Malawi likely formed due to magmatic underplating based on recorded anti-clockwise, isobaric cooling P-T paths in other granulites from surrounding areas. Although the Mangochi charnockites studied in this thesis did not allow for P-T path constraint, the low-pressure, high-temperature conditions recorded, coupled with the distinct granoblastic texture, can be explained by both magmatic underplating and/or a magmatic arc environment.

All pressure and temperature conditions as well as metamorphic facies conditions of each sample are summarised in Table 8.1.

	Chilumba gt-amphibolites	Mlowe gt-cd-granulites	Maganga amphibolites	Maganga schist	Mangochi charnockites
Temperature	M08: 575-660°C	M13: 760°C	M17: 525-750°C	M18: 650°C	M21: 770-780°C
	M09: 565-630°C	M14: 760°C			M22: 770-780°C
Pressure	M08: 4.9-8.7kb	M13: 5kb	M17: $\leq$8.5kb	M18: 15kb	M21: 4-6kb
	M09: 5.5-7.9kb	M14: 4.5kb			M22: 4-6kb
Facies Conditions	amphibolite facies	granulite facies	amphibolite facies facies	high P amphibolites facies	granulite facies

Table 8.1: Summary of temperatures, pressures, and facies conditions for all samples, determined through calculated pseudosections.

8.2 Geochronology

Results from U-Pb isotopic analyses yielded the ages of five samples, taken from four localities, which generally span from Eburnian to Pan African in age.

Two samples, M08 and M09, from Chilumba were dated using U-Pb analyses to yield ages of 580±11 Ma and 563±12 Ma, respectively. If taken to be the same within uncertainty, the ages yielded can give the same age range of roughly 575-569 Ma. Subsequently, the slight difference in ages is not significantly different and the age of metamorphism is around 570 Ma. This result suggests that the formation of the garnet-amphibolites is associated with the Neoproterozoic Pan African Orogeny. However, according the map in Fig. 8.5, Chilumba is situated in the middle of the Palaeoproterozoic Ubendian Belt. A possible explanation for the presence of Pan African amphibolites in the purported Ubendian terrane is that the Pan African terrane present just east of, and truncated by, the Ruhuhu Trough (Fig. 8.5) actually extends further West, underneath Lake Malawi to encompass the Chilumba region as well. Since the areas surrounding Lake Malawi are generally dissected by multiple faults, as a result of modern-day rift propagation, orogenic terranes may be displaced and do not always form perfect continuous belts. Ring *et al.* (2002) discussed similar-aged amphibolites and suggested that these were formed during a 580-550 Ma shearing event south of the Mugesse Shear Zone.

Sample M14 of the Mlowe granulites yielded a Concordia age of 1980±6 Ma and Discordia age of 1977±8 Ma which are within uncertainty of each other and suggests that the granulites are associated with the Palaeoproterozoic Ubendian Orogeny occurred at 1985-1974 Ma. This is in agreement with the proposed map by which shows the Mlowe area to be part of the Ubendian Belt. As mentioned before, Ring *et al.* (1997) reported similar granulites less than 50 km from Mlowe, referred to as cordierite-garnet granulites, which record similar P-T conditions as those recorded by the Mlowe granulites in this study. The granulites discussed by Ring *et al.* (1997) also yielded a Ubendian age of 1985-1995 Ma which is in relatively close agreement with the ages determined in this study.

The Maganga amphibolite (sample M17) is the youngest of the Pan African rocks analysed and yielded an age of 542±32 Ma but has a higher uncertainty than the ages yielded by the Chilumba amphibolites. However, this age is still within uncertainty of that determined in Chilumba and most likely falls within that range as well. Overall, the age results suggested by sample M17 proves to be in disagreement with the map in Fig. 8.5. According to Fagereng (2013), the Maganga region lies within the Ubendian terrane whilst the ages suggest Pan African metamorphism, or at least reworking. As a result, it is likely that the Mozambique Belt to the south of Malawi actually extends further north to include the Maganga region.

Sample M22 of the Mangochi charnockites yields a large spread of ages, all perfectly along the Concordia. The ages range from Grenvillian (i.e. Kibaran/Irumide Orogeny) to Pan African 1100 Ma to 600 Ma. The Pan African overprint in Mangochi places it as part of the Mozambique Belt but there is certainly a Kibaran/Irumide remnant within the charnockites. The Pan African age signatures at 900-800Ma and 650-600Ma roughly coincide with the East African orogen.

A summary of P-T conditions as well as ages in relation to each rock type's respective localities are shown on Fig. 8.5.

8.3 Implications

Findings of this thesis show that the metamorphic evolution of Malawian basement rocks from 4 localities around Lake Malawi span from Eburnian to Pan African in age. The oldest rocks analysed in this study are the 1985-1974 Ma Mlowe granulites which were determined to have formed under 760°C at 4.5-5 kbar. These results are relatively consistent with those of Ring *et al.* (1997) who suggested an age of 1995-1985 Ma and a P-T range of 750-850°C at 5-5.5 kbar. Even though Ring *et al.* (1997) suggest these granulites were part of the upper plate during Ubendian-age subduction, this was based on the presence of intercalated high pressure enderbitic gneiss. The hypothesis revolved around the idea that the intercalated nature of high and low pressure granulites can be explained by categorising it as a paired metamorphic belt which experienced two different pressure conditions at the same time (Ring *et al.*, 1997). The Mlowe granulites in this study do indeed share similar P-T conditions and ages to the supposed "upper plate" granulites. However, this thesis did not analyse the associated enderbitic gneiss and, hence, cannot be used to confirm or deny this theory. Nonetheless, the recorded age of 1985-1974Ma in Mlowe is consistent with an approximately 2000 Ma Ubendian subduction event recorded in other parts of the Mozambique Belt (Moller *et al.*, 1995; Boven *et al.*, 1999; Ring *et al.*, 1997). For future work, it would be highly beneficial to observe the enderbitic gneiss reported by Ring *et al.* (1997) in order to further explore this hypothesis.

Kibaran-age metamorphism is relatively poorly preserved in the samples analysed. Although age signatures of 1100-950Ma is recorded in the Mangochi charnockites, peaks at 900-800 Ma and 650-600 Ma were also observed. Andreoli (1984) and Kroner *et al.* (2001) have reported charnockites and other granulites in southern Malawi in the Zomba-Blantyre region and have suggested their

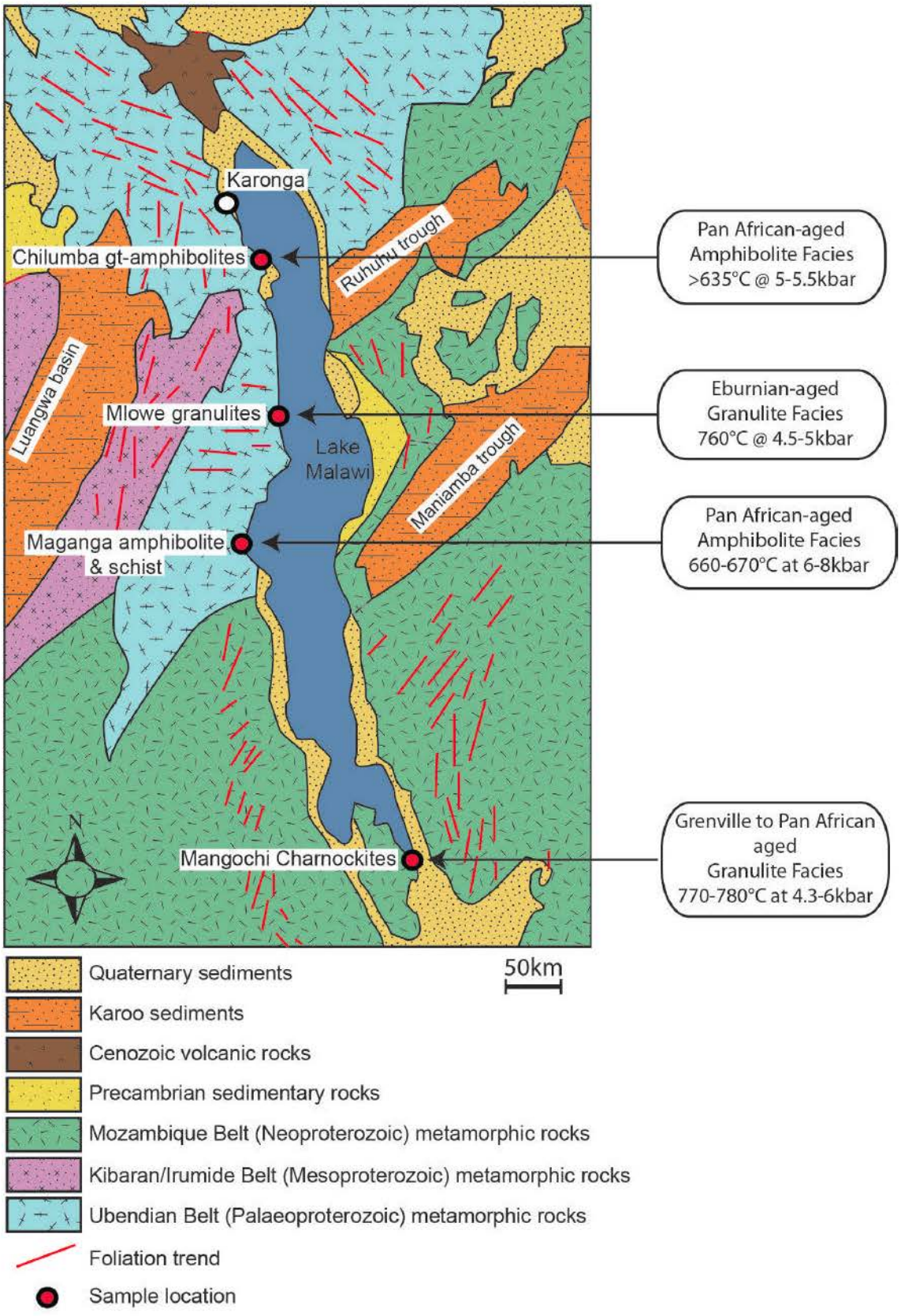

Figure 8.5: Regional Map of Malawi showing sample localities and their associated P-T conditions, metamorphic facies and age. Map was modified after Fagereng, 2013.

origin to be associated with magmatic underplating in a magmatic arc environment during the Kibaran times. These charnockites were mentioned by Andreoli (1984) but did not provide calculated P-T conditions for them. Kroner *et al.* (2001) suggested a temperature range of 940-848°C but no pressure estimates were provided. As a result, charnockites in southern Malawi are not extensively discussed and their P-T conditions are relatively poorly constrained. Pseudosection modelling conducted in this thesis suggests that the charnockites experienced peak conditions at 770-780°C and 4.3-6 kbar. These temperatures are roughly 80-170°C less than proposed by Kroner *et al.* (2001). Additionally, Kroner *et al.* (2001) used isobaric cooling P-T paths recorded in other granulites found in the region to propose magmatic underplating. However, such a P-T path could not be confirmed from the charnockites analysed in this study. Nonetheless, Kibaran-age magmatic underplating (possibly in a magmatic arc setting as suggested by Ring *et al.* (1997)) may still be a possible explanation for the 1100-950 Ma age signatures recorded in the charnockites as well as the associated granoblastic texture which formed at high temperatures and low pressures. In terms of the 900-800 Ma and 650-600 Ma age signatures observed in the charnockites, the lack of any distinct retrograde textures seen in the rocks make it difficult to determine any obvious metamorphic overprinting features that can be associated with these ages. Since the East African Orogen was proposed to have occurred between 800-650 Ma by Meert *et al.* (1995); Meert & van der Voo (1997) and Rodinia break-up occurred between 1300-900 Ma (Li *et al.*, 2008), it is possible that the 900-800 Ma signature in the charnockites either represents a metamorphic event during the early stages of the East African Orogen or the late stages of Rodinia break-up. The 650-600 Ma signature could then represent the late stages of the East African Orogen. However, the findings of this thesis do not provide any immediate evidence to support those conclusions. All that can be inferred is that these charnockites were likely emplaced during Kibaran-age magmatism and later experienced two other metamorphic events at 900-800 Ma and 650-600 Ma.

The Pan African rocks analysed are fairly similar in age, ranging from roughly 575-569 Ma and 574-510 Ma for Chilumba and Maganga, respectively. As mentioned previously, the Maganga age range has high uncertainty and therefore can be interpreted to overlap with the ages yielded in Chilumba. This would suggest that the Maganga and Chilumba regions likely experienced the same metamorphic event. However, while the Chilumba garnet-amphibolites formed at peak conditions of $\geq$635°C and 5-5.5 kbar, the Maganga region experienced conditions of 660-670°C and 6-8 kbar. Although the temperature range for the Chilumba amphibolites are relatively poorly constrained, pressure conditions recorded in Maganga are slightly higher. Different P-T conditions may not be entirely unexpected as the two regions differ quite significantly petrolog-

ically. The Chilumba garnet-amphibolites yield similar ages and P-T conditions to Malawian amphibolites reported by Ring *et al.* (2002) in the same area and proposed that they were formed during a shearing event at 580-550 Ma. This theory was essentially based on the discovery of 530 Ma eclogites in Chilumba which were concluded to have formed during the subduction-collision transition which marked the final amalgamation of east and west Gondwana (Ring *et al.*, 2002). Subsequently, it was stated that the 580-550 Ma amphibolites could not have been a result of crustal thickening during this amalgamation event since (1) they do not preserve any high pressures and (2) they pre-date this supposed eclogite facies metamorphism by 20-50 Ma (Ring *et al.*, 2002). However, this study revealed that such a characteristic granoblastic texture observed in the garnet-amphibolites is not quite consistent with shearing-induced metamorphism. The Maganga amphibolite and schist, on the other hand, have not been mentioned in previous literature despite their interesting contrast in texture and mineral assemblage. Maganga rocks are similarly aged to the Chilumba rocks and yield relatively similar P-T conditions as well. However, they are strongly foliated and are not at all similar to the granoblastic texture observed in Chilumba.

Although Ring *et al.* (2002) concluded that amphibolites of this age were definitely not formed during the final collision of east and west Gondwana at 530 Ma, it is still possible that the observed Chilumba and Maganga rocks could have formed during the early stages of the Kuunga Orogeny which occurred from 570 Ma to 530 Ma (Meert *et al.*, 1995; Meert & van der Voo, 1997; Meert, 2003). Since these regions do not preserve any textures that suggest high pressure conditions, it cannot be determined to what extent these rocks were affected by the Kuunga Orogeny itself. Nonetheless, the extensive amounts of retrogression experienced in northern Malawi (both during and after the Pan African and Kuunga orogenies) must be considered. Given that Malawi is a site of modern tectonism, it is also likely that any remnants of high pressure conditions may have been heavily retrogressed and overprinted during deformation associated with modern rift related normal faulting. Distinct annealed quartz is already observed in the Maganga schists, suggesting that re-equilibration and recrystallisation has occurred in Malawi.

Chapter 9

Conclusion

Calculated P-T conditions and U-Pb age results confirm that multiple metamorphic events, ranging from Eburnian to Pan African in age, have affected the Malawian basement geology. Results show that during Ubendian times, low pressure and high temperature granulites were emplaced at 1985-1974 Ma in the Mlowe region. This emplacement may have been the result of subduction-related magmatism in the upper plate. There is then almost a 900 Ma gap in the chronological history as the next event recorded in the sample set is the 1100-950 Ma emplacement of Mangochi charnockites during Kibaran-age metamorphism. Pseudosection modelling was able to provide a more precise P-T range of 770-780°C and 4.3-6 kbar of charnockites which were previously recorded by Andreoli (1984) in southern Malawi. The high temperature, low pressure conditions combined with the characteristic granoblastic texture observed is consistent with metamorphism associated with magmatic underplating. Subsequently, a 900-800 Ma metamorphic event that possibly occurred during early stages of the East African orogen is recorded in Mangochi. The Mangochi region then experienced another metamorphic event during late stages of the East African orogen at 650-600 Ma. Amphibolite facies metamorphism then occurred throughout the Malawian region around 570 Ma. Although the Chilumba amphibolites were proposed to have formed during a shearing event (Ring *et al.*, 2002), observations of granoblastic textures preserved by the samples show that this likely was not the case. Instead, this thesis proposes that the amphibolite facies metamorphism occurred during the late stages of the Kuunga Orogeny which spanned from 580-530 Ma. Similar P-T conditions of $\geq$635°C at 5-5.5 kbar and 660-670°C at 6-8 kbar are recorded in Chilumba and Maganga, respectively. Overlap in these conditions suggests that these regions likely experienced the same metamorphic event. Findings of this study have allowed for a more detailed metamorphic history of Malawi which has, to some extent, helped unravel the geological complexity by not only identifying features of older orogenic events, but constraining their P-T conditions as well. Future studies should include the comparison of high

pressure rocks reported by Ring *et al.* (2002) and Ring *et al.* (1997) and rock types analysed in this thesis. Such analysis would provide further insight in terms of why rocks found in such close proximity preserve vastly different P-T conditions and textures which ultimately lead to contrasting interpretations of their tectonic environments.

References

Aleinikoff, J., Schenck, W., Srogi, L., Fanning, C., Kamo, S. & Bosbyshell, H., 2006. Deciphering igneous and metamorphic events in high-grade rocks of the Wilmington Complex, Delaware: Morphology, cathodoluminescence and backscattered electron zoning, and SHRIMP U-Pb geochronology of zircon and monazite. *GSA Bulletin*, **118**, 39–64.

Andreoli, M., 1984. Petrochemistry, tectonic evolution and metasomatic mineralisation of Mozambique Belt granulites from S. Malawi and Tete (Mozambique). *Precambrian Research*, **25**, 161–186.

Appel, P., Moller, A. & Schenk, V., 1998. High-pressure granulite facoes metamorphism in the Pan African belt of eastern Tanzania: P-T-t evidence against granulite formation by continental collision. *Journal of Metamorphic Geology*, **16**, 491–509.

Boniface, N., 2009. *Eburnian, Kibaran and Pan-African metamorphic events in the Ubendian belt of Tanzania: Petrology, zircon and monazite geochronology.* PhD thesis, University of Kiel.

Boven, A., Theunissen, K., Sklyarov, E., Klerkx, J., Melnikov, A., Mruma, A. & Punzalan, L., 1999. Timing of exhumation of a high-pressure mafic granulite terrane of the Paleoproterozoic Ubende belt (West Tanzania). *Precambrian Research*, **93**, 119–137.

Buiter, S. & Torsvik, T., 2014. A review of Wilson Cycle plate margins: A role for mantle plumes in continental break-up along sutures? *Gondwana Research*, **26**, 627–653.

Busch, J., Mezger, K. & van der Pluijm, B., 1997. Suturing and extensional reactivation in the Grenville orogen, Canada. *Geology*, **25**, 507–510.

Collins, A. & Pisarevsky, S., 2005. Amalgamating eastern Gondwana: The evolution of the Circum-Indian Orogens. *Earth-Science Reviews*, **71**, 229–270.

Corrigan, D., Culshaw, N. & Mortensen, J., 1994. Pre-Grenvillian evolution and Grenvillian overprinting of the Parautochthonous Belt in Key Harbour, Ontario: UPb and field constraints. *Canadian Journal of Earth Sciences*, **31**, 583–596.

Corvino, A., Boger, S., Henjes-Kunst, F., Wilson, C. & Fitzsimons, C., 2008. Superimposed tectonic events at 2450 Ma, 2100 Ma, 900 Ma and 500 Ma in the North Mawson Escarpment, Antarctic Prince Charles Mountains. *Precambrian Research*, **167**, 281–302.

Daly, M., 1986. The intracratonic Irumide Belt of Zambia and its bearing on collision orogeny during the Proterozoic of Africa. *Geological Society, London, Special Publications*, **19**, 321–328.

De Waele, B. & Mapani, B., 2002. Geology and correlation of the central Irumide belt). *Journal of African Earth Sciences*, **35**, 385–397.

De Waele, B., Wingate, M., Fitzsimons, I. & Mapani, B., 2003. Untying the Kibaran knot: A reassessment of Mesoproterozoic correlations in southern Africa based on SHRIMP U-Pb data from the Irumide belt). *Geological Society of America*, **31**, 509–512.

Diener, J., White, R. & Powell, R., 2008. Granulite facies metamorphism and subsolidus fluid-absentreworking, Strangways Range, Arunta Block, central Australia. *Journal of Metamorphic Geology*, **26**, 603–622.

Engvik, A., Tveten, E., Bingen, B., Viola, G., Erambert, M., Feito, P. & De Azavedo, S., 2007. PTt evolution and textural evidence for decompression of Pan-African high-pressure granulites, Lurio Belt, north-eastern Mozambique. *Journal of Metamorphic Geology*, **25**, 935–952.

Fagereng, A., 2013. Fault segmentation, deep rift earthquakes and crustal rheology: Insights from the 2009 Karonga sequence and seismicity in the RukwaMalawi rift zone. *Tectonophysics*, **601**, 216–225.

Frei, D. & Gerdes, A., 2009. Precise and accurate in situ UPb dating of zircon with high sample throughput by automated LA-SF-ICP-MS. *Chemical Geology*, **261**, 261–270.

Frost, B., Chamberlain, K. & Schumacher, J., 2000. Sphene titanite: phase relations and role as a geochronometer. *Chemical Geology*, **172**, 131–148.

Goncalves, G., Lana, C., Scholz, R., Buick, I., Gerdes, A., Kamo, S., Corfu, F., Marinho, M., Chaves, A., Valeriano, C. & Nalini, J. H., 2016. An assessment of monazite from the Itamb pegmatite district for use as U-Pb isotope reference material for microanalysis and implications for the origin of the Moacyr monazite. *Chemical Geology*, **424**, 30–50.

Green, E., White, R., Diener, J., Powell, R., Holland, T. & Palin, R., 2016. Activitycomposition relations for the calculation of partial melting equilibria in metabasic rocks. *Journal of Metamorphic Geology*, **34**, 845–869.

Heaman, L., 2009. The application of UPb geochronology to mafic, ultramafic, and alkaline rocks: An evaluation of three mineral standards. *Chemical Geology*, **261**, 43–52.

Jackson, S., Pearson, N., Griffin, W. & Belousova, E., 2004. The application of laser ablation - inductively coupled plasma - mass spectrometry to in situ U-Pb zircon geochronology. *Chemical Geology*, **211**, 47–69.

Johnson, A., Rivers, T. & De Waele, B., 2005. A review of the Mesoproterozoic to early Palaeozoic magmatic and tectonothermal history of south-central Africa: implications for Rodinia and Gondwana. *Journal of the Geological Society, London*, **162**, 433–450.

Karmakar, S. & Schenk, V., 2016. Mesoproterozoic UHT metamorphism in the Southern Irumide Belt,Chipata, Zambia: Petrology and in situ monazite dating. *Precambrian Research*, **275**, 332–356.

Kazimoto, E., Schenk, V. & Appel, P., 2015. Granulite-facies metamorphic events in the north-western Ubendian Belt of Tanzania: Implications for the Neoarchean to Paleoproterozoic crustal evolution. *Precambrian Research*, **256**, 31–47.

Kelsey, D., Clark, C. & Hand, M., 2008. Thermobarometric modelling of zircon and monazite growth in melt-bearing systems: examples using model metapelitic and metapsammitic granulites. *Journal of Metamorphic Geology*, **26**, 199–212.

Kroner, A., Sacchi, R., Jaeckel, P. & Costa, M., 1997. Kibaran magmatism and Pan African granulite metamorphism in northern Mozambique: single zircon ages and regional implications. *Journal of African Earth Sciences*, **25**, 467–484.

Kroner, A., Willner, A., Hegner, E., Jaeckel, P. & Nemchin, A., 2001. Single zircon ages, PT evolution and Nd isotopic systematics of high-grade gneisses in southern Malawi and their bearing on the evolution of the Mozambique belt in southeastern Africa. *Precambrian Research*, **109**, 257–291.

Lenardic, A., Moresi, L. & Muhlhaus, H., 2000. The role of mobile belts for the longevity of deep cratonic lithosphere' The crumple zone model. *Geophysical Research Letters*, **27**, 1235–1238.

Li, Z., Bogdanova, S., Collins, A., Davidson, A., De Waele, B., Ernst, R., Fitzsimons, I., Fuck, R., Gladkochub, D., Jacobs, J., Karlstrom, K., Lu, S., Natapov, L., Pease, V., Pisarevsky, S., Thrane, K. & Vernikovsky, V., 2008. Assembly, configuration, and break-up history of Rodinia: A synthesis. *Precambrian Research*, **160**, 179–210.

Ludwig, K., 2003. Isoplot/Ex version 3: a Geochronological toolkit for Microsoft Excel. *Geochronology Center*, **Berkeley**.

Manhica, A., Grantham, G., Armstrong, R., Guise, P. & Kruger, F., 2001. Polyphase deformation and metamorphism at the Kalahari Craton Mozambique Belt boundary. *Geological Society, London, Special Publications*, **184**, 303–322.

Mattinson, J., 2010. Analysis of the relative decay constants of 235U and 238U by multi-step CA-TIMS measurements of closed-system natural zircon samples. *Chemical Geology*, **275**, 186–198.

Meert, J., 2003. A synopsis of events related to the assembly of eastern Gondwana. *Tectonophysics*, **362**, 1–40.

Meert, J. & van der Voo, R., 1997. The Assembly of Gondwana 880-550Ma. *Journal of Geodynamics*, **23**, 223–235.

Meert, J., van der Voo, R. & Ayub, S., 1995. Paleomagnetic investigation of the Neoproterozoic Gagwe lavas and Mbozi complex, Tanzania and the assembly of Gondwana. *Precambrian Research*, **74**, 225–244.

Moller, A., Appel, P., Mezger, K. & Schenk, V., 1995. Evidence for a 2 Ga subduction zone: Eclogites in the Usagaran belt of Tanzania. *Geology*, **23**, 1067–1070.

Moller, A., Mezger, K. & Schenk, V., 2000. UPb dating of metamorphic minerals: Pan-African metamorphism and prolonged slow cooling of high pressure granulites in Tanzania, East Africa. *Precambrian Research*, **104**, 123–146.

Muhongo, S. & Lenoir, J., 1994. Pan-African granulite-facies metamorphism in the Mozambique Belt of Tanzania: U-Pb zircon geochronology. *Journal of the Geological Society, London*, **151**, 343–347.

Muhongo, S., Tuisku, P., Mnali, S., Temu, E., Appel, P. & Stendal, H., 2002. High-pressure granulite-facies metagabbros in the Ubendian Belt of SW Tanzania: preliminary petrography and PT estimates). *Journal of African Earth Sciences*, **34**, 279–285.

Nasdala, L., Hofmeister, W., Norberg, N., Mattinson, J., Corfu, F., Dorr, W., Kamo, S., Kennedy, A., Kronz, A., Reiners, P., Frei, D., Kosler, J., Wan, Y., Gotze, J., Hager, T., Kroner, A. & Valley, J., 2008. Zircon M257a homogeneous natural reference material for the ion microprobe U-Pb analysis of zircon. *Geostandards and Geoanalytical Research*, **32**, 247–265.

Phillips, G., Kelsey, D., Corvino, A. & Dutch, R., 2009. Continental Reworking during Overprinting Orogenic Events, Southern Prince Charles Mountains, East Antarctica. *Journal of Petrology*, **50**, 2017–2041.

Powell, R. & Holland, T., 1988. An internally consistent dataset with uncertainties and correlations: 3. Applications to geobarometry, worked examples and a computer program. *Journal of Metamorphic Geology*, **6**, 173–204.

Ray, G., 1974. The Structural and Metamorphic geology of Northern Malawi. *Journal of the Geological Society, London*, **130**, 427–440.

Ring, U., 1993. Aspects of the kinematic history and mechanisms of superposition of the proterozoic mobile belts of eastern Central Africa (northern Malawi and southern Tanzania). *Precambrian Research*, **62**, 207–226.

Ring, U., 1994. The influence of pre-existing structure on the evolution of the Cenozoic Malawi rift (East African rift system). *Tectonics*, **13**, 313–326.

Ring, U., Betzler, C. & Delvaux, D., 1992. Normal vs. strike-slip faulting during rift development in East Africa: The Malawi rift. *Geology*, **20**, 1015–1018.

Ring, U., Kroner, A. & Toulkeridis, T., 1997. Palaeoproterozoic granulite-facies metamorphism and granitoid intrusions in the Ubendian-Usagaran Orogen of northern Malawi, east-central Africa. *Precambrian Research*, **85**, 27–51.

Ring, U., Kroner, A., Buchwaldt, R., Toulkeridis, T. & Layer, P., 2002. Shear-zone patterns and eclogite-facies metamorphism in the Mozambique belt of northern Malawi, east-central Africa: implications for the assembly of Gondwana. *Precambrian Research*, **116**, 19–56.

Slama, J., Kosler, J., Condon, D., Crowley, J., Gerdes, A., Hanchar, J., Horstwood, M., Morris, G., Nasdala, L., Norberg, N., Schaltegger, U., Schoene, B., Tubrett, M. & Whitehouse, M., 2008. Pleovice zircona new natural reference material for UPb and Hf isotopic microanalysis. *Chemical Geology*, **249**, 1–35.

Sommer, H., Kroner, A., Hauzenberger, C., Muhongo, S. & Windgate, M., 2003. Metamorphic petrology and zircon geochronology of high-grade rocks from the central Mozambique Belt of Tanzania: crustal recycling of Archean and Palaeoproterozoic material during the Pan-African orogeny. *Journal of Metamorphic Geology*, **21**, 915–934.

Spear, F. & Pyle, J., 2010. Theoretical modeling of monazite growth in a low-Ca metapelite. *Chemical Geology*, **273**, 111–119.

White, R. & Powell, R., 2002. Melt loss and the preservation of granulite facies mineral assemblages. *Journal of Metamorphic Geology*, **20**, 621–632.

White, R., Powell, R., Holland, T., Johnson, T. & Green, E., 2014. New mineral activitycomposition relations for thermodynamic calculations in metapelitic systems). *Journal of Metamorphic Geology*, **32**, 261–286.

Williams, I., Buick, I. & Cartwright, I., 1996. An extended episode of early Mesoproterozoic metamorphic fluid flow in the Reynolds Range, central Australia. *Journal of Metamorphic Geology*, **14**, 29–48.

Wilson, T., 1966. Did the Atlantic Close and then Re-open? *Nature*, **211**, 676–681.

Appendix

MINERAL CHEMISTRY FOR CHILUMBA GARNET-AMPHIBOLITES (SAMPLE M07)

	7-hb-1	7-hb-2	7-hb-3	7-hb-4	7-hb-5	7-hb-6	7-hb-7	7-hb-8	7-hb-9	7-hb-10	7-hb-11	7-pl-1	7-pl-2
	hb	hb	hb	hb	hb	hb	hb	hb	hb	hb	hb	pl	pl
SiO2	43.03	42.70	42.55	42.15	43.82	43.14	41.76	42.60	42.44	42.47	42.26	48.79	52.71
TiO2	0.95	0.91	1.00	1.14	0.82	0.91	1.13	1.10	0.87	0.94	1.09	0.00	0.00
Al2O3	15.20	14.85	15.13	15.15	14.22	14.96	15.62	15.31	15.05	14.90	15.43	33.40	30.49
Cr2O3	0.02	0.00	0.00	0.01	0.07	0.01	0.04	0.00	0.00	0.01	0.00	0.06	0.04
FeO	15.92	15.85	15.78	15.72	15.74	15.77	16.00	15.56	16.06	16.06	16.11	0.23	0.12
MnO	0.63	0.56	0.55	0.49	0.58	0.59	0.55	0.47	0.61	0.63	0.65	0.01	0.10
MgO	11.19	11.15	10.97	10.86	11.46	11.23	11.11	11.14	11.03	10.82	10.54	0.01	0.00
CaO	11.17	11.12	11.30	11.27	11.11	11.12	11.27	11.35	11.25	11.18	11.06	15.94	12.96
Na2O	1.28	1.30	1.28	1.21	1.35	1.20	1.38	1.37	1.40	1.23	1.35	2.46	4.05
K2O	0.61	0.62	0.73	0.78	0.50	0.60	0.81	0.64	0.67	0.77	0.71	0.04	0.03
Total	**100.00**	**99.05**	**99.30**	**98.77**	**99.67**	**99.53**	**99.68**	**99.54**	**99.38**	**99.01**	**99.19**	**100.93**	**100.50**
num ox	23.00	23.00	23.00	23.00	23.00	23.00	23.00	23.00	23.00	23.00	23.00	8.00	8.00
Si	6.24	6.26	6.23	6.20	6.36	6.28	6.11	6.21	6.22	6.24	6.20	2.21	2.38
Ti	0.10	0.10	0.11	0.13	0.09	0.10	0.12	0.12	0.10	0.10	0.12	0.00	0.00
Al	2.60	2.57	2.61	2.63	2.43	2.57	2.69	2.63	2.60	2.58	2.67	1.79	1.62
Cr	0.00	0.00	0.00	0.00	0.01	0.00	0.00	0.00	0.00	0.00	0.00	0.00	0.00
Fe	1.93	1.94	1.93	1.93	1.91	1.92	1.96	1.90	1.97	1.97	1.98	0.01	0.00
Mn	0.08	0.07	0.07	0.06	0.07	0.07	0.07	0.06	0.08	0.08	0.08	0.00	0.00
Mg	2.42	2.44	2.39	2.38	2.48	2.44	2.42	2.42	2.41	2.37	2.30	0.00	0.00
Ca	1.74	1.75	1.77	1.78	1.73	1.73	1.77	1.77	1.77	1.76	1.74	0.77	0.63
Na	0.36	0.37	0.36	0.34	0.38	0.34	0.39	0.39	0.40	0.35	0.38	0.22	0.35
K	0.11	0.12	0.14	0.15	0.09	0.11	0.15	0.12	0.12	0.15	0.13	0.00	0.00
Total	**15.59**	**15.60**	**15.61**	**15.60**	**15.56**	**15.56**	**15.69**	**15.61**	**15.65**	**15.61**	**15.60**	**5.00**	**4.99**
xfe	0.59	0.59	0.59	0.59	0.58	0.58	0.59	0.58	0.59	0.60	0.60		
XAb												0.22	0.36
XAn												0.78	0.64
XOr												0.00	0.00

	7-pl-3	7-pl-4	7-pl-5	7-pl-6	7-pl-7	7-pl-8	7-pl-9	7-pl-10	7-gt-1	7-gt-2	7-gt-3	7-gt-4	7-gt-5
	pl	pl	pl	pl	pl	pl	pl	pl	gt	gt	gt	gt	gt
SiO2	48.40	47.84	55.38	52.77	51.39	50.97	48.78	48.47	37.33	37.35	37.48	37.45	37.43
TiO2	0.00	0.00	0.01	0.02	0.00	0.00	0.00	0.02	0.02	0.06	0.06	0.04	0.02
Al2O3	33.64	33.42	28.91	30.43	31.41	31.67	33.44	33.45	21.99	21.96	21.67	21.91	21.64
Cr2O3	0.00	0.00	0.01	0.00	0.06	0.00	0.01	0.03	0.03	0.00	0.03	0.05	0.00
FeO	0.09	0.09	0.07	0.11	0.12	0.26	0.16	0.16	27.27	26.39	27.09	27.29	27.60
MnO	0.00	0.03	0.04	0.03	0.03	0.07	0.03	0.03	3.59	3.43	1.19	2.64	1.99
MgO	0.00	0.00	0.02	0.00	0.00	0.00	0.01	0.01	2.86	3.44	3.73	3.24	3.34
CaO	16.44	16.32	11.01	12.45	13.73	13.97	15.71	16.04	7.38	7.32	8.16	7.54	7.64
Na2O	2.23	2.30	5.21	4.43	3.93	3.68	2.58	2.43	0.00	0.00	0.01	0.03	0.01
K2O	0.02	0.02	0.04	0.03	0.04	0.03	0.02	0.03					
Total	**100.82**	**100.02**	**100.70**	**100.27**	**100.70**	**100.64**	**100.73**	**100.66**	**100.47**	**99.95**	**99.42**	**100.19**	**99.68**
num ox	8.00	8.00	8.00	8.00	8.00	8.00	8.00	8.00	12.00	12.00	12.00	12.00	12.00
Si	2.20	2.19	2.48	2.38	2.32	2.31	2.21	2.20	2.95	2.96	2.97	2.96	2.97
Ti	0.00	0.00	0.00	0.00	0.00	0.00	0.00	0.00	0.00	0.00	0.00	0.00	0.00
Al	1.80	1.81	1.52	1.62	1.67	1.69	1.79	1.79	2.05	2.05	2.03	2.04	2.03
Cr	0.00	0.00	0.00	0.00	0.00	0.00	0.00	0.00	0.00	0.00	0.00	0.00	0.00
Fe	0.00	0.00	0.00	0.00	0.00	0.01	0.01	0.01	1.80	1.75	1.80	1.80	1.83
Mn	0.00	0.00	0.00	0.00	0.00	0.00	0.00	0.00	0.24	0.23	0.08	0.18	0.13
Mg	0.00	0.00	0.00	0.00	0.00	0.00	0.00	0.00	0.34	0.41	0.44	0.38	0.40
Ca	0.80	0.80	0.53	0.60	0.66	0.68	0.76	0.78	0.63	0.62	0.69	0.64	0.65
Na	0.20	0.20	0.45	0.39	0.34	0.32	0.23	0.21	0.00	0.00	0.00	0.01	0.00
K	0.00	0.00	0.00	0.00	0.00	0.00	0.00	0.00	0.00	0.00	0.00	0.00	0.00
Total	**5.00**	**5.01**	**4.99**	**5.00**	**5.01**	**5.01**	**5.00**	**5.01**	**8.02**	**8.01**	**8.01**	**8.02**	**8.01**
xfe													
XAb	0.20	0.20	0.46	0.39	0.34	0.32	0.23	0.21					
XAn	0.80	0.80	0.54	0.61	0.66	0.68	0.77	0.78					
XOr	0.00	0.00	0.00	0.00	0.00	0.00	0.00	0.00					
Xalm									0.60	0.58	0.60	0.60	0.61
Xgrs									0.21	0.21	0.23	0.21	0.22
Xpyr									0.11	0.14	0.15	0.13	0.13
Xsps									0.08	0.08	0.03	0.06	0.04

	7-gt-6 gt	7-gt-7 gt	7-gt-8 gt	7-gt-9 gt	7-gt-10 gt	7-bi-1 bi	7-bi-2 bi	7-bi-3 bi	7-bi-4 bi	7-bi-6 bi	7-bi-7 bi	7-bi-8 bi
SiO2	37.37	37.34	37.07	37.24	36.99	37.60	36.97	37.68	37.94	37.11	37.71	37.82
TiO2	0.05	0.03	0.03	0.06	0.00	1.57	2.13	1.63	2.01	1.49	1.34	1.85
Al2O3	21.88	21.82	21.97	21.94	21.82	17.07	17.07	17.43	16.67	16.84	16.23	16.69
Cr2O3	0.00	0.01	0.01	0.00	0.00	0.04	0.02	0.01	0.04	0.04	0.05	0.00
FeO	26.44	27.02	27.46	28.11	26.92	15.91	16.33	16.28	15.34	17.31	16.42	15.94
MnO	2.92	3.45	3.66	3.34	3.22	0.07	0.12	0.10	0.18	0.14	0.15	0.07
MgO	3.68	3.05	2.70	2.72	3.12	14.67	13.75	14.09	14.83	14.51	14.59	14.53
CaO	7.59	7.48	7.38	7.45	7.51	0.19	0.00	0.02	0.00	0.36	0.13	0.03
Na2O	0.00	0.00	0.00	0.00	0.05	0.19	0.20	0.13	0.20	0.24	0.15	0.16
K2O						8.04	8.96	8.72	8.86	7.50	7.94	8.72
Total	**99.93**	**100.20**	**100.28**	**100.86**	**99.63**	**95.35**	**95.56**	**96.09**	**96.07**	**95.53**	**94.70**	**95.81**
num ox	12.00	12.00	12.00	12.00	12.00	11.00	11.00	11.00	11.00	11.00	11.00	11.00
Si	2.96	2.96	2.95	2.94	2.95	2.78	2.76	2.78	2.79	2.76	2.82	2.80
Ti	0.00	0.00	0.00	0.00	0.00	0.09	0.12	0.09	0.11	0.08	0.08	0.10
Al	2.04	2.04	2.06	2.05	2.05	1.49	1.50	1.52	1.45	1.48	1.43	1.46
Cr	0.00	0.00	0.00	0.00	0.00	0.00	0.00	0.00	0.00	0.00	0.00	0.00
Fe	1.75	1.79	1.82	1.86	1.79	0.99	1.02	1.00	0.94	1.08	1.03	0.99
Mn	0.20	0.23	0.25	0.22	0.22	0.00	0.01	0.01	0.01	0.01	0.01	0.00
Mg	0.43	0.36	0.32	0.32	0.37	1.62	1.53	1.55	1.63	1.61	1.63	1.60
Ca	0.64	0.64	0.63	0.63	0.64	0.01	0.00	0.00	0.00	0.03	0.01	0.00
Na	0.00	0.00	0.00	0.00	0.01	0.03	0.03	0.02	0.03	0.04	0.02	0.02
K	0.00	0.00	0.00	0.00	0.00	0.76	0.85	0.82	0.83	0.71	0.76	0.82
Total	**8.02**	**8.02**	**8.02**	**8.03**	**8.03**	**7.77**	**7.81**	**7.79**	**7.80**	**7.79**	**7.78**	**7.80**
xfe						0.52	0.54	0.54	0.51	0.54	0.53	0.52
Xalm	0.58	0.59	0.60	0.61	0.59							
Xgrs	0.21	0.21	0.21	0.21	0.21							
Xpyr	0.14	0.12	0.11	0.11	0.12							
Xsps	0.06	0.08	0.08	0.07	0.07							

	7-bi-9 bi	7-bi-10 bi
SiO2	37.81	37.88
TiO2	1.84	1.85
Al2O3	16.99	16.79
Cr2O3	0.00	0.00
FeO	15.96	15.85
MnO	0.16	0.08
MgO	14.41	14.74
CaO	0.02	0.02
Na2O	0.22	0.14
K2O	8.73	8.91
Total	**96.14**	**96.26**
num ox	11.00	11.00
Si	2.79	2.79
Ti	0.10	0.10
Al	1.48	1.46
Cr	0.00	0.00
Fe	0.98	0.98
Mn	0.01	0.01
Mg	1.58	1.62
Ca	0.00	0.00
Na	0.03	0.02
K	0.82	0.84
Total	**7.80**	**7.81**
xfe	0.53	0.52

MINERAL CHEMISTRY FOR CHILUMBA GARNET-AMPHIBOLITES (SAMPLE M08)

	08-hb-1	08-hb-2	08-hb-3	08-hb-4	08-hb-5	08-hb-6	08-hb-7	08-hb-8	08-hb-9	08-hb-10	08-pl-1	08-pl-2
	hb	hb	hb	hb	hb	hb	hb	hb	hb	hb	pl	pl
SiO2	40.73	41.24	41.46	41.12	41.47	40.99	41.29	41.23	41.36	41.34	56.04	56.83
TiO2	1.73	1.75	1.65	1.81	1.71	1.83	1.82	1.88	1.84	1.91	0.01	0.01
Al2O3	14.73	14.82	14.89	14.66	14.44	14.55	14.53	14.59	14.51	14.76	28.24	28.11
Cr2O3	0.00	0.00	0.00	0.03	0.00	0.00	0.03	0.01	0.00	0.07	0.03	0.02
FeO	18.39	17.95	18.47	17.96	18.27	17.99	17.86	18.43	18.39	18.49	0.20	0.21
MnO	0.24	0.23	0.14	0.18	0.19	0.18	0.22	0.22	0.22	0.20	0.00	0.02
MgO	9.34	9.22	9.28	9.22	9.62	9.35	9.52	9.15	9.50	9.16	0.00	0.00
CaO	11.99	11.71	11.89	11.95	11.85	11.77	11.85	11.89	11.95	11.86	8.79	10.19
Na2O	1.42	1.59	1.59	1.57	1.57	1.49	1.64	1.60	1.51	1.53	5.60	5.68
K2O	1.44	1.42	1.42	1.43	1.42	1.43	1.33	1.41	1.44	1.47	0.22	0.23
Total	**100.01**	**99.93**	**100.79**	**99.93**	**100.54**	**99.58**	**100.09**	**100.41**	**100.72**	**100.79**	**99.14**	**101.31**
num ox	23.00	23.00	23.00	23.00	23.00	23.00	23.00	23.00	23.00	23.00	8.00	8.00
Si	6.05	6.11	6.10	6.10	6.12	6.10	6.11	6.10	6.10	6.09	2.53	2.52
Ti	0.19	0.19	0.18	0.20	0.19	0.20	0.20	0.21	0.20	0.21	0.00	0.00
Al	2.58	2.59	2.58	2.56	2.51	2.55	2.53	2.54	2.52	2.56	1.50	1.47
Cr	0.00	0.00	0.00	0.00	0.00	0.00	0.00	0.00	0.00	0.01	0.00	0.00
Fe	2.29	2.22	2.27	2.23	2.25	2.24	2.21	2.28	2.27	2.28	0.01	0.01
Mn	0.03	0.03	0.02	0.02	0.02	0.02	0.03	0.03	0.03	0.02	0.00	0.00
Mg	2.07	2.04	2.03	2.04	2.11	2.07	2.10	2.02	2.09	2.01	0.00	0.00
Ca	1.91	1.86	1.87	1.90	1.87	1.88	1.88	1.88	1.89	1.87	0.43	0.48
Na	0.41	0.46	0.45	0.45	0.45	0.43	0.47	0.46	0.43	0.44	0.49	0.49
K	0.27	0.27	0.27	0.27	0.27	0.27	0.25	0.27	0.27	0.28	0.01	0.01
Total	**15.80**	**15.76**	**15.79**	**15.78**	**15.80**	**15.77**	**15.78**	**15.78**	**15.79**	**15.77**	**4.97**	**4.99**
xfe	0.66	0.66	0.67	0.66	0.66	0.66	0.65	0.67	0.66	0.67		
XAb											0.53	0.50
XAn											0.46	0.49
XOr											0.01	0.01

	08-pl-3	08-pl-4	08-pl-5	08-pl-6	08-pl-7	08-pl-08	08-pl-9	08-pl-10	08-pl-11	08-gt-1	08-gt-2	08-gt-3
	pl	pl	pl	pl	pl	pl	pl	pl	pl	gt	gt	gt
SiO2	58.00	56.29	55.25	56.53	56.91	57.14	57.08	57.70	56.45	38.76	38.56	38.73
TiO2	0.02	0.01	0.03	0.02	0.00	0.00	0.00	0.01	0.01	0.05	0.04	0.07
Al2O3	27.34	28.30	28.92	28.37	28.00	28.13	27.95	27.46	28.68	21.91	21.80	22.32
Cr2O3	0.00	0.00	0.01	0.04	0.04	0.02	0.01	0.03	0.04	0.01	0.00	0.02
FeO	0.09	0.16	0.16	0.16	0.11	0.14	0.12	0.11	0.21	24.72	25.00	24.64
MnO	0.06	0.02	0.00	0.02	0.08	0.00	0.05	0.01	0.00	1.71	1.42	1.63
MgO	0.01	0.00	0.00	0.00	0.00	0.00	0.00	0.01	0.01	4.60	4.70	4.75
CaO	8.30	9.10	9.70	8.75	8.78	8.69	8.83	8.52	9.29	9.09	9.11	8.42
Na2O	6.20	5.62	5.27	5.84	5.90	5.70	5.72	6.07	5.42	0.04	0.00	0.00
K2O	0.26	0.17	0.16	0.21	0.21	0.24	0.26	0.22	0.17			
Total	**100.27**	**99.67**	**99.50**	**99.93**	**100.04**	**100.06**	**100.02**	**100.14**	**100.28**	**100.89**	**100.63**	**100.58**
num ox	8.00	8.00	8.00	8.00	8.00	8.00	8.00	8.00	8.00	12.00	12.00	12.00
Si	2.58	2.53	2.49	2.53	2.55	2.55	2.55	2.57	2.52	3.00	2.99	3.00
Ti	0.00	0.00	0.00	0.00	0.00	0.00	0.00	0.00	0.00	0.00	0.00	0.00
Al	1.44	1.50	1.54	1.50	1.48	1.48	1.47	1.44	1.51	2.00	1.99	2.04
Cr	0.00	0.00	0.00	0.00	0.00	0.00	0.00	0.00	0.00	0.00	0.00	0.00
Fe	0.00	0.01	0.01	0.01	0.00	0.01	0.00	0.00	0.01	1.60	1.62	1.59
Mn	0.00	0.00	0.00	0.00	0.00	0.00	0.00	0.00	0.00	0.11	0.09	0.11
Mg	0.00	0.00	0.00	0.00	0.00	0.00	0.00	0.00	0.00	0.53	0.54	0.55
Ca	0.40	0.44	0.47	0.42	0.42	0.42	0.42	0.41	0.44	0.75	0.76	0.70
Na	0.54	0.49	0.46	0.51	0.51	0.49	0.50	0.53	0.47	0.01	0.00	0.00
K	0.01	0.01	0.01	0.01	0.01	0.01	0.01	0.01	0.01	0.00	0.00	0.00
Total	**4.97**	**4.97**	**4.97**	**4.98**	**4.98**	**4.96**	**4.97**	**4.97**	**4.96**	**8.00**	**8.01**	**7.98**
XAb	0.57	0.52	0.49	0.54	0.54	0.53	0.53	0.56	0.51			
XAn	0.42	0.47	0.50	0.45	0.45	0.45	0.45	0.43	0.48			
XOr	0.02	0.01	0.01	0.01	0.01	0.01	0.02	0.01	0.01			
Xalm										0.53	0.54	0.54
Xgrs										0.25	0.25	0.24
Xpyr										0.18	0.18	0.19
Xsps										0.04	0.03	0.04

	08-gt-4	08-gt-5	08-gt-6	08-gt-7	08-gt-9	08-gt-10	08-gt-11
	gt	gt	gt	gt	gt	gt	gt
SiO2	38.19	38.05	38.34	38.37	38.39	38.49	41.05
TiO2	0.13	0.16	0.08	0.02	0.06	0.06	1.88
Al2O3	21.92	21.10	21.49	22.27	22.22	22.12	13.73
Cr2O3	0.03	0.01	0.04	0.01	0.00	0.05	0.03
FeO	25.11	24.87	23.09	25.61	25.44	24.25	17.44
MnO	1.82	1.12	0.99	2.03	1.80	1.39	0.24
MgO	4.22	4.39	4.11	4.43	4.61	4.55	9.20
CaO	8.98	9.23	9.66	7.66	7.92	9.69	10.89
Na2O	0.00	0.09	0.04	0.02	0.00	0.02	1.45
K2O							
Total	**100.41**	**99.02**	**97.83**	**100.42**	**100.44**	**100.62**	**95.91**
num ox	12.00	12.00	12.00	12.00	12.00	12.00	12.00
Si	2.98	3.01	3.04	2.99	2.99	2.98	3.27
Ti	0.01	0.01	0.00	0.00	0.00	0.00	0.11
Al	2.02	1.96	2.01	2.04	2.04	2.02	1.29
Cr	0.00	0.00	0.00	0.00	0.00	0.00	0.00
Fe	1.64	1.64	1.53	1.67	1.65	1.57	1.16
Mn	0.12	0.08	0.07	0.13	0.12	0.09	0.02
Mg	0.49	0.52	0.49	0.51	0.53	0.53	1.09
Ca	0.75	0.78	0.82	0.64	0.66	0.80	0.93
Na	0.00	0.01	0.01	0.00	0.00	0.00	0.22
K	0.00	0.00	0.00	0.00	0.00	0.00	0.00
Total	**8.00**	**8.01**	**7.96**	**7.99**	**7.99**	**8.00**	**8.09**
Xalm	0.55	0.54	0.53	0.56	0.56	0.53	0.36
Xgrs	0.25	0.26	0.28	0.22	0.22	0.27	0.29
Xpyr	0.16	0.17	0.17	0.17	0.18	0.18	0.34
Xsps	0.04	0.02	0.02	0.05	0.04	0.03	0.01

MINERAL CHEMISTRY FOR CHILUMBA GARNET-AMPHIBOLITES (SAMPLE M09)

	09-hb-1	09-hb-2	09-hb-3	09-gt-4	09-hb-5	09-hb-6	09-hb-7	09-hb-8	09-gt-1	09-gt-2	09-gt-3	09-gt-4
	hb	hb	hb	hb	hb	hb	hb	hb	gt	gt	gt	gt
SiO2	41.46	41.23	41.22	41.55	40.96	41.33	41.35	41.12	37.93	38.33	38.29	38.43
TiO2	1.75	1.87	1.79	1.80	1.96	1.68	1.92	1.70	0.05	0.01	0.00	0.00
Al2O3	13.99	14.30	14.92	14.55	14.60	14.81	14.50	14.64	21.54	21.93	21.92	22.33
Cr2O3	0.02	0.03	0.01	0.08	0.03	0.01	0.03	0.01	0.02	0.00	0.00	0.05
FeO	18.72	18.97	18.51	18.82	18.81	18.33	18.43	18.30	25.75	25.18	26.35	27.47
MnO	0.14	0.15	0.15	0.19	0.19	0.15	0.13	0.19	1.44	1.36	1.47	1.57
MgO	9.51	9.00	8.75	9.01	8.96	9.12	9.28	9.01	4.27	4.39	4.39	4.54
CaO	11.87	11.83	12.06	11.99	12.12	12.04	11.97	11.85	8.38	8.65	8.10	6.56
Na2O	1.55	1.51	1.62	1.62	1.67	1.48	1.50	1.75	0.01	0.04	0.02	0.01
K2O	1.22	1.29	1.27	1.29	1.32	1.24	1.28	1.28				
Total	**100.23**	**100.19**	**100.30**	**100.90**	**100.62**	**100.20**	**100.39**	**99.85**	**99.39**	**99.89**	**100.54**	**100.96**
num ox	23.00	23.00	23.00	23.00	23.00	23.00	23.00	23.00	12.00	12.00	12.00	12.00
Si	6.14	6.12	6.10	6.12	6.06	6.11	6.11	6.11	2.99	3.00	2.99	2.98
Ti	0.19	0.21	0.20	0.20	0.22	0.19	0.21	0.19	0.00	0.00	0.00	0.00
Al	2.44	2.50	2.60	2.53	2.55	2.58	2.52	2.56	2.00	2.02	2.02	2.04
Cr	0.00	0.00	0.00	0.01	0.00	0.00	0.00	0.00	0.00	0.00	0.00	0.00
Fe	2.32	2.35	2.29	2.32	2.33	2.27	2.28	2.27	1.70	1.65	1.72	1.78
Mn	0.02	0.02	0.02	0.02	0.02	0.02	0.02	0.02	0.10	0.09	0.10	0.10
Mg	2.10	1.99	1.93	1.98	1.98	2.01	2.04	2.00	0.50	0.51	0.51	0.53
Ca	1.88	1.88	1.91	1.89	1.92	1.91	1.89	1.89	0.71	0.72	0.68	0.55
Na	0.45	0.43	0.46	0.46	0.48	0.42	0.43	0.50	0.00	0.01	0.00	0.00
K	0.23	0.24	0.24	0.24	0.25	0.23	0.24	0.24	0.00	0.00	0.00	0.00
Total	**15.78**	**15.76**	**15.75**	**15.77**	**15.81**	**15.74**	**15.75**	**15.79**	**8.00**	**8.00**	**8.01**	**7.99**
xfe	0.66	0.68	0.68	0.68	0.68	0.67	0.67	0.67				
Xalm									0.57	0.55	0.57	0.60
Xgrs									0.24	0.24	0.23	0.18
Xpyr									0.17	0.17	0.17	0.18
Xsps									0.03	0.03	0.03	0.03

	09-gt-5	09-gt-6	09-gt-7	09-gt-8	09-gt-9	09-gt-10	9-pl-01	9-pl-02	9-pl-3	9-pl-4	9-pl-5	9-pl-06
	gt	gt	gt	gt	gt	gt	pl	pl	pl	pl	pl	pl
SiO2	38.76	38.66	38.52	38.31	38.61	40.67	57.38	56.94	58.90	60.16	58.75	58.41
TiO2	0.03	0.02	0.08	0.07	0.10	1.83	0.00	0.01	0.00	0.02	0.01	0.00
Al2O3	21.69	21.95	21.65	21.49	21.80	13.97	27.62	27.33	26.73	25.38	26.32	27.01
Cr2O3	0.01	0.02	0.04	0.02	0.01	0.04	0.01	0.02	0.00	0.01	0.00	0.00
FeO	25.95	25.42	25.76	26.24	25.04	17.80	0.17	0.10	0.14	0.11	0.16	0.15
MnO	1.41	1.33	1.24	1.46	1.26	0.11	0.03	0.01	0.04	0.06	0.03	0.04
MgO	4.52	4.25	4.46	4.38	4.21	8.53	0.00	0.00	0.02	0.01	0.01	0.00
CaO	8.63	9.20	8.86	8.67	8.96	10.90	8.77	8.80	8.33	7.10	8.14	8.79
Na2O	0.05	0.05	0.02	0.05	0.05	1.51	6.32	6.24	6.51	6.92	6.78	5.91
K2O							0.18	0.22	0.24	0.29	0.23	0.22
Total	**101.05**	**100.90**	**100.64**	**100.70**	**100.03**	**95.35**	**100.48**	**99.66**	**100.91**	**100.06**	**100.42**	**100.54**
num ox	12.00	12.00	12.00	12.00	12.00	12.00	8.00	8.00	8.00	8.00	8.00	8.00
Si	3.00	3.00	3.00	2.99	3.01	3.26	2.56	2.56	2.61	2.68	2.62	2.60
Ti	0.00	0.00	0.00	0.00	0.01	0.11	0.00	0.00	0.00	0.00	0.00	0.00
Al	1.98	2.01	1.99	1.98	2.00	1.32	1.45	1.45	1.40	1.33	1.38	1.41
Cr	0.00	0.00	0.00	0.00	0.00	0.00	0.00	0.00	0.00	0.00	0.00	0.00
Fe	1.68	1.65	1.68	1.71	1.63	1.19	0.01	0.00	0.01	0.00	0.01	0.01
Mn	0.09	0.09	0.08	0.10	0.08	0.01	0.00	0.00	0.00	0.00	0.00	0.00
Mg	0.52	0.49	0.52	0.51	0.49	1.02	0.00	0.00	0.00	0.00	0.00	0.00
Ca	0.72	0.76	0.74	0.72	0.75	0.94	0.42	0.42	0.40	0.34	0.39	0.42
Na	0.01	0.01	0.00	0.01	0.01	0.23	0.55	0.54	0.56	0.60	0.59	0.51
K	0.00	0.00	0.00	0.00	0.00	0.00	0.01	0.01	0.01	0.02	0.01	0.01
Total	**8.01**	**8.00**	**8.01**	**8.02**	**7.98**	**8.08**	**4.99**	**4.99**	**4.98**	**4.97**	**4.99**	**4.96**
XAb							0.56	0.55	0.58	0.63	0.59	0.54
XAn							0.43	0.43	0.41	0.36	0.39	0.45
XOr							0.01	0.01	0.01	0.02	0.01	0.01
Xalm	0.56	0.55	0.56	0.56	0.55	0.38						
Xgrs	0.24	0.26	0.25	0.24	0.25	0.30						
Xpyr	0.17	0.16	0.17	0.17	0.17	0.32						
Xsps	0.03	0.03	0.03	0.03	0.03	0.00						

	9-pl-7 pl	9-pl-8 pl	9-pl-9 pl	9-pl-10 pl	9-pl-11 pl
SiO2	58.03	57.98	57.77	56.76	56.56
TiO2	0.00	0.01	0.00	0.00	0.03
Al2O3	26.99	27.14	27.32	28.22	27.91
Cr2O3	0.00	0.00	0.00	0.03	0.00
FeO	0.13	0.10	0.20	0.15	0.15
MnO	0.05	0.00	0.00	0.04	0.01
MgO	0.01	0.00	0.00	0.01	0.00
CaO	8.69	8.80	8.67	9.68	9.93
Na2O	6.36	6.39	6.22	5.92	5.89
K2O	0.22	0.22	0.24	0.11	0.18
Total	**100.47**	**100.64**	**100.42**	**100.91**	**100.66**
num ox	8.00	8.00	8.00	8.00	8.00
Si	2.59	2.58	2.57	2.53	2.53
Ti	0.00	0.00	0.00	0.00	0.00
Al	1.42	1.42	1.44	1.48	1.47
Cr	0.00	0.00	0.00	0.00	0.00
Fe	0.00	0.00	0.01	0.01	0.01
Mn	0.00	0.00	0.00	0.00	0.00
Mg	0.00	0.00	0.00	0.00	0.00
Ca	0.41	0.42	0.41	0.46	0.48
Na	0.55	0.55	0.54	0.51	0.51
K	0.01	0.01	0.01	0.01	0.01
Total	**4.99**	**4.99**	**4.98**	**4.99**	**5.00**
XAb	0.56	0.56	0.56	0.52	0.51
XAn	0.42	0.43	0.43	0.47	0.48
XOr	0.01	0.01	0.01	0.01	0.01

MINERAL CHEMISTRY FOR MLOWE GRANULITES (SAMPLE M13)

	13 pl 3	13 pl 6	13 pl 9	13 ksp 11	13 ksp 12	13 ksp 13	13 ksp 14	13 ksp 15	13 ksp 16	13 ksp 17	13 ksp 18	13 ksp 19
	pl	pl	pl	ksp	ksp	ksp	ksp	ksp	ksp	ksp	ksp	ksp
SiO2	69.46	68.91	68.58	65.93	65.94	65.52	65.21	65.34	66.30	65.70	65.00	65.20
TiO2	0.01	0.02	0.00	0.03	0.03	0.03	0.02	0.00	0.03	0.02	0.01	0.00
Al2O3	19.59	19.69	19.42	18.72	18.86	18.56	18.62	18.78	18.89	18.57	18.43	18.30
Cr2O3	0.00	0.00	0.00	0.00	0.00	0.01	0.00	0.00	0.00	0.00	0.00	0.02
FeO	0.03	0.02	0.02	0.02	0.00	0.00	0.07	0.03	0.08	0.03	0.00	0.01
MnO	0.05	0.02	0.02	0.10	0.05	0.05	0.02	0.01	0.04	0.01	0.01	0.04
MgO	0.01	0.00	0.02	0.00	0.00	0.00	0.00	0.00	0.01	0.03	0.00	0.03
CaO	0.19	0.28	0.26	0.00	0.00	0.00	0.00	0.00	0.00	0.00	0.00	0.00
Na2O	11.04	11.00	10.86	1.37	2.18	0.92	0.82	0.80	1.59	0.88	0.76	0.73
K2O	0.06	0.05	0.05	14.46	13.28	15.32	15.58	15.58	13.74	15.48	15.76	15.56
Total	**100.44**	**99.99**	**99.23**	**100.63**	**100.35**	**100.42**	**100.36**	**100.53**	**100.69**	**100.72**	**99.98**	**99.89**
num ox	8.00	8.00	8.00	8.00	8.00	8.00	8.00	8.00	8.00	8.00	8.00	8.00
Si	3.01	3.00	3.01	3.00	3.00	3.00	2.99	2.99	3.01	3.00	3.00	3.01
Ti	0.00	0.00	0.00	0.00	0.00	0.00	0.00	0.00	0.00	0.00	0.00	0.00
Al	1.00	1.01	1.00	1.01	1.01	1.00	1.01	1.01	1.01	1.00	1.00	0.99
Cr	0.00	0.00	0.00	0.00	0.00	0.00	0.00	0.00	0.00	0.00	0.00	0.00
Fe	0.00	0.00	0.00	0.00	0.00	0.00	0.00	0.00	0.00	0.00	0.00	0.00
Mn	0.00	0.00	0.00	0.00	0.00	0.00	0.00	0.00	0.00	0.00	0.00	0.00
Mg	0.00	0.00	0.00	0.00	0.00	0.00	0.00	0.00	0.00	0.00	0.00	0.00
Ca	0.01	0.01	0.01	0.00	0.00	0.00	0.00	0.00	0.00	0.00	0.00	0.00
Na	0.93	0.93	0.92	0.12	0.19	0.08	0.07	0.07	0.14	0.08	0.07	0.07
K	0.00	0.00	0.00	0.84	0.77	0.90	0.91	0.91	0.79	0.90	0.93	0.92
Total	**4.95**	**4.96**	**4.95**	**4.97**	**4.98**	**4.98**	**4.99**	**4.99**	**4.96**	**4.99**	**5.00**	**4.99**
xfe												
XAb	0.99	0.98	0.98	0.13	0.20	0.08	0.07	0.07	0.15	0.08	0.07	0.07
XAn	0.01	0.01	0.01	0.00	0.00	0.00	0.00	0.00	0.00	0.00	0.00	0.00
XOr	0.00	0.00	0.00	0.87	0.80	0.92	0.93	0.93	0.85	0.92	0.93	0.93

	13 ksp 20	13 cor 3	13 cor 5	13 cor 6	13 cor 9	13 cor 10	13-gt-1	13-gt-4	13-gt-7	13-gt-10	13-cd-2	13-cd-3
	ksp	cor	cor	cor	cor	cor	gt	gt	gt	gt	cd	cd
SiO2	64.98	0.01	0.02	0.01	0.03	0.02	37.47	37.03	37.46	37.49	49.92	49.72
TiO2	0.01	0.00	0.00	0.06	0.00	0.00	0.02	0.03	0.02	0.04	0.00	0.01
Al2O3	18.58	101.26	102.50	101.87	103.19	102.47	22.07	21.85	22.05	22.12	32.90	32.72
Cr2O3	0.01	0.10	0.06	0.07	0.15	0.11	0.00	0.03	0.04	0.04	0.00	0.00
FeO	0.08	0.64	0.52	0.60	0.59	0.54	32.35	31.87	31.70	32.43	6.52	6.56
MnO	0.08	0.05	0.02	0.01	0.04	0.02	1.78	2.20	2.13	1.98	0.10	0.03
MgO	0.00	0.03	0.00	0.00	0.01	0.02	5.70	5.29	5.46	5.34	10.05	9.58
CaO	0.02	0.00	0.01	0.00	0.00	0.01	0.75	0.99	0.95	0.89	0.02	0.00
Na2O	1.72	0.01	0.01	0.00	0.01	0.00	0.01	0.00	0.04	0.00	0.12	0.11
K2O	14.21	0.01	0.00	0.00	0.00	0.02					0.00	0.02
Total	**99.69**	**102.12**	**103.15**	**102.63**	**104.02**	**103.22**	**100.14**	**99.29**	**99.86**	**100.33**	**99.64**	**98.74**
num ox	8.00	3.00	3.00	3.00	3.00	3.00	12.00	12.00	12.00	12.00	18.00	18.00
Si	2.99	0.00	0.00	0.00	0.00	0.00	2.96	2.96	2.97	2.96	5.03	5.05
Ti	0.00	0.00	0.00	0.00	0.00	0.00	0.00	0.00	0.00	0.00	0.00	0.00
Al	1.01	1.99	1.99	1.99	1.99	1.99	2.06	2.06	2.06	2.06	3.91	3.92
Cr	0.00	0.00	0.00	0.00	0.00	0.00	0.00	0.00	0.00	0.00	0.00	0.00
Fe	0.00	0.01	0.01	0.01	0.01	0.01	2.14	2.13	2.10	2.14	0.55	0.56
Mn	0.00	0.00	0.00	0.00	0.00	0.00	0.12	0.15	0.14	0.13	0.01	0.00
Mg	0.00	0.00	0.00	0.00	0.00	0.00	0.67	0.63	0.64	0.63	1.51	1.45
Ca	0.00	0.00	0.00	0.00	0.00	0.00	0.06	0.09	0.08	0.07	0.00	0.00
Na	0.15	0.00	0.00	0.00	0.00	0.00	0.00	0.00	0.01	0.00	0.02	0.02
K	0.83	0.00	0.00	0.00	0.00	0.00	0.00	0.00	0.00	0.00	0.00	0.00
Total	**5.00**	**2.00**	**2.00**	**2.00**	**2.00**	**2.00**	**8.01**	**8.01**	**8.00**	**8.00**	**11.03**	**11.00**
xfe		0.96	1.00	1.00	0.98	0.97	0.85	0.86	0.85	0.86	0.39	0.41
XAb	0.16											
XAn	0.00											
XOr	0.84											
Xalm							0.71	0.71	0.71	0.72		
Xgrs							0.02	0.03	0.03	0.03		
Xpyr							0.22	0.21	0.22	0.21		
Xsps							0.04	0.05	0.05	0.04		

	13-cd-5	13-cd-6	13-cd-8	13-cd-9	13-cd-10	13-bi-1	13-bi-2	13-bi-3	13-bi-4	13-bi-6	13-bi-7	13-bi-8
	cd	cd	cd	cd	cd	bi	bi	bi	bi	bi	bi	bi
SiO2	50.06	49.97	49.68	49.88	49.63	36.78	36.62	36.92	36.92	36.93	36.84	36.90
TiO2	0.00	0.00	0.03	0.00	0.00	2.70	2.78	3.13	2.79	3.18	3.04	2.78
Al2O3	33.50	33.60	33.02	33.58	33.89	17.97	17.72	17.80	17.76	17.88	17.97	17.62
Cr2O3	0.01	0.00	0.00	0.01	0.00	0.09	0.06	0.05	0.02	0.01	0.12	0.07
FeO	6.42	6.11	6.81	6.62	6.44	17.95	18.17	19.15	19.05	19.22	18.44	18.57
MnO	0.02	0.06	0.07	0.10	0.08	0.00	0.00	0.08	0.10	0.05	0.09	0.04
MgO	10.17	10.28	9.93	9.56	9.63	13.04	12.72	11.95	12.03	12.12	12.51	12.71
CaO	0.01	0.01	0.01	0.00	0.00	0.00	0.01	0.00	0.00	0.00	0.00	0.00
Na2O	0.08	0.09	0.09	0.10	0.06	0.26	0.28	0.27	0.28	0.28	0.28	0.19
K2O	0.00	0.00	0.00	0.00	0.02	10.19	10.23	10.29	10.13	10.25	10.19	10.11
Total	**100.28**	**100.13**	**99.64**	**99.86**	**99.74**	**98.97**	**98.59**	**99.64**	**99.09**	**99.92**	**99.48**	**98.99**
num ox	18.00	18.00	18.00	18.00	18.00	11.00	11.00	11.00	11.00	11.00	11.00	11.00
Si	5.01	5.00	5.01	5.01	4.99	2.68	2.69	2.69	2.70	2.69	2.68	2.70
Ti	0.00	0.00	0.00	0.00	0.00	0.15	0.15	0.17	0.15	0.17	0.17	0.15
Al	3.95	3.96	3.93	3.98	4.02	1.55	1.53	1.53	1.53	1.53	1.54	1.52
Cr	0.00	0.00	0.00	0.00	0.00	0.00	0.00	0.00	0.00	0.00	0.01	0.00
Fe	0.54	0.51	0.57	0.56	0.54	1.10	1.12	1.17	1.17	1.17	1.12	1.14
Mn	0.00	0.01	0.01	0.01	0.01	0.00	0.00	0.01	0.01	0.00	0.01	0.00
Mg	1.52	1.53	1.49	1.43	1.44	1.42	1.39	1.30	1.31	1.31	1.36	1.39
Ca	0.00	0.00	0.00	0.00	0.00	0.00	0.00	0.00	0.00	0.00	0.00	0.00
Na	0.02	0.02	0.02	0.02	0.01	0.04	0.04	0.04	0.04	0.04	0.04	0.03
K	0.00	0.00	0.00	0.00	0.00	0.95	0.96	0.96	0.95	0.95	0.95	0.94
Total	**11.03**	**11.03**	**11.03**	**11.01**	**11.01**	**7.88**	**7.89**	**7.87**	**7.87**	**7.87**	**7.87**	**7.87**
xfe	0.39	0.37	0.41	0.41	0.40	0.58	0.59	0.62	0.61	0.61	0.60	0.59

	13-bi-9	13-bi-10	13-bi-11	13-sill-5	13-sill-7	13-sill-8	13-sill-9	13-sill-10	13-sill-11	13-sill-2	13-sill-3	13-sill-4
	bi	bi	bi	sill	sill	sill	sill	sill	sill	sill	sill	sill
SiO2	36.77	37.23	36.78	37.32	37.34	37.21	36.76	36.94	37.71	37.54	37.72	37.60
TiO2	2.78	2.93	2.37	0.01	0.01	0.00	0.00	0.00	0.00	0.01	0.00	0.01
Al2O3	17.89	18.44	18.17	62.90	62.32	62.30	61.50	61.81	61.96	62.88	62.40	62.78
Cr2O3	0.07	0.06	0.12	0.04	0.05	0.06	0.08	0.05	0.01	0.02	0.03	0.04
FeO	18.28	17.77	17.93	0.62	0.48	0.69	0.64	0.70	0.70	0.70	0.68	0.74
MnO	0.04	0.08	0.04	0.06	0.02	0.02	0.02	0.04	0.03	0.05	0.04	0.04
MgO	12.82	12.46	13.13	0.00	0.01	0.02	0.03	0.00	0.01	0.01	0.02	0.00
CaO	0.01	0.00	0.00	0.00	0.01	0.00	0.01	0.00	0.02	0.00	0.00	0.01
Na2O	0.22	0.23	0.18	0.01	0.02	0.00	0.03	0.02	0.02	0.00	0.00	0.02
K2O	10.14	9.81	9.97	0.02	0.00	0.00	0.01	0.02	0.00	0.00	0.01	0.00
Total	**99.03**	**99.01**	**98.70**	**100.97**	**100.25**	**100.29**	**99.08**	**99.58**	**100.46**	**101.21**	**100.90**	**101.24**
num ox	11.00	11.00	11.00	5.00	5.00	5.00	5.00	5.00	5.00	5.00	5.00	5.00
Si	2.69	2.70	2.69	1.00	1.01	1.00	1.00	1.00	1.02	1.00	1.01	1.01
Ti	0.15	0.16	0.13	0.00	0.00	0.00	0.00	0.00	0.00	0.00	0.00	0.00
Al	1.54	1.58	1.57	1.99	1.98	1.98	1.98	1.98	1.97	1.98	1.97	1.98
Cr	0.00	0.00	0.01	0.00	0.00	0.00	0.00	0.00	0.00	0.00	0.00	0.00
Fe	1.12	1.08	1.10	0.01	0.01	0.02	0.01	0.02	0.02	0.02	0.02	0.02
Mn	0.00	0.00	0.00	0.00	0.00	0.00	0.00	0.00	0.00	0.00	0.00	0.00
Mg	1.40	1.35	1.43	0.00	0.00	0.00	0.00	0.00	0.00	0.00	0.00	0.00
Ca	0.00	0.00	0.00	0.00	0.00	0.00	0.00	0.00	0.00	0.00	0.00	0.00
Na	0.03	0.03	0.03	0.00	0.00	0.00	0.00	0.00	0.00	0.00	0.00	0.00
K	0.95	0.91	0.93	0.00	0.00	0.00	0.00	0.00	0.00	0.00	0.00	0.00
Total	**7.88**	**7.82**	**7.87**	**3.01**	**3.00**	**3.00**	**3.01**	**3.01**	**3.00**	**3.00**	**3.00**	**3.00**
xfe	0.59	0.59	0.58	1.00	0.99	0.97	0.96	1.00	0.98	0.99	0.97	1.00

	13-sp-2	13-sp-3	13-sp-4	13-sp-5	13-sp-6	13-sp-7	13-sp-8	13-sp-9	13-sp-10	13-sp-11
	sp	sp	sp	sp	sp	sp	sp	sp	sp	sp
SiO2	0.00	0.00	0.00	0.00	0.00	0.00	0.00	0.00	0.00	0.00
TiO2	0.00	0.03	0.02	0.00	0.07	0.00	0.03	0.07	0.00	0.00
Al2O3	57.27	57.15	57.61	58.14	58.08	59.13	58.75	55.65	57.42	58.01
Cr2O3	2.32	2.67	1.84	0.55	0.64	0.61	0.55	1.19	1.76	1.19
FeO	33.45	32.55	34.12	34.03	33.87	32.72	33.00	35.00	33.20	32.82
MnO	0.14	0.07	0.15	0.14	0.14	0.14	0.08	0.10	0.13	0.05
MgO	7.01	7.38	7.14	7.23	7.07	7.37	7.14	6.75	6.96	7.10
CaO	0.00	0.00	0.00	0.00	0.00	0.00	0.00	0.00	0.00	0.00
Na2O	0.00	0.00	0.00	0.00	0.00	0.00	0.00	0.00	0.00	0.00
K2O	0.00	0.00	0.00	0.00	0.00	0.00	0.00	0.00	0.00	0.00
NiO	0.34	0.41	0.35	0.34	0.32	0.39	0.32	0.35	0.38	0.40
ZnO	0.00	0.00	0.00	0.00	0.00	0.00	0.00	0.00	0.00	0.00
Total	**100.53**	**100.26**	**101.22**	**100.43**	**100.17**	**100.36**	**99.87**	**99.12**	**99.85**	**99.57**
num ox	4.00	4.00	4.00	4.00	4.00	4.00	4.00	4.00	4.00	4.00
Si	0.00	0.00	0.00	0.00	0.00	0.00	0.00	0.00	0.00	0.00
Ti	0.00	0.00	0.00	0.00	0.00	0.00	0.00	0.00	0.00	0.00
Al	1.89	1.89	1.89	1.92	1.92	1.94	1.94	1.88	1.90	1.92
Cr	0.05	0.06	0.04	0.01	0.01	0.01	0.01	0.03	0.04	0.03
Fe	0.78	0.76	0.79	0.80	0.79	0.76	0.77	0.84	0.78	0.77
Mn	0.00	0.00	0.00	0.00	0.00	0.00	0.00	0.00	0.00	0.00
Mg	0.29	0.31	0.30	0.30	0.30	0.30	0.30	0.29	0.29	0.30
Ca	0.00	0.00	0.00	0.00	0.00	0.00	0.00	0.00	0.00	0.00
Na	0.00	0.00	0.00	0.00	0.00	0.00	0.00	0.00	0.00	0.00
K	0.00	0.00	0.00	0.00	0.00	0.00	0.00	0.00	0.00	0.00
Ni	0.01	0.01	0.01	0.01	0.01	0.01	0.01	0.01	0.01	0.01
Zn	0.00	0.00	0.00	0.00	0.00	0.00	0.00	0.00	0.00	0.00
Total	**3.03**	**3.03**	**3.03**	**3.04**	**3.03**	**3.03**	**3.03**	**3.05**	**3.03**	**3.03**
xfe	0.83	0.82	0.83	0.82	0.83	0.82	0.82	0.84	0.83	0.82

MINERAL CHEMISTRY FOR MLOWE GRANULITES (SAMPLE M14)

	14 ksp 2 ksp	14 ksp 3 ksp	14 ksp 4 ksp	14 ksp 5 ksp	14 ksp 6 ksp	14 ksp 7 ksp	14 ksp 10 ksp	14 ksp 11 ksp	14 ksp 12 ksp	14 ksp 13 ksp	14 pl 7 pl
SiO2	65.51	65.34	66.24	65.88	65.44	65.53	65.36	64.91	64.86	64.62	63.05
TiO2	0.01	0.06	0.02	0.00	0.02	0.00	0.00	0.02	0.07	0.02	0.00
Al2O3	19.18	18.88	19.14	18.86	19.13	18.93	18.82	18.67	18.60	18.45	23.45
Cr2O3	0.00	0.00	0.01	0.02	0.02	0.06	0.00	0.02	0.00	0.00	0.00
FeO	0.00	0.01	0.04	0.01	0.00	0.03	0.00	0.03	0.00	0.02	0.05
MnO	0.00	0.00	0.02	0.01	0.01	0.05	0.05	0.00	0.11	0.00	0.00
MgO	0.00	0.00	0.01	0.02	0.03	0.00	0.00	0.00	0.00	0.02	0.00
CaO	0.47	0.00	0.08	0.02	0.00	0.03	0.00	0.00	0.00	0.01	4.24
Na2O	2.13	0.76	3.34	1.74	1.13	1.95	0.76	0.75	0.87	0.82	8.48
K2O	13.48	15.67	11.65	14.19	15.33	13.79	15.79	15.90	15.55	15.61	0.12
Total	**100.78**	**100.73**	**100.56**	**100.75**	**101.11**	**100.37**	**100.78**	**100.30**	**100.06**	**99.57**	**99.40**
num ox	8.00	8.00	8.00	8.00	8.00	8.00	8.00	8.00	8.00	8.00	8.00
Si	2.98	2.99	2.99	3.00	2.98	2.99	2.99	2.99	2.99	2.99	2.80
Ti	0.00	0.00	0.00	0.00	0.00	0.00	0.00	0.00	0.00	0.00	0.00
Al	1.03	1.02	1.02	1.01	1.03	1.02	1.02	1.01	1.01	1.01	1.23
Cr	0.00	0.00	0.00	0.00	0.00	0.00	0.00	0.00	0.00	0.00	0.00
Fe	0.00	0.00	0.00	0.00	0.00	0.00	0.00	0.00	0.00	0.00	0.00
Mn	0.00	0.00	0.00	0.00	0.00	0.00	0.00	0.00	0.00	0.00	0.00
Mg	0.00	0.00	0.00	0.00	0.00	0.00	0.00	0.00	0.00	0.00	0.00
Ca	0.02	0.00	0.00	0.00	0.00	0.00	0.00	0.00	0.00	0.00	0.20
Na	0.19	0.07	0.29	0.15	0.10	0.17	0.07	0.07	0.08	0.07	0.73
K	0.78	0.91	0.67	0.82	0.89	0.80	0.92	0.93	0.91	0.92	0.01
Total	**4.99**	**4.99**	**4.98**	**4.99**	**5.00**	**4.99**	**5.00**	**5.00**	**5.00**	**5.00**	**4.96**
xfe											
XAb	0.19	0.07	0.30	0.16	0.10	0.18	0.07	0.07	0.08	0.07	0.78
XAn	0.02	0.00	0.00	0.00	0.00	0.00	0.00	0.00	0.00	0.00	0.21
XOr	0.79	0.93	0.69	0.84	0.90	0.82	0.93	0.93	0.92	0.93	0.01

	14 pl 8	14-gt-3	14-gt-6	14-gt-8	14-gt-10	14-bi-1	14-bi-2	14-bi-3	14-bi-4	14-bi-5	14-bi-6	14-bi-7
	pl	gt	gt	gt	gt	bi	bi	bi	bi	bi	bi	bi
SiO2	61.91	37.36	37.79	37.75	37.59	37.07	37.50	37.63	37.57	37.53	37.24	37.70
TiO2	0.05	0.03	0.06	0.00	0.04	2.80	1.88	2.01	1.96	2.13	2.34	2.49
Al2O3	24.61	21.89	22.05	22.09	22.10	17.23	17.49	17.73	18.00	17.64	17.31	17.43
Cr2O3	0.01	0.02	0.00	0.01	0.05	0.03	0.04	0.02	0.04	0.01	0.04	0.01
FeO	0.08	32.70	31.45	31.82	31.85	16.54	16.68	16.66	16.68	16.14	16.49	15.48
MnO	0.02	2.48	2.25	2.29	2.20	0.07	0.06	0.04	0.02	0.04	0.07	0.00
MgO	0.00	5.77	5.79	5.70	5.72	13.74	14.18	13.66	13.94	14.25	14.43	13.88
CaO	5.43	0.36	0.85	0.79	1.15	0.04	0.00	0.00	0.01	0.00	0.00	0.03
Na2O	8.19	0.02	0.04	0.02	0.00	0.14	0.14	0.15	0.15	0.10	0.09	0.11
K2O	0.09					10.48	10.60	10.77	10.70	10.92	10.86	10.60
Total	**100.39**	**100.63**	**100.28**	**100.47**	**100.70**	**98.14**	**98.59**	**98.67**	**99.06**	**98.76**	**98.87**	**97.72**
num ox	8.00	12.00	12.00	12.00	12.00	11.00	11.00	11.00	11.00	11.00	11.00	11.00
Si	2.73	2.95	2.97	2.97	2.96	2.72	2.73	2.74	2.72	2.73	2.71	2.76
Ti	0.00	0.00	0.00	0.00	0.00	0.15	0.10	0.11	0.11	0.12	0.13	0.14
Al	1.28	2.04	2.05	2.05	2.05	1.49	1.50	1.52	1.54	1.51	1.49	1.50
Cr	0.00	0.00	0.00	0.00	0.00	0.00	0.00	0.00	0.00	0.00	0.00	0.00
Fe	0.00	2.16	2.07	2.09	2.09	1.01	1.02	1.01	1.01	0.98	1.00	0.95
Mn	0.00	0.17	0.15	0.15	0.15	0.00	0.00	0.00	0.00	0.00	0.00	0.00
Mg	0.00	0.68	0.68	0.67	0.67	1.50	1.54	1.48	1.51	1.54	1.57	1.51
Ca	0.26	0.03	0.07	0.07	0.10	0.00	0.00	0.00	0.00	0.00	0.00	0.00
Na	0.70	0.00	0.01	0.00	0.00	0.02	0.02	0.02	0.02	0.01	0.01	0.02
K	0.01	0.00	0.00	0.00	0.00	0.98	0.99	1.00	0.99	1.01	1.01	0.99
Total	**4.98**	**8.03**	**8.00**	**8.01**	**8.02**	**7.88**	**7.91**	**7.90**	**7.90**	**7.91**	**7.93**	**7.86**
xfe		0.85	0.84	0.85	0.85	0.55	0.54	0.55	0.54	0.53	0.53	0.53
XAb	0.73											
XAn	0.27											
XOr	0.01											
Xalm		0.71	0.70	0.70	0.70							
Xgrs		0.01	0.02	0.02	0.03							
Xpyr		0.22	0.23	0.22	0.22							
Xsps		0.05	0.05	0.05	0.05							

	14-bi-8 bi	14-bi-9 bi	14-bi-10 bi	14-bi-11 bi	14-sill-1 sill	14-sill-2 sill	14-sill-3 sill	14-sill-5 sill	14-sill-6 sill	14-sill-7 sill
SiO2	37.87	37.51	38.10	37.56	37.52	38.48	37.12	36.76	37.82	37.17
TiO2	1.47	1.80	1.93	1.99	0.05	0.00	0.05	0.01	0.00	0.02
Al2O3	18.34	17.51	19.46	17.94	62.28	60.25	61.67	61.02	63.02	62.53
Cr2O3	0.00	0.00	0.04	0.04	0.00	0.00	0.02	0.03	0.03	0.00
FeO	12.83	15.05	14.53	15.87	1.00	0.82	0.74	1.00	0.85	0.74
MnO	0.11	0.09	0.00	0.03	0.02	0.01	0.03	0.02	0.01	0.05
MgO	16.84	15.30	13.91	14.55	0.02	0.04	0.00	0.00	0.01	0.02
CaO	0.00	0.00	0.00	0.02	0.00	0.00	0.01	0.01	0.01	0.01
Na2O	0.27	0.22	0.13	0.12	0.00	0.01	0.00	0.00	0.00	0.03
K2O	10.47	10.65	9.85	10.59	0.01	0.00	0.01	0.00	0.01	0.02
Total	**98.20**	**98.13**	**97.96**	**98.72**	**100.89**	**99.61**	**99.65**	**98.86**	**101.76**	**100.59**
num ox	11.00	11.00	11.00	11.00	5.00	5.00	5.00	5.00	5.00	5.00
Si	2.72	2.73	2.74	2.72	1.01	1.04	1.01	1.01	1.01	1.00
Ti	0.08	0.10	0.10	0.11	0.00	0.00	0.00	0.00	0.00	0.00
Al	1.55	1.50	1.65	1.53	1.97	1.93	1.98	1.97	1.98	1.99
Cr	0.00	0.00	0.00	0.00	0.00	0.00	0.00	0.00	0.00	0.00
Fe	0.77	0.92	0.87	0.96	0.02	0.02	0.02	0.02	0.02	0.02
Mn	0.01	0.01	0.00	0.00	0.00	0.00	0.00	0.00	0.00	0.00
Mg	1.80	1.66	1.49	1.57	0.00	0.00	0.00	0.00	0.00	0.00
Ca	0.00	0.00	0.00	0.00	0.00	0.00	0.00	0.00	0.00	0.00
Na	0.04	0.03	0.02	0.02	0.00	0.00	0.00	0.00	0.00	0.00
K	0.96	0.99	0.90	0.98	0.00	0.00	0.00	0.00	0.00	0.00
Total	**7.92**	**7.93**	**7.79**	**7.90**	**3.01**	**2.99**	**3.00**	**3.01**	**3.00**	**3.01**
xfe	0.43	0.50	0.51	0.52	0.98	0.96	0.99	1.00	0.99	0.98

	14-sill-8	14-sill-9	14-sill-10	14-sill-11	14-sill-12	14-sill-13	14-sp-1	14-sp-2	14-sp-3	14-sp-4	14-cd-1
	sill	sill	sill	sill	sill	sill	sp	sp	sp	sp	cd
SiO2	37.54	37.17	36.95	37.31	37.35	37.35	0.00	0.00	0.00	0.00	49.58
TiO2	0.03	0.01	0.03	0.01	0.00	0.01	0.02	0.00	0.00	0.03	0.00
Al2O3	63.05	61.73	61.13	62.26	61.09	61.61	58.50	58.60	58.56	56.81	33.58
Cr2O3	0.02	0.02	0.02	0.03	0.02	0.00	0.65	0.67	0.66	0.73	0.00
FeO	0.61	0.82	0.71	0.81	1.22	0.69	26.04	25.85	26.65	24.01	6.25
MnO	0.03	0.00	0.00	0.04	0.03	0.01	0.13	0.10	0.15	0.13	0.10
MgO	0.00	0.00	0.01	0.00	0.06	0.01	3.84	3.87	3.94	3.83	9.59
CaO	0.00	0.01	0.01	0.01	0.02	0.01	0.00	0.00	0.00	0.00	0.03
Na2O	0.00	0.02	0.00	0.01	0.00	0.02	0.00	0.00	0.00	0.00	0.16
K2O	0.00	0.01	0.00	0.01	0.00	0.02	0.00	0.00	0.00	0.00	0.02
NiO							0.13	0.13	0.16	0.12	
ZnO							14.67	15.02	14.56	16.20	
Total	**101.29**	**99.80**	**98.86**	**100.49**	**99.80**	**99.73**	**103.98**	**104.24**	**104.67**	**101.86**	**99.31**
num ox	5.00	5.00	5.00	5.00	5.00	5.00	4.00	4.00	4.00	4.00	18.00
Si	1.00	1.01	1.01	1.01	1.02	1.01	0.00	0.00	0.00	0.00	5.00
Ti	0.00	0.00	0.00	0.00	0.00	0.00	0.00	0.00	0.00	0.00	0.00
Al	1.99	1.97	1.97	1.98	1.96	1.97	1.93	1.93	1.92	1.92	4.00
Cr	0.00	0.00	0.00	0.00	0.00	0.00	0.01	0.01	0.01	0.02	0.00
Fe	0.01	0.02	0.02	0.02	0.03	0.02	0.61	0.60	0.62	0.58	0.53
Mn	0.00	0.00	0.00	0.00	0.00	0.00	0.00	0.00	0.00	0.00	0.01
Mg	0.00	0.00	0.00	0.00	0.00	0.00	0.16	0.16	0.16	0.16	1.44
Ca	0.00	0.00	0.00	0.00	0.00	0.00	0.00	0.00	0.00	0.00	0.00
Na	0.00	0.00	0.00	0.00	0.00	0.00	0.00	0.00	0.00	0.00	0.03
K	0.00	0.00	0.00	0.00	0.00	0.00	0.00	0.00	0.00	0.00	0.00
Ni							0.00	0.00	0.00	0.00	
Zn							0.30	0.31	0.30	0.34	
Total	**3.00**	**3.00**	**3.00**	**3.00**	**3.01**	**3.00**	**3.03**	**3.03**	**3.03**	**3.03**	**11.01**
xfe	1.00	1.00	0.99	1.00	0.95	0.99	0.87	0.87	0.87	0.86	0.39

	14-cd-3	14-cd-4	14-cd-7	14-cor-2	14-cor-3	14-cor-6
	cd	cd	cd	cor	cor	cor
SiO2	49.61	49.68	49.95	0.03	0.24	0.00
TiO2	0.02	0.00	0.00	0.01	0.01	0.00
Al2O3	33.56	33.26	33.05	101.76	100.28	102.94
Cr2O3	0.00	0.00	0.02	0.09	0.11	0.08
FeO	6.51	6.53	6.88	0.64	0.54	0.63
MnO	0.02	0.10	0.08	0.02	0.03	0.01
MgO	9.98	9.78	9.74	0.01	0.07	0.00
CaO	0.00	0.00	0.00	0.00	0.06	0.01
Na2O	0.10	0.13	0.08	0.01	0.00	0.00
K2O	0.01	0.00	0.01	0.00	0.02	0.01
Total	**99.82**	**99.48**	**99.81**	**102.58**	**101.35**	**103.67**
num ox	18.00	18.00	18.00	3.00	3.00	3.00
Si	4.99	5.01	5.03	0.00	0.00	0.00
Ti	0.00	0.00	0.00	0.00	0.00	0.00
Al	3.98	3.96	3.92	1.99	1.99	1.99
Cr	0.00	0.00	0.00	0.00	0.00	0.00
Fe	0.55	0.55	0.58	0.01	0.01	0.01
Mn	0.00	0.01	0.01	0.00	0.00	0.00
Mg	1.50	1.47	1.46	0.00	0.00	0.00
Ca	0.00	0.00	0.00	0.00	0.00	0.00
Na	0.02	0.03	0.02	0.00	0.00	0.00
K	0.00	0.00	0.00	0.00	0.00	0.00
Total	**11.03**	**11.02**	**11.02**	**2.00**	**2.00**	**2.00**
xfe	0.39	0.40	0.41	0.98	0.89	1.00

MINERAL CHEMISTRY FOR MAGANGA AMPHIBOLITES (SAMPLE M16)

	16 amph 2	16 hb 3	16 hb 4	16 hb 5	16 hb 6	16 hb 8	16 hb 11	16 pl 2	16 pl 4	16 pl 13	16 pl 14	16 pl 8
	hb	hb	hb	hb	hb	hb	hb	pl	pl	pl	pl	sph
SiO2	42.64	42.41	41.98	42.52	42.83	42.73	42.55	60.19	61.33	60.48	61.05	31.00
TiO2	0.49	0.56	0.64	0.50	0.53	0.56	0.56	0.00	0.01	0.00	0.00	38.02
Al2O3	13.35	14.30	14.11	13.89	13.56	13.21	13.42	24.47	23.80	24.32	24.12	1.10
Cr2O3	0.03	0.00	0.01	0.01	0.00	0.00	0.06	0.00	0.00	0.02	0.01	0.00
FeO	19.72	19.17	19.63	19.37	18.53	19.67	19.37	0.26	0.16	0.21	0.18	0.82
MnO	0.28	0.32	0.40	0.34	0.34	0.33	0.28	0.02	0.02	0.05	0.07	0.07
MgO	8.75	8.68	8.56	8.68	8.93	9.09	8.93	0.00	0.00	0.00	0.02	0.02
CaO	11.70	11.52	11.57	11.59	11.58	11.66	11.83	6.85	6.11	6.68	6.41	27.81
Na2O	1.17	1.22	1.31	1.34	1.29	1.18	1.11	7.43	7.57	7.18	7.34	0.00
K2O	0.50	0.47	0.55	0.44	0.42	0.59	0.51	0.06	0.05	0.09	0.06	0.00
Total	**98.62**	**98.65**	**98.76**	**98.69**	**98.00**	**99.02**	**98.62**	**99.28**	**99.05**	**99.03**	**99.26**	**98.84**
num ox	23.00	23.00	23.00	23.00	23.00	23.00	23.00	8.00	8.00	8.00	8.00	5.00
Si	6.39	6.33	6.29	6.36	6.42	6.38	6.37	2.70	2.74	2.71	2.73	1.02
Ti	0.05	0.06	0.07	0.06	0.06	0.06	0.06	0.00	0.00	0.00	0.00	0.94
Al	2.36	2.52	2.49	2.45	2.40	2.33	2.37	1.29	1.26	1.29	1.27	0.04
Cr	0.00	0.00	0.00	0.00	0.00	0.00	0.01	0.00	0.00	0.00	0.00	0.00
Fe	2.47	2.39	2.46	2.42	2.32	2.46	2.43	0.01	0.01	0.01	0.01	0.02
Mn	0.04	0.04	0.05	0.04	0.04	0.04	0.04	0.00	0.00	0.00	0.00	0.00
Mg	1.96	1.93	1.91	1.93	1.99	2.02	1.99	0.00	0.00	0.00	0.00	0.00
Ca	1.88	1.84	1.86	1.86	1.86	1.87	1.90	0.33	0.29	0.32	0.31	0.98
Na	0.34	0.35	0.38	0.39	0.37	0.34	0.32	0.65	0.66	0.62	0.64	0.00
K	0.10	0.09	0.11	0.08	0.08	0.11	0.10	0.00	0.00	0.01	0.00	0.00
Total	**15.59**	**15.57**	**15.63**	**15.60**	**15.55**	**15.62**	**15.59**	**4.98**	**4.96**	**4.96**	**4.96**	**3.01**
xfe	0.69	0.69	0.70	0.69	0.67	0.68	0.68					0.98
XAb								0.66	0.69	0.66	0.67	
XAn								0.34	0.31	0.34	0.32	
XOr								0.00	0.00	0.01	0.00	

	16 pl 9 sph	16 pl 10 sph	16-mica-3 bi	16-mica-4 bi	16-mica-8 bi	16-mica-9 bi
SiO2	31.06	31.32	36.05	36.20	36.77	36.59
TiO2	38.52	39.00	1.65	1.62	1.71	1.77
Al2O3	1.10	1.10	17.54	17.09	17.28	17.15
Cr2O3	0.04	0.00	0.05	0.04	0.08	0.10
FeO	0.82	0.90	22.71	22.85	22.48	22.49
MnO	0.16	0.10	0.19	0.20	0.17	0.11
MgO	0.02	0.03	13.25	13.44	12.84	12.82
CaO	28.08	27.82	0.07	0.07	0.05	0.05
Na2O	0.02	0.02	0.11	0.09	0.18	0.12
K2O	0.00	0.00	7.07	7.49	8.47	8.39
Total	**99.82**	**100.28**	**98.70**	**99.09**	**100.02**	**99.58**
num ox	5.00	5.00	11.00	11.00	11.00	11.00
Si	1.02	1.02	2.66	2.67	2.69	2.69
Ti	0.95	0.95	0.09	0.09	0.09	0.10
Al	0.04	0.04	1.52	1.48	1.49	1.48
Cr	0.00	0.00	0.00	0.00	0.00	0.01
Fe	0.02	0.02	1.40	1.41	1.37	1.38
Mn	0.00	0.00	0.01	0.01	0.01	0.01
Mg	0.00	0.00	1.46	1.48	1.40	1.40
Ca	0.98	0.97	0.01	0.01	0.00	0.00
Na	0.00	0.00	0.02	0.01	0.03	0.02
K	0.00	0.00	0.66	0.70	0.79	0.79
Total	**3.02**	**3.01**	**7.83**	**7.86**	**7.88**	**7.87**
xfe	0.97	0.97	0.63	0.63	0.64	0.64

MINERAL CHEMISTRY FOR MAGANGA AMPHIBOLITES (SAMPLE M17)

	17 hb 2	17 hb 3	17 hb 4	17 hb 6	17 hb 7	17 hb 8	17 hb 9	17 hb 10	17 ap 1	17 pl 1	17 pl 2	17 pl 3
	hb	hb	hb	hb	hb	hb	hb	hb	sph	pl	pl	pl
SiO2	42.94	42.61	43.05	43.41	42.47	43.09	43.90	43.52	30.72	58.51	60.34	58.80
TiO2	0.60	0.64	0.59	0.56	0.64	0.60	0.52	0.51	39.11	0.01	0.04	0.01
Al2O3	13.27	14.10	13.18	12.76	13.45	13.23	12.35	12.83	1.07	26.77	25.69	26.75
Cr2O3	0.00	0.02	0.06	0.00	0.05	0.00	0.04	0.02	0.00	0.00	0.00	0.00
FeO	20.09	20.38	20.15	19.66	20.11	20.17	19.71	19.50	0.45	0.08	0.01	0.09
MnO	0.23	0.22	0.19	0.24	0.23	0.32	0.23	0.24	0.15	0.01	0.00	0.08
MgO	9.14	8.57	8.93	9.12	8.69	8.78	9.29	9.30	0.00	0.00	0.00	0.02
CaO	11.75	11.74	11.88	11.94	11.81	11.74	11.92	11.88	28.81	7.54	6.64	7.96
Na2O	1.26	1.11	1.22	1.17	1.18	1.17	1.16	1.20	0.00	6.67	7.19	6.44
K2O	0.50	0.60	0.57	0.52	0.63	0.57	0.50	0.50	0.00	0.08	0.05	0.07
Total	**99.78**	**99.98**	**99.81**	**99.39**	**99.26**	**99.66**	**99.62**	**99.51**	**100.30**	**99.67**	**99.97**	**100.21**
num ox	23.00	23.00	23.00	23.00	23.00	23.00	23.00	23.00	5.00	8.00	8.00	8.00
Si	6.37	6.32	6.39	6.45	6.35	6.40	6.51	6.45	1.00	2.61	2.68	2.61
Ti	0.07	0.07	0.07	0.06	0.07	0.07	0.06	0.06	0.96	0.00	0.00	0.00
Al	2.32	2.46	2.31	2.24	2.37	2.32	2.16	2.24	0.04	1.41	1.34	1.40
Cr	0.00	0.00	0.01	0.00	0.01	0.00	0.00	0.00	0.00	0.00	0.00	0.00
Fe	2.49	2.53	2.50	2.44	2.51	2.51	2.44	2.42	0.01	0.00	0.00	0.00
Mn	0.03	0.03	0.02	0.03	0.03	0.04	0.03	0.03	0.00	0.00	0.00	0.00
Mg	2.02	1.89	1.98	2.02	1.94	1.94	2.05	2.06	0.00	0.00	0.00	0.00
Ca	1.87	1.86	1.89	1.90	1.89	1.87	1.89	1.89	1.01	0.36	0.32	0.38
Na	0.36	0.32	0.35	0.34	0.34	0.34	0.33	0.35	0.00	0.58	0.62	0.56
K	0.09	0.11	0.11	0.10	0.12	0.11	0.09	0.09	0.00	0.00	0.00	0.00
Total	**15.63**	**15.60**	**15.62**	**15.59**	**15.63**	**15.59**	**15.57**	**15.59**	**3.02**	**4.97**	**4.96**	**4.96**
xfe	0.69	0.70	0.69	0.68	0.70	0.70	0.68	0.68	1.00			
XAb										0.61	0.66	0.59
XAn										0.38	0.34	0.40
XOr										0.00	0.00	0.00

	17 pl 5 pl	17 pl 6 pl	17 pl 7 pl	17 pl 9 pl	17 pl 10 pl	17 pl 11 pl
SiO2	61.66	60.70	59.09	58.40	60.43	60.47
TiO2	0.03	0.00	0.04	0.01	0.02	0.00
Al2O3	25.11	25.20	26.95	27.42	25.96	25.78
Cr2O3	0.01	0.00	0.02	0.00	0.02	0.02
FeO	0.03	0.06	0.07	0.09	0.09	0.13
MnO	0.03	0.02	0.07	0.00	0.03	0.00
MgO	0.02	0.01	0.03	0.02	0.01	0.00
CaO	5.91	6.38	7.84	8.69	6.93	6.93
Na2O	7.57	7.26	6.49	6.17	7.01	6.87
K2O	0.07	0.07	0.06	0.07	0.10	0.09
Total	**100.44**	**99.70**	**100.67**	**100.88**	**100.59**	**100.29**
num ox	8.00	8.00	8.00	8.00	8.00	8.00
Si	2.72	2.70	2.61	2.58	2.67	2.68
Ti	0.00	0.00	0.00	0.00	0.00	0.00
Al	1.30	1.32	1.41	1.43	1.35	1.34
Cr	0.00	0.00	0.00	0.00	0.00	0.00
Fe	0.00	0.00	0.00	0.00	0.00	0.00
Mn	0.00	0.00	0.00	0.00	0.00	0.00
Mg	0.00	0.00	0.00	0.00	0.00	0.00
Ca	0.28	0.30	0.37	0.41	0.33	0.33
Na	0.65	0.63	0.56	0.53	0.60	0.59
K	0.00	0.00	0.00	0.00	0.01	0.01
Total	**4.96**	**4.96**	**4.96**	**4.97**	**4.96**	**4.95**
XAb	0.70	0.67	0.60	0.56	0.64	0.64
XAn	0.30	0.33	0.40	0.44	0.35	0.36
XOr	0.00	0.00	0.00	0.00	0.01	0.01

MINERAL CHEMISTRY FOR MAGANGA SCHIST (SAMPLE M18)

	18 pl 3	18 pl 5	18-g-2	18-ky-46	18-st-47	18-ky-54	18-st-55	18-st-58	18-st-59	18-st-60	18-st-61	18-st-62
	pl	pl	st	st	st	st	st	st	st	st	st	st
SiO2	64.65	64.06	27.66	27.90	28.21	28.08	28.34	27.48	27.94	27.90	28.12	28.09
TiO2	0.00	0.03	0.51	0.45	0.44	0.47	0.49	0.55	0.51	0.43	0.59	0.48
Al2O3	22.20	22.52	55.50	54.01	54.62	55.38	54.70	54.55	55.13	54.91	55.26	54.68
Cr2O3	0.00	0.01	0.02	0.03	0.03	0.07	0.00	0.06	0.02	0.03	0.05	0.00
FeO	0.06	0.06	14.04	14.60	14.51	14.51	14.74	14.90	14.61	14.64	14.68	14.70
MnO	0.03	0.04	0.55	0.55	0.56	0.61	0.61	0.65	0.59	0.64	0.58	0.66
MgO	0.02	0.00	1.73	1.73	1.74	1.79	1.82	1.63	1.83	1.68	1.60	1.78
CaO	3.61	3.92	0.01	0.01	0.01	0.00	0.01	0.00	0.00	0.00	0.01	0.01
Na2O	8.81	8.57	0.02	0.07	0.02	0.00	0.00	0.00	0.04	0.01	0.05	0.02
K2O	0.04	0.03		0.00	0.00	0.00	0.02	0.00	0.00	0.00	0.00	0.01
Total	**99.42**	**99.24**	**100.04**	**99.35**	**100.14**	**100.92**	**100.72**	**99.83**	**100.68**	**100.24**	**100.93**	**100.43**
num ox	8.00	8.00	26.00	26.00	26.00	26.00	26.00	26.00	26.00	26.00	26.00	26.00
Si	2.86	2.84	4.25	4.33	4.34	4.29	4.34	4.26	4.28	4.30	4.30	4.32
Ti	0.00	0.00	0.06	0.05	0.05	0.05	0.06	0.06	0.06	0.05	0.07	0.06
Al	1.16	1.18	10.06	9.89	9.91	9.97	9.88	9.97	9.96	9.97	9.96	9.91
Cr	0.00	0.00	0.00	0.00	0.00	0.01	0.00	0.01	0.00	0.00	0.01	0.00
Fe	0.00	0.00	1.81	1.90	1.87	1.85	1.89	1.93	1.87	1.88	1.88	1.89
Mn	0.00	0.00	0.07	0.07	0.07	0.08	0.08	0.09	0.08	0.08	0.07	0.09
Mg	0.00	0.00	0.40	0.40	0.40	0.41	0.42	0.38	0.42	0.39	0.37	0.41
Ca	0.17	0.19	0.00	0.00	0.00	0.00	0.00	0.00	0.00	0.00	0.00	0.00
Na	0.75	0.74	0.01	0.02	0.01	0.00	0.00	0.00	0.01	0.00	0.01	0.01
K	0.00	0.00	0.00	0.00	0.00	0.00	0.00	0.00	0.00	0.00	0.00	0.00
Total	**4.94**	**4.94**	**16.66**	**16.68**	**16.65**	**16.67**	**16.67**	**16.69**	**16.68**	**16.67**	**16.66**	**16.68**
xfe			0.89	0.89	0.89	0.89	0.89	0.90	0.89	0.90	0.90	0.89
XAb	0.81	0.80										
XAn	0.18	0.20										
XOr	0.00	0.00										

	18-st-63	18-st-64	18-st-65	18-mica-3	18-bi-9	18-bi-16	18-bi-17	18-bi-18	18-bi-19	18-bi-20	18-gt-16	18-gt-17
	st	st	st	bi	bi	bi	bi	bi	bi	bi	gt	gt
SiO2	27.81	28.11	28.37	38.00	36.83	35.94	35.82	36.87	36.28	36.74	37.15	37.37
TiO2	0.48	0.45	0.45	1.46	1.40	1.39	1.35	1.53	1.53	1.64	0.07	0.04
Al2O3	55.41	55.10	53.99	19.53	19.69	19.51	19.79	18.50	18.75	18.80	21.15	21.44
Cr2O3	0.08	0.04	0.02	0.03	0.04	0.02	0.03	0.06	0.04	0.00	0.03	0.00
FeO	14.64	14.80	14.99	21.00	19.03	20.10	19.85	19.80	19.83	19.50	27.30	27.86
MnO	0.66	0.59	0.55	0.20	0.19	0.27	0.29	0.16	0.14	0.17	8.40	8.58
MgO	1.74	1.83	2.03	11.76	11.81	11.99	12.07	11.49	11.35	11.65	2.67	2.75
CaO	0.01	0.01	0.01	0.01	0.00	0.03	0.03	0.00	0.05	0.00	2.75	2.01
Na2O	0.01	0.01	0.03	0.30	0.30	0.28	0.19	0.36	0.33	0.36	0.05	0.01
K2O	0.00	0.01	0.01	9.41	9.57	8.12	7.29	9.67	9.46	9.55		
Total	**100.84**	**100.94**	**100.44**	**101.70**	**98.86**	**97.66**	**96.71**	**98.44**	**97.76**	**98.41**	**99.56**	**100.05**
num ox	26.00	26.00	26.00	11.00	11.00	11.00	11.00	11.00	11.00	11.00	12.00	12.00
Si	4.26	4.30	4.37	2.71	2.69	2.66	2.66	2.72	2.69	2.70	3.00	3.00
Ti	0.05	0.05	0.05	0.08	0.08	0.08	0.08	0.08	0.09	0.09	0.00	0.00
Al	10.00	9.93	9.79	1.64	1.69	1.70	1.73	1.61	1.64	1.63	2.01	2.03
Cr	0.01	0.00	0.00	0.00	0.00	0.00	0.00	0.00	0.00	0.00	0.00	0.00
Fe	1.87	1.89	1.93	1.25	1.16	1.24	1.23	1.22	1.23	1.20	1.84	1.87
Mn	0.09	0.08	0.07	0.01	0.01	0.02	0.02	0.01	0.01	0.01	0.57	0.58
Mg	0.40	0.42	0.47	1.25	1.28	1.32	1.33	1.26	1.26	1.28	0.32	0.33
Ca	0.00	0.00	0.00	0.00	0.00	0.00	0.00	0.00	0.00	0.00	0.24	0.17
Na	0.00	0.00	0.01	0.04	0.04	0.04	0.03	0.05	0.05	0.05	0.01	0.00
K	0.00	0.00	0.00	0.86	0.89	0.77	0.69	0.91	0.90	0.90	0.00	0.00
Total	**16.68**	**16.68**	**16.69**	**7.84**	**7.85**	**7.82**	**7.76**	**7.87**	**7.87**	**7.86**	**8.00**	**7.99**
xfe	0.89	0.89	0.88	0.64	0.62	0.63	0.62	0.63	0.64	0.63		
Xalm											0.62	0.63
Xgrs											0.08	0.06
Xpyr											0.11	0.11
Xsps											0.19	0.20

	18-bi-21	18-bi-10	18-bi-12	18-mu-7	18-mu-35	18-mu-36	18-mu-37	18-mu-38	18-mu-39	18-mu-40	18-mu-41	18-mu-42
	bi	bi	bi	musc	musc	musc	musc	musc	musc	musc	musc	musc
SiO2	36.79	37.56	35.98	47.88	45.83	45.67	45.93	46.68	46.09	46.25	46.77	46.29
TiO2	1.55	1.42	1.35	0.45	0.72	0.55	0.33	0.33	0.55	0.45	0.58	0.80
Al2O3	18.61	19.81	19.40	36.66	34.48	34.31	34.72	35.59	35.40	34.97	33.80	35.23
Cr2O3	0.05	0.03	0.04	0.00	0.05	0.05	0.00	0.03	0.06	0.08	0.00	0.03
FeO	19.33	19.26	20.29	2.31	2.59	2.43	2.37	2.66	2.29	2.44	2.49	2.57
MnO	0.14	0.14	0.14	0.03	0.04	0.00	0.00	0.00	0.04	0.03	0.05	0.02
MgO	11.53	11.83	12.72	0.47	0.49	0.52	0.56	0.55	0.45	0.59	0.84	0.52
CaO	0.03	0.00	0.03	0.00	0.01	0.02	0.00	0.00	0.00	0.00	0.00	0.00
Na2O	0.38	0.28	0.32	1.53	1.49	1.41	1.48	1.55	1.56	1.47	1.36	1.67
K2O	9.68	9.51	8.25	9.68	9.63	9.69	9.51	9.52	9.95	9.66	9.87	9.49
Total	**98.09**	**99.84**	**98.52**	**99.01**	**95.33**	**94.66**	**94.90**	**96.91**	**96.39**	**95.94**	**95.76**	**96.62**
num ox	11.00	11.00	11.00	11.00	11.00	11.00	11.00	11.00	11.00	11.00	11.00	11.00
Si	2.72	2.71	2.64	3.07	3.07	3.08	3.08	3.07	3.05	3.07	3.11	3.05
Ti	0.09	0.08	0.07	0.02	0.04	0.03	0.02	0.02	0.03	0.02	0.03	0.04
Al	1.62	1.68	1.68	2.77	2.72	2.72	2.74	2.76	2.76	2.74	2.65	2.74
Cr	0.00	0.00	0.00	0.00	0.00	0.00	0.00	0.00	0.00	0.00	0.00	0.00
Fe	1.19	1.16	1.24	0.12	0.15	0.14	0.13	0.15	0.13	0.14	0.14	0.14
Mn	0.01	0.01	0.01	0.00	0.00	0.00	0.00	0.00	0.00	0.00	0.00	0.00
Mg	1.27	1.27	1.39	0.05	0.05	0.05	0.06	0.05	0.04	0.06	0.08	0.05
Ca	0.00	0.00	0.00	0.00	0.00	0.00	0.00	0.00	0.00	0.00	0.00	0.00
Na	0.05	0.04	0.05	0.19	0.19	0.18	0.19	0.20	0.20	0.19	0.18	0.21
K	0.91	0.88	0.77	0.79	0.82	0.83	0.81	0.80	0.84	0.82	0.84	0.80
Total	**7.87**	**7.83**	**7.86**	**7.01**	**7.04**	**7.04**	**7.03**	**7.04**	**7.06**	**7.04**	**7.04**	**7.04**
xfe	0.63	0.62	0.61	0.83	0.84	0.82	0.81	0.83	0.83	0.81	0.75	0.83

	18-mu-43	18-chl-26	18-chl-27	18-chl-28	18-chl-29	18-chl-30	18-chl-31	18-chl-32	18-chl-33	18-chl-34	18-st-44	18-ky-45
	musc	chl	chl	chl	chl	chl	chl	chl	chl	chl	ky	ky
SiO2	45.76	25.06	25.40	25.67	25.19	25.44	25.26	25.08	25.15	25.08	37.58	37.19
TiO2	0.75	0.07	0.06	0.07	0.07	0.02	0.04	0.07	0.11	0.07	0.06	0.04
Al2O3	34.79	23.31	23.46	23.65	23.36	23.58	23.18	22.92	23.26	23.57	62.89	62.82
Cr2O3	0.02	0.02	0.02	0.01	0.03	0.02	0.03	0.01	0.03	0.02	0.07	0.04
FeO	2.51	24.52	24.90	24.70	24.31	24.62	24.67	24.48	24.57	24.63	1.40	1.50
MnO	0.05	0.36	0.30	0.27	0.33	0.32	0.37	0.31	0.36	0.24	0.09	0.00
MgO	0.55	17.08	16.83	16.56	17.14	16.72	17.34	17.22	17.41	17.05	0.02	0.05
CaO	0.00	0.00	0.00	0.00	0.00	0.00	0.03	0.05	0.00	0.02	0.01	0.01
Na2O	1.50	0.01	0.01	0.03	0.00	0.05	0.01	0.00	0.00	0.01	0.03	0.01
K2O	9.71	0.01	0.01	0.01	0.00	0.00	0.02	0.00	0.00	0.01	0.02	0.01
Total	**95.64**	**90.43**	**90.98**	**90.98**	**90.43**	**90.77**	**90.95**	**90.15**	**90.89**	**90.71**	**102.16**	**101.66**
num ox	11.00	14.00	14.00	14.00	14.00	14.00	14.00	14.00	14.00	14.00	5.00	5.00
Si	3.05	2.55	2.57	2.59	2.56	2.57	2.55	2.56	2.54	2.54	1.00	0.99
Ti	0.04	0.01	0.00	0.01	0.01	0.00	0.00	0.01	0.01	0.01	0.00	0.00
Al	2.74	2.79	2.79	2.81	2.79	2.81	2.76	2.76	2.77	2.81	1.97	1.98
Cr	0.00	0.00	0.00	0.00	0.00	0.00	0.00	0.00	0.00	0.00	0.00	0.00
Fe	0.14	2.08	2.10	2.08	2.06	2.08	2.09	2.09	2.08	2.09	0.03	0.03
Mn	0.00	0.03	0.03	0.02	0.03	0.03	0.03	0.03	0.03	0.02	0.00	0.00
Mg	0.05	2.59	2.53	2.49	2.59	2.52	2.61	2.62	2.62	2.57	0.00	0.00
Ca	0.00	0.00	0.00	0.00	0.00	0.00	0.00	0.01	0.00	0.00	0.00	0.00
Na	0.19	0.00	0.00	0.01	0.00	0.01	0.00	0.00	0.00	0.00	0.00	0.00
K	0.83	0.00	0.00	0.00	0.00	0.00	0.00	0.00	0.00	0.00	0.00	0.00
Total	**7.05**	**10.05**	**10.03**	**10.01**	**10.04**	**10.03**	**10.06**	**10.06**	**10.06**	**10.05**	**3.01**	**3.01**
xfe	0.82	0.59	0.60	0.60	0.59	0.60	0.59	0.59	0.59	0.59	0.99	0.97
Al (iv)		1.45	1.43	1.41	1.44	1.43	1.45	1.44	1.46	1.46		

	18-st-48 ky	18-ky-49 ky	18-ky-50 ky	18-ky-51 ky	18-ky-52 ky	18-ky-53 ky	18-st-56 ky	18-ky-57 ky
SiO2	37.34	37.07	37.09	37.00	37.28	37.08	37.03	37.38
TiO2	0.05	0.01	0.00	0.02	0.03	0.00	0.01	0.03
Al2O3	62.47	62.90	62.55	63.53	62.80	62.85	62.25	63.37
Cr2O3	0.01	0.04	0.00	0.02	0.04	0.00	0.05	0.04
FeO	1.30	1.20	1.30	1.38	1.38	1.31	1.45	1.23
MnO	0.03	0.02	0.04	0.00	0.00	0.02	0.09	0.06
MgO	0.06	0.08	0.06	0.06	0.04	0.05	0.07	0.08
CaO	0.00	0.01	0.00	0.01	0.00	0.01	0.02	0.00
Na2O	0.01	0.00	0.00	0.00	0.01	0.01	0.00	0.00
K2O	0.00	0.00	0.01	0.01	0.00	0.01	0.01	0.00
Total	**101.28**	**101.32**	**101.05**	**102.03**	**101.59**	**101.34**	**100.98**	**102.20**
num ox	5.00	5.00	5.00	5.00	5.00	5.00	5.00	5.00
Si	1.00	0.99	1.00	0.99	1.00	0.99	1.00	0.99
Ti	0.00	0.00	0.00	0.00	0.00	0.00	0.00	0.00
Al	1.97	1.99	1.98	2.00	1.98	1.99	1.98	1.99
Cr	0.00	0.00	0.00	0.00	0.00	0.00	0.00	0.00
Fe	0.03	0.03	0.03	0.03	0.03	0.03	0.03	0.03
Mn	0.00	0.00	0.00	0.00	0.00	0.00	0.00	0.00
Mg	0.00	0.00	0.00	0.00	0.00	0.00	0.00	0.00
Ca	0.00	0.00	0.00	0.00	0.00	0.00	0.00	0.00
Na	0.00	0.00	0.00	0.00	0.00	0.00	0.00	0.00
K	0.00	0.00	0.00	0.00	0.00	0.00	0.00	0.00
Total	**3.01**	**3.01**	**3.01**	**3.02**	**3.01**	**3.01**	**3.01**	**3.01**
xfe	0.95	0.94	0.95	0.96	0.97	0.96	0.95	0.94

MINERAL CHEMISTRY FOR MANGOCHI (SAMPLE M21)

	21 opx 1 cpx	21 opx 2 cpx	21 opx 3 cpx	21 cpx 4 cpx	21 cpx 5 cpx	21 cpx 6 cpx	21 cpx 8 cpx	21 cpx 10 cpx	21 ksp 1 ksp	21 ksp 2 ksp	21 ksp 3 ksp
SiO2	49.00	48.81	48.73	48.55	48.59	48.94	48.22	49.04	65.70	65.34	65.20
TiO2	0.11	0.08	0.12	0.19	0.09	0.13	0.17	0.11	0.02	0.06	0.05
Al2O3	1.04	0.98	0.91	0.91	0.93	0.84	1.04	1.02	19.25	19.10	19.00
Cr2O3	0.01	0.00	0.00	0.03	0.00	0.00	0.02	0.02	0.01	0.03	0.00
FeO	28.17	27.71	27.84	29.68	29.92	30.01	32.70	27.11	0.03	0.00	0.02
MnO	1.16	1.15	1.14	1.19	1.24	1.21	1.35	1.14	0.08	0.00	0.02
MgO	2.09	2.07	2.06	2.17	1.98	1.94	2.23	2.18	0.02	0.00	0.01
CaO	18.82	19.13	19.03	17.24	17.16	17.47	14.26	19.31	0.08	0.04	0.05
Na2O	0.32	0.37	0.35	0.34	0.33	0.28	0.28	0.40	1.68	1.41	1.60
K2O	0.01	0.01	0.01	0.00	0.01	0.00	0.00	0.01	13.50	14.56	14.53
Total	**100.74**	**100.30**	**100.18**	**100.30**	**100.25**	**100.81**	**100.27**	**100.35**	**100.36**	**100.54**	**100.48**
num ox	6.00	6.00	6.00	6.00	6.00	6.00	6.00	6.00	8.00	8.00	8.00
Si	1.98	1.98	1.98	1.98	1.99	1.99	1.98	1.99	2.99	2.98	2.98
Ti	0.00	0.00	0.00	0.01	0.00	0.00	0.01	0.00	0.00	0.00	0.00
Al	0.05	0.05	0.04	0.04	0.04	0.04	0.05	0.05	1.03	1.03	1.02
Cr	0.00	0.00	0.00	0.00	0.00	0.00	0.00	0.00	0.00	0.00	0.00
Fe	0.95	0.94	0.95	1.01	1.02	1.02	1.12	0.92	0.00	0.00	0.00
Mn	0.04	0.04	0.04	0.04	0.04	0.04	0.05	0.04	0.00	0.00	0.00
Mg	0.13	0.13	0.13	0.13	0.12	0.12	0.14	0.13	0.00	0.00	0.00
Ca	0.82	0.83	0.83	0.75	0.75	0.76	0.63	0.84	0.00	0.00	0.00
Na	0.03	0.03	0.03	0.03	0.03	0.02	0.02	0.03	0.15	0.12	0.14
K	0.00	0.00	0.00	0.00	0.00	0.00	0.00	0.00	0.78	0.85	0.85
Total	**4.00**	**4.00**	**4.00**	**4.00**	**4.00**	**4.00**	**4.00**	**4.00**	**4.96**	**4.99**	**5.00**
xfe	0.93	0.93	0.93	0.93	0.94	0.94	0.94	0.93			
XAb									0.16	0.13	0.14
XAn									0.00	0.00	0.00
XOr									0.84	0.87	0.85
Jadeite content	0.03	0.03	0.03	0.03	0.03	0.03	0.03	0.04			

	21 ksp 4	21 ksp 5	21 ksp 6	21 ksp 7	21 ksp 8	21 ksp 9	21 ksp 10	21 pl 1	21 pl 2	21 pl 3	21 pl 4
	ksp	ksp	ksp	ksp	ksp	ksp	ksp	pl	pl	pl	pl
SiO2	65.33	65.11	65.14	65.14	65.25	64.77	64.98	63.18	62.99	63.06	62.70
TiO2	0.01	0.01	0.06	0.03	0.01	0.06	0.02	0.03	0.03	0.02	0.01
Al2O3	19.12	19.01	18.88	19.14	18.97	18.83	18.81	23.87	24.03	23.42	23.63
Cr2O3	0.00	0.00	0.00	0.00	0.00	0.00	0.02	0.01	0.00	0.00	0.00
FeO	0.04	0.04	0.05	0.00	0.05	0.02	0.05	0.09	0.09	0.08	0.01
MnO	0.06	0.05	0.00	0.02	0.00	0.00	0.01	0.03	0.05	0.04	0.02
MgO	0.01	0.00	0.00	0.02	0.01	0.00	0.01	0.00	0.00	0.00	0.00
CaO	0.07	0.00	0.04	0.01	0.00	0.00	0.01	4.88	4.88	4.81	5.11
Na2O	1.70	1.48	1.18	1.33	1.37	1.06	0.99	8.31	8.15	8.22	8.21
K2O	14.17	14.76	15.22	14.77	14.84	15.15	15.24	0.33	0.21	0.22	0.10
Total	**100.52**	**100.47**	**100.57**	**100.46**	**100.50**	**99.89**	**100.13**	**100.73**	**100.43**	**99.87**	**99.80**
num ox	8.00	8.00	8.00	8.00	8.00	8.00	8.00	8.00	8.00	8.00	8.00
Si	2.98	2.98	2.98	2.98	2.98	2.98	2.99	2.77	2.77	2.79	2.78
Ti	0.00	0.00	0.00	0.00	0.00	0.00	0.00	0.00	0.00	0.00	0.00
Al	1.03	1.03	1.02	1.03	1.02	1.02	1.02	1.24	1.25	1.22	1.23
Cr	0.00	0.00	0.00	0.00	0.00	0.00	0.00	0.00	0.00	0.00	0.00
Fe	0.00	0.00	0.00	0.00	0.00	0.00	0.00	0.00	0.00	0.00	0.00
Mn	0.00	0.00	0.00	0.00	0.00	0.00	0.00	0.00	0.00	0.00	0.00
Mg	0.00	0.00	0.00	0.00	0.00	0.00	0.00	0.00	0.00	0.00	0.00
Ca	0.00	0.00	0.00	0.00	0.00	0.00	0.00	0.23	0.23	0.23	0.24
Na	0.15	0.13	0.11	0.12	0.12	0.09	0.09	0.71	0.70	0.70	0.70
K	0.82	0.86	0.89	0.86	0.87	0.89	0.89	0.02	0.01	0.01	0.01
Total	**4.99**	**5.00**	**5.00**	**4.99**	**5.00**	**5.00**	**4.99**	**4.97**	**4.96**	**4.96**	**4.96**
XAb	0.15	0.13	0.11	0.12	0.12	0.10	0.09	0.74	0.74	0.75	0.74
XAn	0.00	0.00	0.00	0.00	0.00	0.00	0.00	0.24	0.25	0.24	0.25
XOr	0.84	0.87	0.89	0.88	0.88	0.90	0.91	0.02	0.01	0.01	0.01

	21 pl 5 pl	21 pl 6 pl	21 pl 7 pl	21 pl 8 pl	21 pl 9 pl	21 pl 10 pl	21 kspbl 1 pl	21 kspbl 2 pl	21 kspbl 3 pl	21 kspbl 4 pl	21 kspbl 5 pl
SiO2	62.82	62.98	62.22	62.55	62.94	63.25	62.71	62.99	62.89	63.08	63.04
TiO2	0.00	0.00	0.01	0.00	0.01	0.00	0.03	0.00	0.00	0.04	0.04
Al2O3	23.58	23.67	23.56	23.81	24.02	23.94	23.74	23.11	22.99	23.68	23.37
Cr2O3	0.00	0.01	0.02	0.01	0.00	0.00	0.01	0.00	0.00	0.00	0.00
FeO	0.07	0.12	0.13	0.07	0.08	0.08	0.08	0.09	0.03	0.12	0.01
MnO	0.01	0.07	0.05	0.06	0.01	0.00	0.02	0.04	0.02	0.04	0.05
MgO	0.00	0.02	0.00	0.00	0.01	0.00	0.00	0.01	0.00	0.00	0.00
CaO	4.98	4.85	4.98	5.06	4.87	4.89	5.14	4.75	4.59	4.98	4.93
Na2O	7.94	7.89	8.15	7.97	8.36	8.24	8.21	8.15	8.45	8.39	8.11
K2O	0.27	0.33	0.26	0.31	0.34	0.17	0.16	0.13	0.13	0.15	0.14
Total	**99.68**	**99.93**	**99.38**	**99.84**	**100.65**	**100.57**	**100.09**	**99.28**	**99.11**	**100.48**	**99.69**
num ox	8.00	8.00	8.00	8.00	8.00	8.00	8.00	8.00	8.00	8.00	8.00
Si	2.78	2.78	2.77	2.77	2.77	2.78	2.77	2.80	2.80	2.78	2.79
Ti	0.00	0.00	0.00	0.00	0.00	0.00	0.00	0.00	0.00	0.00	0.00
Al	1.23	1.23	1.24	1.24	1.24	1.24	1.24	1.21	1.21	1.23	1.22
Cr	0.00	0.00	0.00	0.00	0.00	0.00	0.00	0.00	0.00	0.00	0.00
Fe	0.00	0.00	0.00	0.00	0.00	0.00	0.00	0.00	0.00	0.00	0.00
Mn	0.00	0.00	0.00	0.00	0.00	0.00	0.00	0.00	0.00	0.00	0.00
Mg	0.00	0.00	0.00	0.00	0.00	0.00	0.00	0.00	0.00	0.00	0.00
Ca	0.24	0.23	0.24	0.24	0.23	0.23	0.24	0.23	0.22	0.23	0.23
Na	0.68	0.68	0.70	0.68	0.71	0.70	0.70	0.70	0.73	0.72	0.70
K	0.02	0.02	0.01	0.02	0.02	0.01	0.01	0.01	0.01	0.01	0.01
Total	**4.95**	**4.95**	**4.97**	**4.96**	**4.98**	**4.96**	**4.97**	**4.95**	**4.96**	**4.97**	**4.95**
XAb	0.73	0.73	0.74	0.73	0.74	0.75	0.74	0.75	0.76	0.75	0.74
XAn	0.25	0.25	0.25	0.25	0.24	0.24	0.25	0.24	0.23	0.24	0.25
XOr	0.02	0.02	0.02	0.02	0.02	0.01	0.01	0.01	0.01	0.01	0.01

	21 kspbl 6 pl	21 kspbl 7 pl	21 kspbl 8 pl	21 kspbl 9 pl	21 kspbl 10 pl	21 plbl 1 ksp	21 plbl 2 ksp	21 plbl 4 ksp	21 plbl 6 ksp	21 plbl 7 ksp	21 plbl 8 ksp
SiO2	62.72	62.74	62.56	62.54	62.84	64.61	64.60	65.63	65.15	65.08	64.93
TiO2	0.00	0.00	0.00	0.01	0.02	0.04	0.01	0.02	0.02	0.05	0.07
Al2O3	23.44	23.04	23.47	23.23	23.16	18.32	18.32	18.05	18.50	18.63	18.51
Cr2O3	0.02	0.00	0.04	0.04	0.00	0.00	0.00	0.02	0.03	0.00	0.00
FeO	0.07	0.12	0.12	0.13	0.08	0.03	0.01	0.04	0.03	0.06	0.06
MnO	0.00	0.04	0.04	0.01	0.03	0.01	0.02	0.04	0.00	0.02	0.05
MgO	0.02	0.02	0.01	0.00	0.00	0.01	0.00	0.00	0.01	0.00	0.03
CaO	4.92	4.86	4.92	4.99	4.79	0.00	0.02	0.00	0.00	0.00	0.00
Na2O	8.08	8.49	8.14	7.92	8.30	0.95	0.93	0.86	0.94	0.79	0.94
K2O	0.18	0.10	0.16	0.16	0.06	15.29	15.38	15.65	15.43	15.73	15.48
Total	**99.45**	**99.41**	**99.46**	**99.04**	**99.28**	**99.27**	**99.30**	**100.30**	**100.11**	**100.37**	**100.07**
num ox	8.00	8.00	8.00	8.00	8.00	8.00	8.00	8.00	8.00	8.00	8.00
Si	2.78	2.79	2.78	2.79	2.79	3.00	3.00	3.02	3.00	2.99	2.99
Ti	0.00	0.00	0.00	0.00	0.00	0.00	0.00	0.00	0.00	0.00	0.00
Al	1.23	1.21	1.23	1.22	1.21	1.00	1.00	0.98	1.00	1.01	1.01
Cr	0.00	0.00	0.00	0.00	0.00	0.00	0.00	0.00	0.00	0.00	0.00
Fe	0.00	0.00	0.00	0.00	0.00	0.00	0.00	0.00	0.00	0.00	0.00
Mn	0.00	0.00	0.00	0.00	0.00	0.00	0.00	0.00	0.00	0.00	0.00
Mg	0.00	0.00	0.00	0.00	0.00	0.00	0.00	0.00	0.00	0.00	0.00
Ca	0.23	0.23	0.23	0.24	0.23	0.00	0.00	0.00	0.00	0.00	0.00
Na	0.70	0.73	0.70	0.68	0.72	0.09	0.08	0.08	0.08	0.07	0.08
K	0.01	0.01	0.01	0.01	0.00	0.91	0.91	0.92	0.91	0.92	0.91
Total	**4.95**	**4.97**	**4.96**	**4.95**	**4.96**	**5.00**	**5.00**	**4.99**	**4.99**	**5.00**	**5.00**
XAb	0.74	0.76	0.74	0.73	0.76	0.09	0.08	0.08	0.08	0.07	0.08
XAn	0.25	0.24	0.25	0.26	0.24	0.00	0.00	0.00	0.00	0.00	0.00
XOr	0.01	0.01	0.01	0.01	0.00	0.91	0.91	0.92	0.92	0.93	0.92

	21 plbl 9	21 plbl 10	21-opx-1	21-opx-2	21-opx-3	21-opx-4	21-opx-5	21-opx-7	21-opx-8	21-opx-9	21-opx-10
	ksp	ksp	opx	opx	opx	opx	opx	opx	opx	opx	opx
SiO2	64.64	64.83	47.36	47.09	47.6	47.0	47.1	47.1	47.4	47.8	47.7
TiO2	0.05	0.01	0.09	0.09	0.0	0.1	0.1	0.1	0.0	0.0	0.1
Al2O3	18.63	18.63	0.34	0.23	0.2	0.2	0.2	0.2	0.2	0.3	0.2
Cr2O3	0.05	0.00	0.00	0.00	0.0	0.0	0.0	0.0	0.0	0.0	0.0
FeO	0.01	0.04	47.24	47.09	46.9	47.0	46.9	47.1	46.6	47.0	46.7
MnO	0.02	0.04	2.18	2.16	2.2	2.0	2.1	2.4	2.3	2.3	2.4
MgO	0.02	0.00	2.07	2.49	2.5	2.2	2.1	2.3	2.3	2.2	2.3
CaO	0.01	0.02	0.94	0.95	0.9	1.6	1.5	0.9	0.9	1.0	0.9
Na2O	1.09	0.93	0.03	0.00	0.0	0.0	0.0	0.0	0.0	0.0	0.0
K2O	15.09	15.53									
Total	**99.61**	**100.04**	**100.26**	**100.09**	**100.3**	**100.0**	**100.1**	**100.0**	**99.8**	**100.5**	**100.3**
num ox	8.00	8.00	6.00	6.00	6.0	6.0	6.0	6.0	6.0	6.0	6.0
Si	2.99	2.99	2.02	2.01	2.0	2.0	2.0	2.0	2.0	2.0	2.0
Ti	0.00	0.00	0.00	0.00	0.0	0.0	0.0	0.0	0.0	0.0	0.0
Al	1.02	1.01	0.02	0.01	0.0	0.0	0.0	0.0	0.0	0.0	0.0
Cr	0.00	0.00	0.00	0.00	0.0	0.0	0.0	0.0	0.0	0.0	0.0
Fe	0.00	0.00	1.68	1.68	1.7	1.7	1.7	1.7	1.7	1.7	1.7
Mn	0.00	0.00	0.08	0.08	0.1	0.1	0.1	0.1	0.1	0.1	0.1
Mg	0.00	0.00	0.13	0.16	0.2	0.1	0.1	0.1	0.1	0.1	0.1
Ca	0.00	0.00	0.04	0.04	0.0	0.1	0.1	0.0	0.0	0.0	0.0
Na	0.10	0.08	0.00	0.00	0.0	0.0	0.0	0.0	0.0	0.0	0.0
K	0.89	0.91	0.00	0.00	0.0	0.0	0.0	0.0	0.0	0.0	0.0
Total	**5.00**	**5.00**	**3.97**	**3.98**	**4.0**	**4.0**	**4.0**	**4.0**	**4.0**	**4.0**	**4.0**
xfe			0.96	0.95	0.9	1.0	1.0	1.0	1.0	1.0	1.0
XAb	0.10	0.08									
XAn	0.00	0.00									
XOr	0.90	0.92									

	21-gt-5	21-gt-11
	gt	gt
SiO2	36.7	36.9
TiO2	0.0	0.0
Al2O3	20.5	20.5
Cr2O3	0.0	0.0
FeO	30.9	30.6
MnO	3.9	3.6
MgO	0.5	0.5
CaO	7.6	7.7
Na2O	0.0	0.0
K2O		
Total	**100.1**	**99.8**
num ox	12.0	12.0
Si	3.0	3.0
Ti	0.0	0.0
Al	2.0	2.0
Cr	0.0	0.0
Fe	2.1	2.1
Mn	0.3	0.2
Mg	0.1	0.1
Ca	0.7	0.7
Na	0.0	0.0
K	0.0	0.0
Total	**8.0**	**8.0**
xfe		
Xalm	0.7	0.7
Xgrs	0.2	0.2
Xpyr	0.0	0.0
Xsps	0.1	0.1

MINERAL CHEMISTRY FOR MANGOCHI (SAMPLE M22)

	22 cpx 1	22 cpx 2	22 cpx 4	22 cpx 8	22 cpx 9	22 cpx 10	22 cpx 11	22 cpx 14	22 cpx 15	22 cpx 17	22 opx 18
	cpx	cpx	cpx	cpx	cpx	cpx	cpx	cpx	cpx	cpx	opx
SiO2	48.67	49.41	48.88	49.57	49.13	49.38	49.25	49.19	49.04	48.26	46.54
TiO2	0.08	0.03	0.03	0.10	0.03	0.09	0.14	0.11	0.11	0.19	0.06
Al2O3	0.85	0.45	0.83	1.06	0.76	0.73	0.82	0.75	0.79	1.05	0.28
Cr2O3	0.05	0.00	0.00	0.02	0.00	0.03	0.00	0.03	0.01	0.00	0.02
FeO	30.31	27.70	30.75	26.73	27.97	28.89	26.48	26.93	26.57	28.22	48.13
MnO	1.14	1.08	1.16	0.96	1.15	1.15	1.05	1.07	1.04	1.13	2.20
MgO	1.66	1.61	1.71	1.72	1.88	1.77	1.97	1.99	1.49	1.92	1.92
CaO	17.88	20.34	16.99	20.27	19.33	18.62	20.53	20.29	20.49	18.99	0.84
Na2O	0.30	0.24	0.32	0.40	0.28	0.24	0.40	0.29	0.33	0.35	0.00
K2O	0.01	0.00	0.01	0.01	0.00	0.01	0.00	0.02	0.00	0.01	0.01
Total	**100.94**	**100.86**	**100.69**	**100.84**	**100.53**	**100.91**	**100.65**	**100.66**	**99.88**	**100.12**	**100.00**
num ox	6.00	6.00	6.00	6.00	6.00	6.00	6.00	6.00	6.00	6.00	6.00
Si	1.98	2.00	1.99	2.00	1.99	2.00	1.99	1.99	2.00	1.97	2.00
Ti	0.00	0.00	0.00	0.00	0.00	0.00	0.00	0.00	0.00	0.01	0.00
Al	0.04	0.02	0.04	0.05	0.04	0.03	0.04	0.04	0.04	0.05	0.01
Cr	0.00	0.00	0.00	0.00	0.00	0.00	0.00	0.00	0.00	0.00	0.00
Fe	1.03	0.94	1.05	0.90	0.95	0.98	0.89	0.91	0.91	0.96	1.73
Mn	0.04	0.04	0.04	0.03	0.04	0.04	0.04	0.04	0.04	0.04	0.08
Mg	0.10	0.10	0.10	0.10	0.11	0.11	0.12	0.12	0.09	0.12	0.12
Ca	0.78	0.88	0.74	0.87	0.84	0.81	0.89	0.88	0.89	0.83	0.04
Na	0.02	0.02	0.03	0.03	0.02	0.02	0.03	0.02	0.03	0.03	0.00
K	0.00	0.00	0.00	0.00	0.00	0.00	0.00	0.00	0.00	0.00	0.00
Total	**4.01**	**4.00**	**4.00**	**3.99**	**4.00**	**3.99**	**4.00**	**4.00**	**3.99**	**4.01**	**3.99**
xfe	0.95	0.95	0.95	0.94	0.94	0.94	0.93	0.93	0.95	0.94	0.96
Jadeite content	0.03	0.02	0.03	0.03	0.03	0.02	0.03	0.03	0.03	0.03	0.00

	22 pl 3	22 pl 6	22 pl 7	22 pl 12	22 pl 13	22 pl 15	22 pl 16	22 ksp 1	22 ksp 2	22 pl 1
	pl	pl	pl	pl	pl	pl	pl	ksp	ksp	ksp
SiO2	63.68	62.94	63.11	63.12	62.71	63.26	63.12	65.58	65.65	66.34
TiO2	0.00	0.02	0.00	0.01	0.00	0.00	0.03	0.01	0.00	0.05
Al2O3	22.80	23.44	23.14	22.79	23.08	23.08	23.02	18.26	18.37	18.67
Cr2O3	0.01	0.03	0.03	0.00	0.03	0.00	0.03	0.00	0.00	0.00
FeO	0.06	0.08	0.10	0.09	0.05	0.06	0.11	0.06	0.00	0.03
MnO	0.03	0.00	0.04	0.07	0.01	0.01	0.04	0.03	0.00	0.04
MgO	0.01	0.00	0.00	0.01	0.00	0.01	0.00	0.00	0.01	0.00
CaO	4.83	4.92	4.76	4.86	4.80	4.90	4.88	0.04	0.06	0.00
Na2O	8.24	8.19	8.34	8.21	8.33	8.24	8.41	1.27	1.43	1.18
K2O	0.08	0.12	0.14	0.14	0.13	0.09	0.15	13.42	13.17	13.68
Total	**99.75**	**99.74**	**99.67**	**99.30**	**99.14**	**99.65**	**99.79**	**98.67**	**98.68**	**99.99**
num ox	8.00	8.00	8.00	8.00	8.00	8.00	8.00	8.00	8.00	8.00
Si	2.81	2.79	2.80	2.81	2.79	2.80	2.80	3.03	3.02	3.02
Ti	0.00	0.00	0.00	0.00	0.00	0.00	0.00	0.00	0.00	0.00
Al	1.19	1.22	1.21	1.19	1.21	1.20	1.20	0.99	1.00	1.00
Cr	0.00	0.00	0.00	0.00	0.00	0.00	0.00	0.00	0.00	0.00
Fe	0.00	0.00	0.00	0.00	0.00	0.00	0.00	0.00	0.00	0.00
Mn	0.00	0.00	0.00	0.00	0.00	0.00	0.00	0.00	0.00	0.00
Mg	0.00	0.00	0.00	0.00	0.00	0.00	0.00	0.00	0.00	0.00
Ca	0.23	0.23	0.23	0.23	0.23	0.23	0.23	0.00	0.00	0.00
Na	0.71	0.70	0.72	0.71	0.72	0.71	0.72	0.11	0.13	0.10
K	0.00	0.01	0.01	0.01	0.01	0.01	0.01	0.79	0.77	0.79
Total	**4.95**	**4.96**	**4.96**	**4.95**	**4.96**	**4.95**	**4.97**	**4.93**	**4.93**	**4.93**
Ab	0.75	0.75	0.75	0.75	0.75	0.75	0.75	0.13	0.14	0.12
An	0.24	0.25	0.24	0.24	0.24	0.25	0.24	0.00	0.00	0.00
Or	0.01	0.01	0.01	0.01	0.01	0.01	0.01	0.87	0.86	0.88

	22 plbl 2 ksp	22 plbl 3 ksp	22 plbl 4 ksp	22 plbl 5 ksp	22 plbl 6 ksp	22 plbl 7 ksp	22 plbl 8 ksp	22 plbl 9 ksp	22 plbl 10 ksp	22 kspbl 1 pl	22 kspbl 4 pl
SiO2	63.87	63.74	63.66	63.73	64.00	64.05	63.71	64.35	63.81	62.88	61.95
TiO2	0.01	0.03	0.06	0.00	0.01	0.02	0.04	0.03	0.04	0.01	0.03
Al2O3	19.23	18.55	19.02	18.85	19.05	19.05	19.00	19.10	18.97	22.96	23.37
Cr2O3	0.03	0.00	0.00	0.01	0.00	0.00	0.04	0.00	0.00	0.00	0.00
FeO	0.02	0.43	0.00	0.03	0.03	0.06	0.02	0.04	0.00	0.11	0.09
MnO	0.01	0.08	0.02	0.02	0.08	0.04	0.01	0.00	0.01	0.01	0.09
MgO	0.01	0.03	0.01	0.00	0.00	0.00	0.00	0.00	0.01	0.03	0.00
CaO	0.00	0.05	0.03	0.00	0.00	0.00	0.01	0.00	0.00	4.80	4.98
Na2O	0.94	0.80	1.17	1.10	1.01	0.93	1.23	1.00	1.40	8.44	8.37
K2O	13.65	13.43	13.49	13.59	13.59	13.82	13.45	13.79	13.05	0.10	0.13
Total	**97.76**	**97.14**	**97.46**	**97.33**	**97.77**	**97.98**	**97.52**	**98.32**	**97.29**	**99.34**	**99.00**
num ox	8.00	8.00	8.00	8.00	8.00	8.00	8.00	8.00	8.00	8.00	8.00
Si	2.98	3.00	2.98	2.99	2.99	2.99	2.98	2.99	2.99	2.80	2.77
Ti	0.00	0.00	0.00	0.00	0.00	0.00	0.00	0.00	0.00	0.00	0.00
Al	1.06	1.03	1.05	1.04	1.05	1.05	1.05	1.05	1.05	1.20	1.23
Cr	0.00	0.00	0.00	0.00	0.00	0.00	0.00	0.00	0.00	0.00	0.00
Fe	0.00	0.02	0.00	0.00	0.00	0.00	0.00	0.00	0.00	0.00	0.00
Mn	0.00	0.00	0.00	0.00	0.00	0.00	0.00	0.00	0.00	0.00	0.00
Mg	0.00	0.00	0.00	0.00	0.00	0.00	0.00	0.00	0.00	0.00	0.00
Ca	0.00	0.00	0.00	0.00	0.00	0.00	0.00	0.00	0.00	0.23	0.24
Na	0.08	0.07	0.11	0.10	0.09	0.08	0.11	0.09	0.13	0.73	0.73
K	0.81	0.81	0.81	0.81	0.81	0.82	0.80	0.82	0.78	0.01	0.01
Total	**4.94**	**4.93**	**4.95**	**4.95**	**4.94**	**4.94**	**4.95**	**4.94**	**4.94**	**4.97**	**4.98**
Ab	0.09	0.08	0.12	0.11	0.10	0.09	0.12	0.10	0.14	0.76	0.75
An	0.00	0.00	0.00	0.00	0.00	0.00	0.00	0.00	0.00	0.24	0.25
Or	0.91	0.91	0.88	0.89	0.90	0.91	0.88	0.90	0.86	0.01	0.01

	22 kspbl 5 pl	22 kspbl 9 pl	22-gt-1 gt	22-gt-2 gt	22-gt-3 gt	22-gt-4 gt	22-gt-5 gt	22-gt-6 gt	22-gt-7 gt	22-gt-8 gt	22-gt-9 gt
SiO2	61.80	61.70	36.82	36.82	36.87	36.80	36.80	36.78	37.16	36.77	36.97
TiO2	0.00	0.01	0.01	0.06	0.10	0.03	0.04	0.08	0.03	0.08	0.02
Al2O3	23.88	24.18	20.96	20.96	20.78	21.03	21.13	20.82	20.94	21.00	21.10
Cr2O3	0.00	0.02	0.02	0.04	0.04	0.00	0.00	0.03	0.00	0.00	0.03
FeO	0.05	0.10	30.62	30.94	30.39	31.08	31.45	31.21	30.80	30.82	30.66
MnO	0.06	0.05	3.94	3.76	4.10	3.54	3.53	3.45	3.99	3.81	3.97
MgO	0.00	0.00	0.33	0.36	0.34	0.32	0.33	0.29	0.35	0.33	0.37
CaO	4.79	4.91	7.61	7.54	7.60	7.57	7.58	7.68	7.53	7.61	7.55
Na2O	8.33	8.15	0.03	0.03	0.06	0.00	0.03	0.01	0.01	0.02	0.02
K2O	0.12	0.15									
Total	**99.03**	**99.27**	**100.34**	**100.51**	**100.28**	**100.37**	**100.88**	**100.35**	**100.81**	**100.44**	**100.68**
num ox	8.00	8.00	12.00	12.00	12.00	12.00	12.00	12.00	12.00	12.00	12.00
Si	2.76	2.75	2.98	2.97	2.98	2.98	2.96	2.98	2.99	2.97	2.98
Ti	0.00	0.00	0.00	0.00	0.01	0.00	0.00	0.00	0.00	0.00	0.00
Al	1.26	1.27	2.00	2.00	1.98	2.00	2.01	1.99	1.99	2.00	2.00
Cr	0.00	0.00	0.00	0.00	0.00	0.00	0.00	0.00	0.00	0.00	0.00
Fe	0.00	0.00	2.07	2.09	2.06	2.10	2.12	2.11	2.07	2.08	2.07
Mn	0.00	0.00	0.27	0.26	0.28	0.24	0.24	0.24	0.27	0.26	0.27
Mg	0.00	0.00	0.04	0.04	0.04	0.04	0.04	0.04	0.04	0.04	0.04
Ca	0.23	0.23	0.66	0.65	0.66	0.66	0.65	0.67	0.65	0.66	0.65
Na	0.72	0.70	0.00	0.00	0.01	0.00	0.00	0.00	0.00	0.00	0.00
K	0.01	0.01	0.00	0.00	0.00	0.00	0.00	0.00	0.00	0.00	0.00
Total	**4.98**	**4.97**	**8.02**	**8.02**	**8.02**	**8.02**	**8.03**	**8.02**	**8.02**	**8.02**	**8.02**
Ab	0.75	0.74									
An	0.24	0.25									
Or	0.01	0.01									
Xalm			0.68	0.69	0.68	0.69	0.69	0.69	0.68	0.68	0.68
Xgrs			0.22	0.21	0.22	0.22	0.21	0.22	0.21	0.22	0.21
Xpyr			0.01	0.01	0.01	0.01	0.01	0.01	0.01	0.01	0.01
Xsps			0.09	0.08	0.09	0.08	0.08	0.08	0.09	0.09	0.09

	22-opx-1	22-opx-2	22-opx-3	22-opx-4	22-opx-5	22-opx-6	22-opx-7	22-opx-9	22-opx-11	22-opx-12
	opx	opx	opx	opx	opx	opx	opx	opx	opx	opx
SiO2	47.44	47.53	47.43	47.56	47.26	47.66	47.34	47.67	47.68	47.54
TiO2	0.03	0.08	0.03	0.03	0.11	0.08	0.04	0.10	0.07	0.08
Al2O3	0.21	0.29	0.20	0.21	0.28	0.19	0.33	0.20	0.19	0.20
Cr2O3	0.00	0.00	0.00	0.00	0.02	0.00	0.00	0.02	0.04	0.02
FeO	47.95	47.40	47.36	47.25	47.67	47.74	47.85	47.51	48.02	48.05
MnO	2.19	2.20	2.11	2.34	1.94	2.07	2.11	2.03	2.02	2.09
MgO	1.86	1.87	2.04	1.93	1.85	2.06	1.98	1.89	1.76	1.82
CaO	0.80	0.89	0.82	0.90	0.90	0.75	0.83	0.92	0.80	0.96
Na2O	0.04	0.01	0.01	0.03	0.05	0.04	0.00	0.04	0.04	0.01
K2O										
Total	**100.51**	**100.26**	**100.00**	**100.26**	**100.07**	**100.58**	**100.48**	**100.37**	**100.61**	**100.77**
num ox	6.00	6.00	6.00	6.00	6.00	6.00	6.00	6.00	6.00	6.00
Si	2.02	2.02	2.02	2.02	2.02	2.02	2.01	2.03	2.03	2.02
Ti	0.00	0.00	0.00	0.00	0.00	0.00	0.00	0.00	0.00	0.00
Al	0.01	0.01	0.01	0.01	0.01	0.01	0.02	0.01	0.01	0.01
Cr	0.00	0.00	0.00	0.00	0.00	0.00	0.00	0.00	0.00	0.00
Fe	1.71	1.69	1.69	1.68	1.70	1.69	1.70	1.69	1.71	1.71
Mn	0.08	0.08	0.08	0.08	0.07	0.07	0.08	0.07	0.07	0.08
Mg	0.12	0.12	0.13	0.12	0.12	0.13	0.13	0.12	0.11	0.12
Ca	0.04	0.04	0.04	0.04	0.04	0.03	0.04	0.04	0.04	0.04
Na	0.00	0.00	0.00	0.00	0.00	0.00	0.00	0.00	0.00	0.00
K	0.00	0.00	0.00	0.00	0.00	0.00	0.00	0.00	0.00	0.00
Total	**3.98**	**3.97**	**3.97**	**3.97**	**3.97**	**3.97**	**3.98**	**3.97**	**3.97**	**3.97**
xfe	0.96	0.96	0.96	0.96	0.96	0.96	0.96	0.96	0.96	0.96